Diesel engine heat release analysis by using newly defined dimensionless parameters

A thesis submitted for the degree of Doctor of Philosophy

By:
G.Abbaszadehmosayebi

School of Engineering and Design
Brunel University
United Kingdom

2014

Abstract

Diesel engine combustion has been studied during the last decades by researchers in terms of improving the performance of the engine. In order to improve the analysis of the diesel engine combustion, dimensionless parameters were used in this study. It was concluded that the newly introduced dimensionless parameters developed in this study facilitate understanding of diesel engine combustion process.

A new method has been proposed to determine the values of the form factor (*m*) and efficiency factors (*a*) of the Wiebe equation. This is achieved by developing a modified form of Wiebe equation with only one constant. The modified version of Wiebe equation facilitates the determination of constants accurately, which enhances the accuracy of evaluating the burn fraction. The error induced on the burn fraction *f* with respect to the values of constants *a* and *m* obtained through different methods is discussed and compared. The form factor affects the burn fraction significantly compared to the efficiency factor. A new non-dimensional parameter 'combustion burn factor (C_i)' has been identified in the modified Wiebe equation. The burn fraction *f* was found to be a function of C_i only, thus the benefits of expressing heat release rate with respect to C_i have been presented.

The errors associated with the determination of apparent heat release rate (*AHRR*) and the cumulative heat release (*Cum.Hrr*) from the measured cylinder pressure data and the assumed specific heat ratio (γ) was determined and compared. The γ affected the calculated AHRR more than the cylinder pressure. Overestimation of γ resulted in an underestimation of the peak value of the *AHRR* and vice versa, this occurred without any shift in the combustion phasing. A new methodology has been proposed to determine the instantaneous and mean value of γ for a given combustion. A two litre Ford puma Zetec diesel engine, four cylinder

and 16 valves was employed to carry out this investigation. This new methodology has been applied to determine γ for a wide range of injection pressure (800 bar to 1200 bar), injection timing (9 deg *BTDC* to -2 deg *BTDC*) and engine loads at 2.7 *BMEP* and 5 *BMEP*. Standard ultra-low sulphur diesel fuel and two bio-diesels (Rapeseed Methyl Ester and Jatropha Methyl Ester) were studied in this investigation.

Ignition delay is one the most important parameter that characterises the combustion and performance of diesel engines. The relation between ignition delay and combustion performance in terms of efficiency and emission was revealed by researchers. Ignition delay period measurements in diesel engine combustion along with the most used correlation for calculating ignition delay are discussed in this work. The effect of constants on accuracy in the correlation were discussed, and induced error on calculated ignition delay periods with respect to constants were calculated and compared. New techniques were proposed to calculate the constant values directly by using the experimental data. It was found that the calculated values for ignition delay using the new techniques matched well with the experimental data. These techniques can improve the accuracy of the ignition delay correlation. Also a new correlation without any constants was introduced in this work. This correlation can be used to predict ignition delay directly by using engine parameters only. The introduced correlation provides better results compared to Arrhenius type correlation presented by Wolfer. This new correlation can be used for feedback control engine combustion process.

Acknowledgments

Words cannot express how grateful I am to my supervisor Dr. Lionel Ganippa who has been a tremendous mentor for me. I would like to thank him for encouraging me to develop my skills as a research scientist and complete the present study. He has given me invaluable advice on pursuing this research and furthering my career. It was an honour to study under the supervision of such a person whose experience and knowledge has greatly contributed to the engine combustion research at Brunel University.

Also I would like to express my special appreciation and thanks to Professor Thanos Megaritis who supported me whenever I needed help. His encouragement always motivated me in my undergraduate and research study.

I should also extend my special thanks to the school of engineering and design at Brunel University and UKIERI for supporting this research.

I would like to express my appreciation to Andy Selway, Ken Anstiss and Clive Barrett for their technical support and advice.

And last but not the least, this research would not have been possible if my little family had not supported me throughout. My wife and two daughters deserve my gratitude for their patience and understanding at all those times when I did not give them the due attention and care.

Abbreviations

AHRR	Apparent heat release rate
ATC	After top dead centre
Bdc	bottom dead centre
BMEP	Break mean effective pressure
BP	Brake Power fraction
BTDC	Before top dead centre
CI	Compression Ignition
CN	Cetane number
CVC	Constant volume combustion
DI	Direct Injection
ECU	Electronic Control Unit
EGR	Exhaust Gas Recirculation
EMS	Electro Mobility Spectrometer
fps	Frame per second
HRTEM	High Resolution Transmission Electron Microscopy
HSDI	High Speed Direct Injection
ICE	Internal Combustion Engine
JME	Jatropha Methyl Ester
LDA	Laser Doppler Anemometry
LHV	lower heating value
LIF	Laser Induced Fluorescence
LRS	Laser Rayleigh Scattering
PAHs	Polycyclic Aromatic Hydrocarbons
PIV	Particle Imaging Velocimetry
PLIF	Planar Laser-Induced Fluorescence
PM	Particulate Matter
RCM	Rapid Compression Machines
RME	Rapeseed Methyl Ester
SI	Spark Ignition
SRS	Spontaneous Raman Scattering
Tdc	top dead centre
TEM	Transmission Electron Microscopy
UHC	Unburned Hydro Carbon
ULSD	Ultra Low Sulfur Diesel
UV	Ultra Violet

Nomenclature

C_i	Combustion burn factor	-
a	Efficiency factor	-
$a(ac)$	Actual value of efficiency factor	-
CO_2	Carbon dioxide	-
Cp	Specific heat at constant pressure	$J/kg.K$
$Cum.Hrr$	cumulative heat release	J
Cv	Specific heat at constant volume	$J/kg.K$
e	Napier's constant (e ≈2.718)	-
E	Error function	J/deg
E_A	Apparent activation energy	-
E_{max}	Maximum absolute error value	J/deg
f	Burn fraction	-
h_i	Specific enthalpy	J/kg
ID	Ignition delay	$msec$
m	mass, polytropic index, Form factor	$Kg,-,-$
$m(ac)$	Actual value of m	-
$m(f)$	The value of polytropic index obtained by curve fitting procedure	-
m^o	Mass rate	Kg/sec
N	Number of molecules	-
Ne	Number of molecules in the effective centres	-
N_o	Number of molecules/moles of reactant at start of combustion	-
NO_x	Nitrogen Oxides	-
Nu	Nusselt number	-
Q	Released heat	J
R	Universal gas constant (8.314)	J/mol.K
Re	Reynolds number	-
RF	Residual function	J/deg
SO_2	Sulphur Dioxide	-
S_p	Piston mean speed	m/sec
t	Time	$msec$
T	Temperature	K
T_c	Temperature at start of combustion	oC
T_i	Temperature at start of compression	oC
U	Internal energy	J
V	Volume	m^3
V_c	Clearance volume	m^3
V_d	Swept volume	m^3

Greek letters

η	Efficiency
α	Relative Apparent heat release rate error
β	Absolute error on Apparent heat release rate
Δ, Π	Dimensionless parameter
$\Delta\Theta$	Combustion duration
Θ	Crank angle
θ_{50}	Location of centre of combustion
θ_{max}	The crank angle where $AHRR/\omega$ reaches to its maximum value
Θ_o	Crank angle at start of combustion
ρ	Density of effective centres
ρr	Relative density of the effective centres
τ	Ignition delay
Υ	Heat capacities ratio
φ	Equivalence ratio
ω	Crank shaft angular velocity, Burn rate

Contents

Abstract i
Acknowledgements iii
Abbreviations iv
Nomenclature v
Greek letters vi
Contents vii
List of Figures ix
List of tables xiv
Chapter 1 - Introduction 1
1.1.Introduction 1
1.2.Vehicle Market Analysis 2
1.3.Internal combustion engines 4
1.3.1. Otto engine 10
1.3.2. Diesel engine 11
1.3.3. Engine operating cycles 12
1.3.4. Diesel engine Advantages 15
1.3.5. Diesel engine disadvantages 16
1.4.Lay out of dissertation 17
1.5.Motivation 19
1.6.Contribution of knowledge 20
Chapter 2 – Literature Review 21
2.1.Engine Research 21
2.1.1 Stationary engines 21
2.1.2. Optical techniques 25
2.1.3.Transmission Electron Microscopy (TEM) 32
2.1.3.1.Definition 32
2.1.3.2.Major problems using TEM 35
2.1.4.Analytical techniques 36
2.2.Wiebe equation 37
2.2.1.Wiebe equation constants (*a* and *m*) 38
2.2.2.Derivation of Wiebe equation 39
2.2.3.Forms of Wiebe equation 46
2.2.4.Applications of Wiebe equation 47
2.3.Heat capacities ratio (γ) 49
2.4.Ignition delay (τ) 51
Chapter 3 – Theoretical methodology 55
3.1.Heat release calculation 55
3.2.Calculation of in-cylinder temperature 59
Chapter 4 – Experimental set up 64
Chapter 5 – Characterising Wiebe Equation for Heat Release Analysis based on Combustion Burn Factor (Ci) 69
5.1.Introduction 69
5.2.Modified Wiebe Equation 70
5.3.Determination of Instantaneous Form (m) and Efficiency (a) Factors 71
5.4.Determination of Overall Form and Efficiency Factors for entire combustion 75

5.6.Comparison of theoretical models 77
5.7.Burn Fraction Error Analysis 79
5.8.Combustion burn factor (Ci) and heat release rate analysis 84
5.9.Conclusions 88
Chapter 6 – Determination of specific heat ratio and error analysis for engine heat release calculations 89
6.1.Introduction 89
6.2.Theory and Results 91
6.2.1.Determination of γ 91
6.2.2.Error associated with pressure on AHRR and γ 100
6.2.3.Effect of variation of γ on AHRR 101
6.2.4.Effect of variation of γ on Cumulative Heat Release 105
6.3.Conclusion 106
Chapter 7 – Characterising ignition delay correlation for diesel engine by using newly proposed analytical methods 108
7.1.Introduction 108
7.2. Error Induced by Constants on Ignition Delay 109
7.3.Determination of A, n and C 112
7.3.1.Analytical approach (Determination of A and n) 113
7.3.2.Line fitting approach (Determination of n) 115
7.3.3.Determination of constant C 116
7.4.New Correlation (Determination of ignition delay) 118
7.5.Results 120
7.5.1.Induced error on ignition delay with respect to A, n and C 120
7.5.2.Analytical approach 121
7.5.3.Line fitting approach 122
7.5.4.Fitting least square function 123
7.6.Discussion 124
7.6.1.Analytical, Line fitting and Fitting a least square methods 124
7.6.2.New correlation 125
7.6.3.Error propagation function 126
7.7.Conclusion 127
Chapter 8 – Conclusion 129
8.1.Wiebe equation 130
8.2.Heat capacities ratio 130
8.3.Ignition delay 131
8.4.Recommendation for future work 132
References 133
Appendix 1 148
Appendix 2 148
Appendix 3 149
Publications of this work 150

List of Figures

Figure (1.1): Number of the cars on the road in some European countries in 2011.

Figure (1.2): Number of passenger cars per 1000 inhabitants (to 2011).

Figure (1.3): European Union emission standards for *PM* and NO_x for engine.

Figure (1.4): Rolls Royce gas turbine internal combustion engine. Type: MT30.

Figure (1.5): An internal combustion engine used in passenger car. Engine type: Mazda skyactiv D Engine1.

Figure (1.6): Typical spark ignition engine.

Figure (1.7): Typical compression ignition engine.

Figure (1.8): Otto cycle.

Figure (1.9): Diesel cycle.

Figure (1.10): Basic geometry of the reciprocating Diesel combustion engine.

Figure (1.11): the four stroke operating cycle.

Figure (2.1): (a): Multi cylinder diesel engine control unit at Brunel University (b): Four cylinder engine equipped with sensors at Brunel University.

Figure (2.2): Several ports at engine exhaust for gas sampling.

Figure (2.3): (a): Ricardo Hydra optical diesel engine at Brunel University. (b): Control unit.

Figure (2.4 a-f): Images of spray and combustion development in a single cylinder diesel engine using high speed camera (10000fps) for diesel fuel at engine condition: fuel injection 5 deg *BTDC*, Fuel injection pressure 1200 bar, Engine speed 1500 rpm and Fuel injection

duration 550 μsec. The frame number is indicated on top right hand side for each image. Each frame number is equivalent to 10^2 μsec. Images a-f indicate the fuel spray development, spray speed and location of start of combustion as well as shape of fuel sprays.

Figure (2.5): *TEM* microscope unit at National Renewable Energy Laboratory,15013 Denver West Parkway, Golden, CO 80401 USA.

Figure (2.6): Image of diesel fuel particle by using *TEM* microscope. Engine condition: fuel injection 9 deg *BTDC*, Fuel injection pressure 800 bar, 0% *EGR*, Engine speed 2000 rpm at 2.7 bar *BMEP*. Multi cylinder diesel engine at Brunel University.

Figure (2.7): Image of *RME* fuel particle by using *TEM* microscope. Engine condition: fuel injection 9 deg *BTDC*, Fuel injection pressure 800 bar, 0% *EGR*, Engine speed 2000 rpm at 2.7 bar *BMEP*. Multi cylinder diesel engine at Brunel University.

Figure (2.8): Variation of efficiency factor (a) against Burn fraction at end of combustion (f_d).

Figure (2.9): Variation of Burn fraction (f) with respect to a.

Figure (2.10): Variation of Burn fraction (f) with respect to m.

Figure (2.11): Variation of Burn rate (ω) with respect to Form factor (m) at $\Delta\theta$=36 and a=4.61.

Figure (3.1): Gross and net heat release profile during combustion, for a turbocharged DI diesel engine in mid load and mid speed range, showing relative magnitude of heat transfer, crevice, and fuel vaporization and heat up effects.

Figure (3.2): Basic geometry of the reciprocating Diesel combustion engine.

Figure (3.3): Variation of in-cylinder temperature at different intake air temperatures for diesel fuel at injection timing 6 deg *BTDC,* injection pressure= 800 bar , BMEP=2.7 and 2000 rpm.

Figure (3.4): variation of in-cylinder temperature at start of combustion at different intake air temperature for diesel fuel at injection timing 6 deg *BTDC,* injection pressure= 800 bar , *BMEP*=2.7 and 2000 rpm.

Figure (3.5): Variation polytropic index (*m*) against piston mean speed for diesel fuel.

Figure (3.6): Variation of in-cylinder temperature using three different methods for diesel fuel at injection timing 6 deg *BTDC,* injection pressure= 800 bar, *BMEP*=2.7 and 2000 rpm. Cylinder wall temperature was considered for T_i for three sets of data.

Figure (4.1): Horiba Mexa-7170 gas analyser.

Figure (4.2): Horiba MEXA-7170 control system.

Figure (4.3): A sample reading by gas analyser type: Horiba MEXA-7170.

Figure (4.4): four cylinder 2 litre Ford Puma Zetec 16 valves High Speed Direct Injection (*HSDI*) diesel engine at Brunel University engine lab.

Figure (5.1): Variation of actual Form factor *m(ac)* and fitted value *m(f)* versus $(\theta-\theta_o)/\Delta\theta$ for the engine operating condition A2.

Figure (5.2): Variation of actual Efficiency factor *a(ac)* and chosen value *a** versus $(\theta-\theta_o)/\Delta\theta$ for the engine operating condition A2.

Figure (5.3): Determination of one overall value of the form factor by taking the slope of $\ln(\frac{\ln(1-f)}{\ln(0.5)})$ and $\ln(\frac{\theta-\theta_o}{\theta_{50}-\theta_o})$.

Figure (5.4): Determination of one overall value of the efficiency factor by taking the slope of $-\ln(1-f)$ and $(\frac{\theta-\theta_o}{\Delta\theta})^{m+1}$.

Figure (5.5): Variation of *f* against $\frac{\theta-\theta_o}{\Delta\theta}$, for four set of data along with experimental data, for the engine operating condition A2.

Figure (5.6): Variation of f for different value of $(\theta-\theta_o)/\Delta\theta$ with respect to *a* and *m* for the engine operating condition A2.

Figure (5.7): Total absolute Burn fraction (*E*) for different value of $(\theta-\theta_o)/\Delta\theta$ with respect to *a* and *m* for the engine operating condition A2.

Figure (5.8): Variation of E_{max} for different values of *a* and *m*.

Figure (5.9): Variation of E_{max} against *m* for *a*=5 and *a*=6.908 for Wiebe equation and modified Wiebe equation.

Figure (5.10): Apparent heat release rate against instantaneous crank angle (θ) at different engine operating conditions A4, A7 and A10.

Figure (5.11): Apparent heat release rate expressed in terms of non-dimensional combustion burn factor (C_i) at conditions A4, A7 and A10.

Figure (6.1). A typical engine measurement system.

Figure (6.2): Pressure transducer type: Kistler 6125A.

Figure (6.3): Variation of in-cylinder pressure against combustion volume. The average of the slope of compression and expansion line provide γ value (*pV* diagram).

Figure (6.4): The value of specific heat ratio γ obtained using logarithmic *pV* diagram for the engine operation conditions A1-A15 described in table (6.1). The most commonly used value in literature γ =1.35 is plotted by dotted line.

Figure (6.5): Variation of sum of square value of Residual Function (*RF*) for three fuels (diesel, Rapeseed Methyl Ester (*RME*) and Jatropha Methyl Ester (*JME*)) at operating conditions A3. The absolute minimum of each curve provide the best γ value.

Figure (6.6): The values of γ obtained using the method based on centre of combustion (θ_{50}) position for the engine operating conditions A1-A15. The most commonly used value in literature γ =1.35 is plotted by dotted line.

Figure (6.7a, 6.7b, 6.7c): The value of γ for the engine operating conditions A1-A15 for diesel fuel , RME and JME using the method based on centre of combustion (θ_{50}) position (new method) and *pV* diagram. The most commonly used value in literature γ =1.35 is plotted by dotted line. γ_{av} corresponds to average value of heat capacities ratio during expansion and compression periods.

Figure (6.8): Absolute Apparent heat release rate error value, d γ =0.01, for the engine operating condition A3.

Figure (6.9): Variation of maximum absolute error (β) for Apparent Heat Release Rate for three fuels (diesel, Rapeseed Methyl Ester (*RME*) and Jatropha Methyl Ester (*JME*)) at engine conditions A1-A15.

Figure (6.10): Apparent heat release rate relative error (α) for a small change in γ value, d γ =0.01, at the engine operating condition A3.

Figure (6.11): Variation of the maximum value relative Apparent Heat Release Rate error for three fuels (diesel, Rapeseed Methyl Ester (*RME*) and Jatropha Methyl Ester (*JME*)) at the engine operating conditions A1-A15.

Figure (7.1): Variation of calculated ignition delay values at given condition for different values of *A* and *n.*

Figure (7.2): The calculated values for *A* and *n* at conditions E1-E13 by using Analytical and line fitting methods.

Figure (7.3): variation of ignition delay for operating conditions E1-E13 by using three analytical techniques along with experimental data.

Figure (7.4): Variation of ignition delay by considering different values for constant C for E1-E13. *A* and *n* were calculated by analytical approach.

Figure (7.5): Variation of ignition delay by considering different values for constant *C* for operating conditions E1-E13. *A* and *n* were calculated by line fitting approach.

Figure (7.6): Variation of ignition delay by considering different values for constant C for E1-E13. *A* and *n* were calculated by fitting a non-linear least square function.

Figure (7.7): Error propagation values (ω) determined for *A* and *n* for different values of *C* obtained from [96, 100&109, 137, 139] along with analytical calculation in present work (analytical) and new correlation.

List of tables

Table (2.1): specification of optical engine

Table (4.1): Specification of engine.

Table (5.1): Engine operating conditions A1 to A30.

Table (6.1): Engine operating conditions A1 to A15.

Table (7.1): Experimental conditions for the tests.

Table (7.2): Values determined for *A* and *n* for different values of *C* obtained from [96, 100&109, 137, 139] along with analytical calculation and Line fitting in present work.

Chapter 1

Introduction

1.1 Introduction

The present work was undertaken at Brunel University as a part of project sponsored by UKIERI (United Kingdom-India Education Research Initiative) and School of Engineering and Design at Brunel University.

Dimensionless parameters are widely used in different fields of science. Reynolds number (*Re*) in fluids and Nusselt number (*Nu*) in heat transfer are good examples for the dimensionless parameters. Dimensionless parameters can help to improve combustion analysis in terms of saving time and extracting more results from the collected data. Also dimensionless parameters can provide valuable results by considering combination effects of parameters. These results could not be achieved if the parameters were studied individually. In this work dimensionless parameters were used to improve engine combustion analysis and proposing a modified form of Wiebe equation. A new technique was proposed to calculate an accurate value for Heat capacities ratio. Also a new correlation was proposed to calculate ignition delay by using dimensionless parameters.

To demonstrate the results a four cylinder 2 litre Ford Puma Zetec 16 valves High Speed Direct Injection (*HSDI*) diesel engine was employed to carry out the measurements. Standard ultra-low sulphur diesel (*ULSD*), and two bio-diesels, Rapeseed Methyl Ester (*RME*), Jatropha Methyl Ester (*JME*) were used in this investigation. The fuel specifications for diesel, *RME* and *JME* can be found in Appendix 1.

1.2. Vehicle Market Analysis

Due to the advantages of Internal Combustion Engines, the number of cars has increased over the last decades. According to the report by Eurostat [1], the statistical office of the European Union situated in Luxembourg, the number of cars in the European countries has increased significantly since 1991. Figure 1.1 indicates the number of cars on the road for 18 counties in Europe. Similar results are available for the rest of European countries.

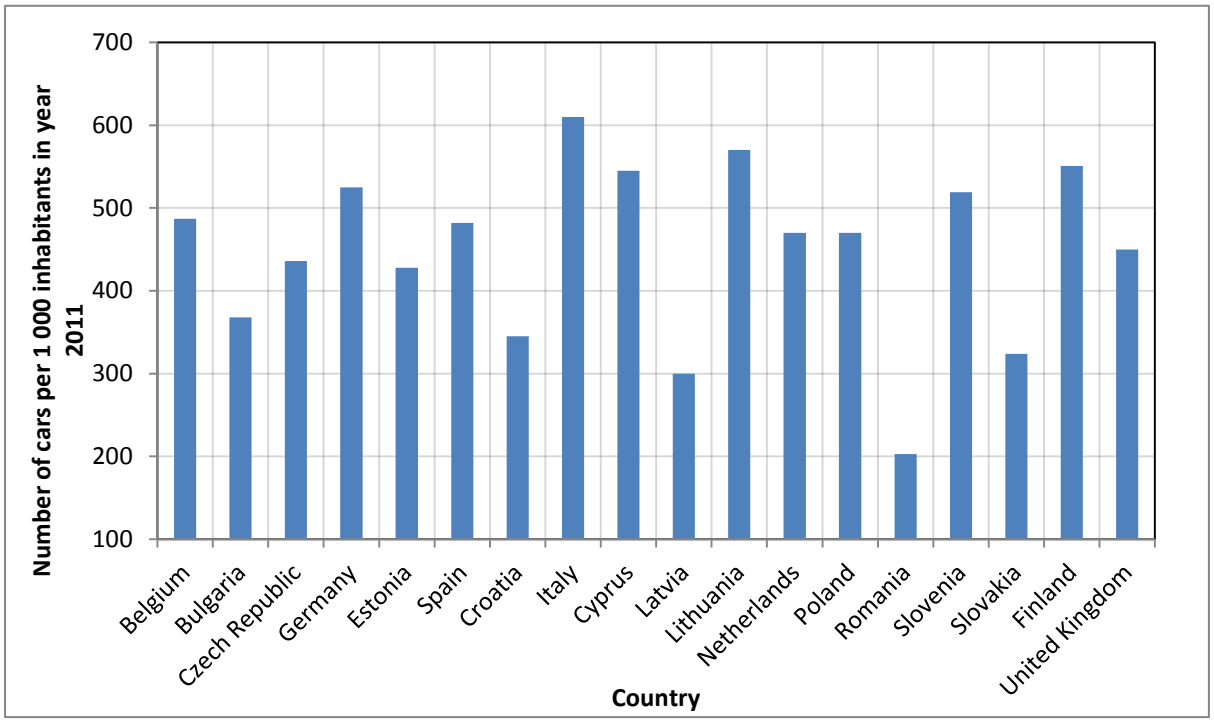

Figure (1.1): Number of the cars on the road in some European countries in 2011.

Figure (1.1) and the statistical study of number of the cars in Europe shows that since 1991 to 2011 the number of cars has increased almost linearly and relatively with a similar large slope for all countries in Europe. Figure 1.2 indicates the number of cars per 1000 inhabitants for The Netherlands, Poland, Czech Republic, Germany, Spain, Italy and United Kingdom during 1991 to 2011. According to this figure the number of cars in Europe has continuously increased up to 75% for Czech Republic during the last two decades and it is expected to

increase in the next decades too. Similar statistical data are available for the other countries around the world.

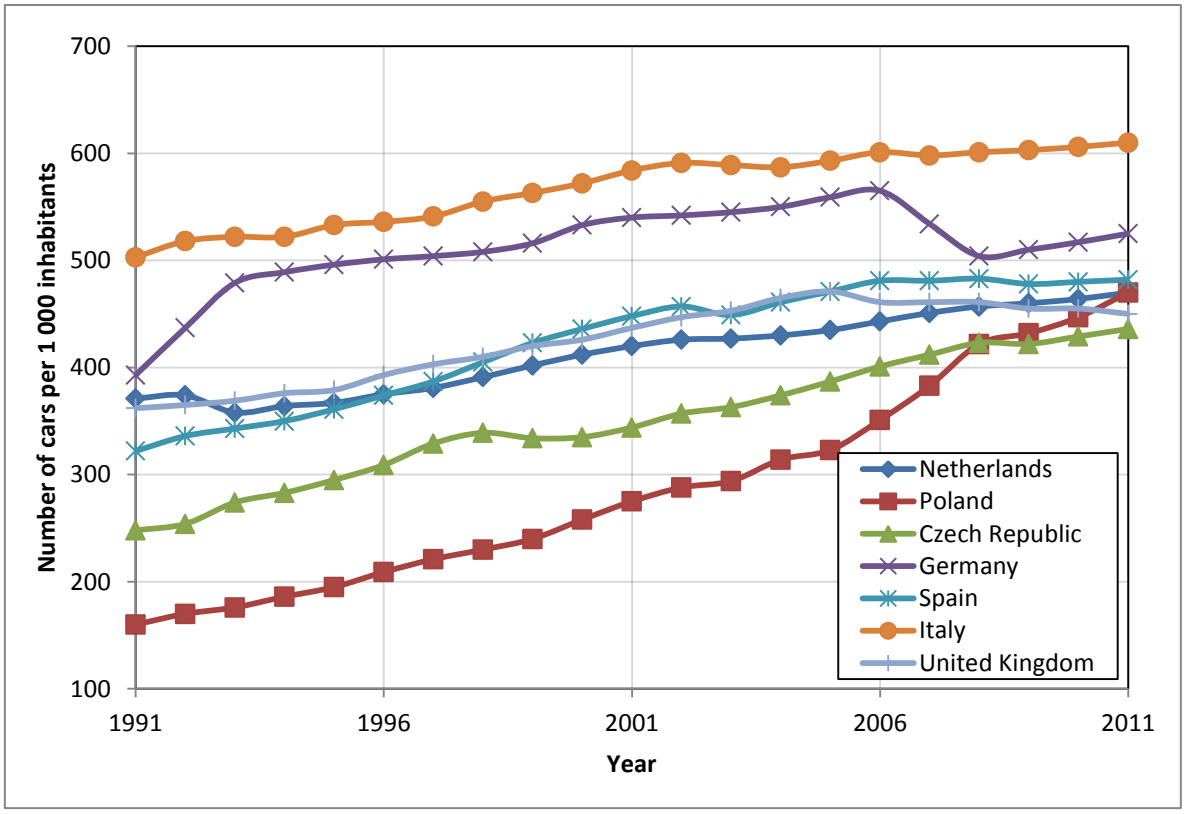

Figure (1.2): Number of passenger cars per 1000 inhabitants (to 2011).

Due to serious damage on health and environment by engine combustion products, improving the combustion efficiency in terms of fuel economy and combustion emission has become more important than ever. This issue is considered as the main challenge facing the engine research community. It is evident that the large number of cars has a considerable potential to increase the air pollution as well as noise pollution in the European countries. This fact clearly indicates that it is vital to establish an operative and efficient procedure to control the dramatic growth of pollutants in terms of quantity and quality all over the world. The significant increase in the number of cars not only in Europe but also in all countries across the world proves the importance of environmental impact of emission, produced by this growing number of cars on human health and environment.

In order to control the harmful effects of engine combustion, automotive companies were forced to follow the issued standards by European Union emission standards (Euro 1 to Euro 6). Since 1992 when European Union suggested the first norm as Euro 1, *PM* was regulated. Euro 2 was issued in 1996 and new regulation was set for *PM*. In 2003 the Euro 3 was issued to set limits for *PM* and NO_x jointly for the first time and it was followed by Euro 4,5 and 6. As shown in figure 1.3 , Euro 6 is in force since the beginning of 2014.

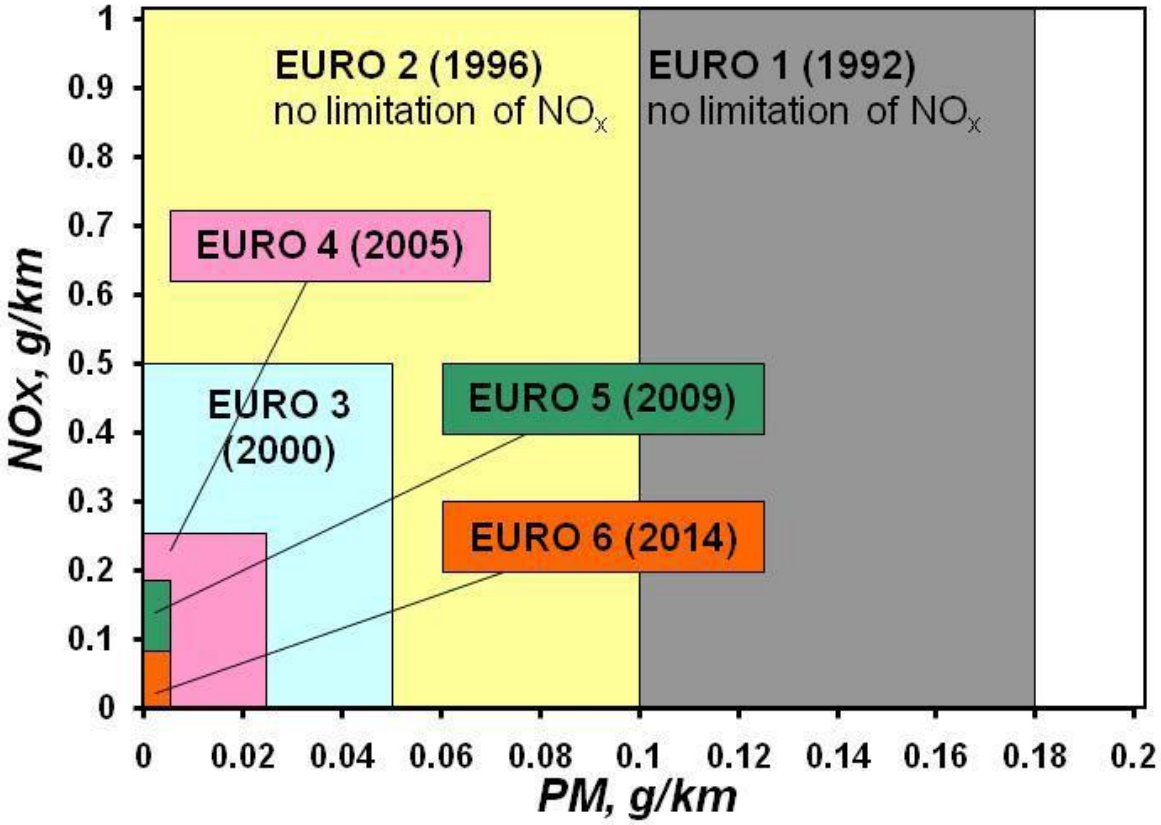

Figure (1.3): European Union emission standards for *PM* and NO_x for engine.

1.3. Internal combustion engines

The internal combustion engine is a heat engine in which the chemical energy of the fuel in form of heat is transformed to mechanical energy. This transformation occurs in combustion

of a fuel and an oxidizer in a combustion chamber (high temperature and pressure air compressed in the cylinder). In an internal combustion engine (*ICE*), direct force is applied to some mechanical components (usually pistons, blades, nozzles or turbines) leading to the rising temperature and pressure of working fluid. The applied force moves some mechanical parts and this movement transforms chemical energy to useful mechanical energy. Internal combustion engines have mostly been used for mobile vehicles due to their excellent power to weight ratio. There are many types of internal combustion engine used in different industries and they can be classified based on their main features [2,3]. These features determine the application of diesel engines and allow the comparison of one engine with another within the same group. Generally all diesel engines can be classified based on the following criteria [4]:

1. Realization of working cycle:
    - four-stroke diesel engines if working cycle requires four piston strokes
    - two-stroke diesel engine if working cycle requires two piston strokes.
2. Application:
    - ship diesel engines
    - Industrial and stationary diesel engines (diesel generators, diesel compressors, etc.)
    - locomotive diesel engines
    - on-road (trucks)
    - off road (tractors) diesel engines
3. Charging of the cylinders with air:
    - naturally aspirated diesel engines (piston sucks the fresh air into the cylinder during its downward motion)

- turbocharged diesel engines (air compressor charges the cylinders with fresh air to increase the diesel engine power)

4. Design:
    - in-line arrangement of the cylinders
    - V arrangement of the cylinders (as a star)
    - trunk-piston diesel engines in which pistons are joined to the connected rod by means of floating piston pin and lower eye of connected rod joint to the crankshaft
    - single-acting diesel engine in which the working process in the cylinder starts from one side of the piston
    - double-acting diesel engines in which each cylinder consists of the upper and lower working chambers around the piston and diesel engines with opposed pistons in which each cylinder consists of two pistons that act in opposite directions.
5. Crank speed:
    - slow-speed diesel engines with crankshaft speed <240 rpm
    - medium-speed diesel engines with crankshaft speed 240 through 750 rpm
    - high speed diesel engines with crankshaft speed 750 through 2500 rpm.
6. Piston speed:
    - diesel engines with slow piston speed if piston speed is <6.5 m/sec
    - diesel engines with medium piston speed if piston is 6.5 through 9 m/sec
    - diesel engines with high piston speed if piston speed is >9 m/sec.
7. Direction of crankshaft rotation:
    - counter clock wise direction of crankshaft rotation
    - clockwise direction of crankshaft rotation

- diesel engines that allow the reversal of the direction of crankshaft rotation.

8. Utilized fuel:
    - diesel engines with utilization of light liquid fuels,
    - diesel engines with utilization of heavy liquid fuels,
    - diesel engines with utilization of natural gas
    - multi fuel diesel engines that utilize various fuels
9. Fuel-air mixture:
    - direct fuel injection in the cylinders,
    - indirect fuel injection into special chambers
    - fuel injection in the piston bowls.

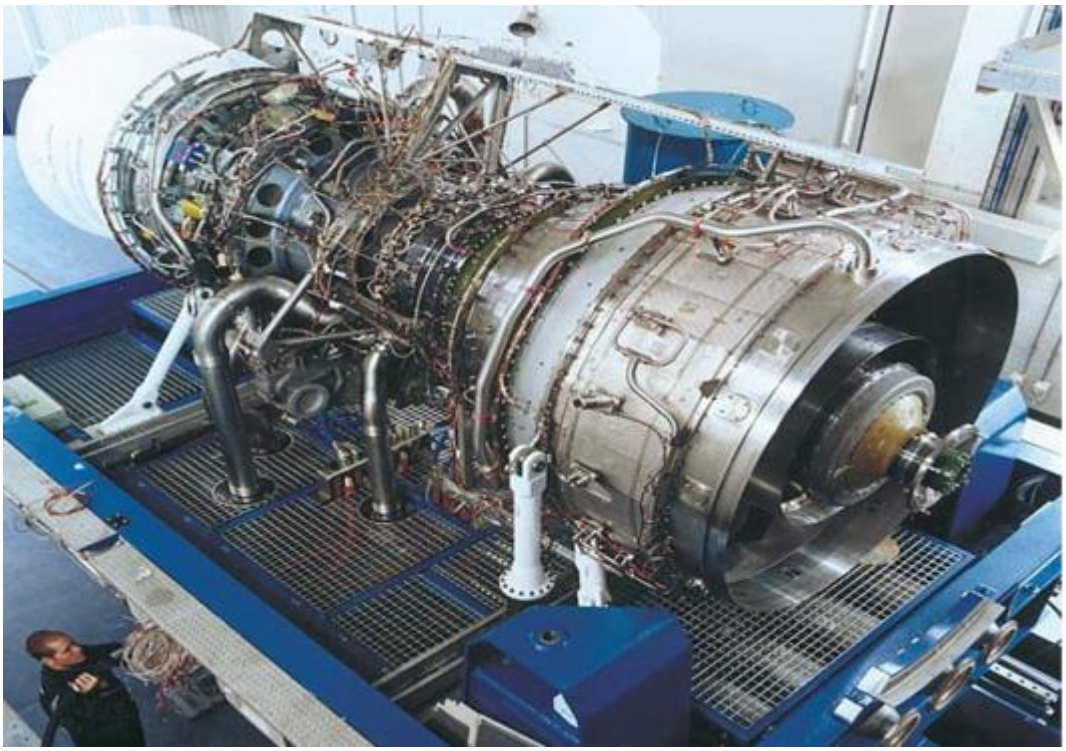

Figure (1.4): Rolls Royce gas turbine internal combustion engine. Type: MT30.

http://worldmaritimenews.com/archives/59507/rolls-royce-to-power-south-korea-navys-frigate-with-mt30-gas-turbine/. 03.09.2014

Figure (1.5): An internal combustion engine used in passenger car. Engine type: Mazda skyactiv D Engine1.

http://wot.motortrend.com/thread-of-the-day-are-diesel-engined-passenger-cars-overhyped-319713.html/2014-mazda6-cockpit-6/. 03.09.2014

Figure 1.4 and figure 1.5 indicate two types of internal combustion engines.

Otto cycle and Diesel cycle engines are the two main types of internal combustion engines. Otto (1832-1891) developed the first spark-ignition (*SI*) engine in 1876. This engine is also called petrol or gasoline engine and uses a spark to ignite the fuel inside the combustion chamber [5].

Later Rudolf Diesel (1858 – 1913) introduced a new type of internal combustion engine called compression ignition (*CI*) engine in 1892. This engine is known as diesel engine [6].

Diesel used the generated heat of compressed air inside the combustion chamber to ignite the fuel which is injected to the chamber almost at end of compression. Components of a typical spark ignition engine and compression ignition engine are shown in figures 1.6 and 1.7 respectively.

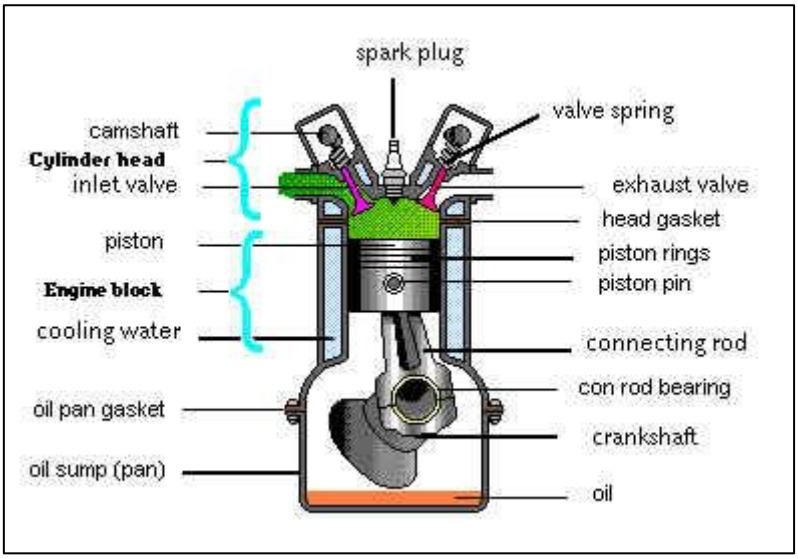

Figure (1.6): A typical spark ignition engine.

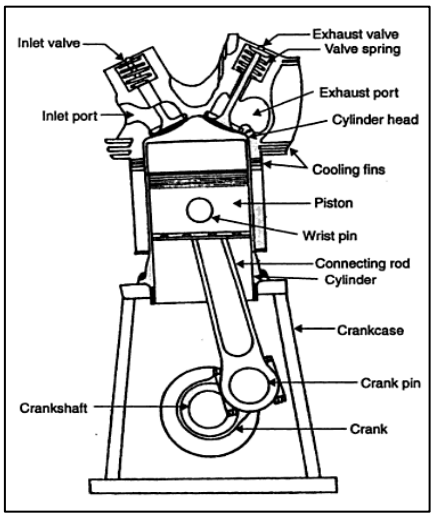

Figure (1.7): A typical compression ignition engine.

Many investigations were carried out to improve the efficiency of internal engines in terms of fuel economy, noise performance, durability and emission performance. As a result of these investigations, the efficiency of engines were enhanced significantly during the last decades.

1.3.1. Otto engine

This type of engine follows the Otto cycle which is known as spark-ignition internal combustion engine. Figure 1.8 shows the Otto cycle on the *pv* diagram [7].

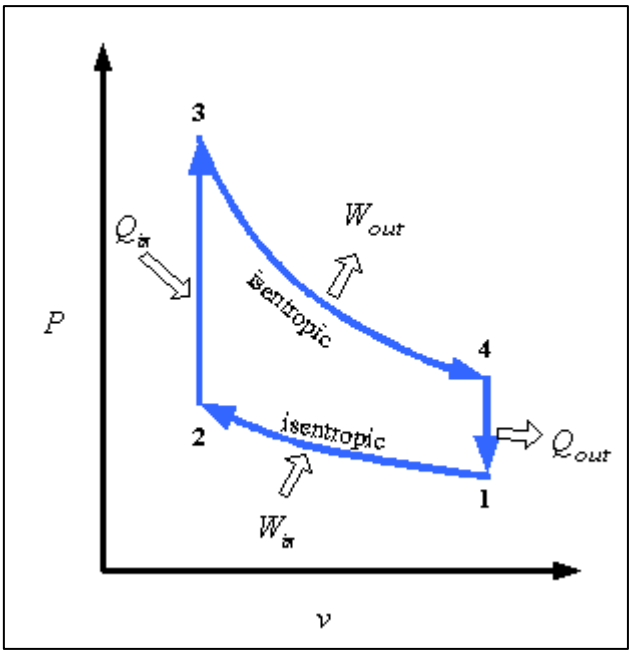

Figure (1.8): Otto cycle.

Process 1-2 is an isentropic compression of the air as the piston moves from bottom dead centre (*BDC*) to the top dead centre (*TDC*). Heat is then added at a constant volume while the piston is momentarily at rest at *TDC*. This process corresponds to the ignition of the fuel-air mixture by the spark and the subsequent burning in the engine. Process 3-4 is an isentropic expansion and process 4-1 is the rejection of heat from the air while the piston is at *BDC*. The thermal efficiency (η_{th}) of this cycle can be calculated by equation (1.1).

$$\eta_{th} = 1 - \frac{T_1}{T_2} \qquad (1.1)$$

Equation (1.1) can be written in terms of compression ratio *r*.

$$\eta_{th} = 1 - \frac{1}{r^{\gamma-1}} \qquad (1.2)$$

Where $r = \frac{V_1}{V_2} = \frac{V_4}{V_3}$ and γ is specific heat capacities ratio.

1.3.2. Diesel engine

Diesel engine follows the standard diesel cycle and is known as compression ignition engine. In this cycle the heat is transferred to the working fluid at a constant pressure. This process corresponds to injection and burning of the fuel in the engine. Diesel cycle is shown in figure 1.9 .

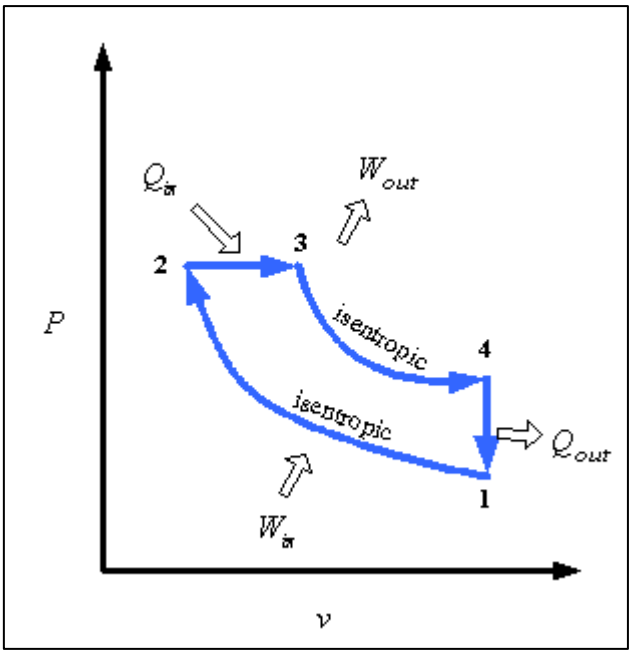

Figure (1.9): Diesel cycle.

Since the gas is expanding during the heat addition in the diesel cycle the heat transfer must be just sufficient to maintain a constant pressure. At state 3, the heat addition ceases and the gas undergoes an isentropic expansion, process 3-4, until the piston reaches the Bottom dead center (*BDC*). As in the Otto cycle, a constant volume rejection of heat at *BDC* replaces the exhaust and intake processes of the engine. The efficiency of the diesel engine can be calculated by equation (1.3).

$$\eta_{th} = 1 - \frac{C_v(T_4 - T_1)}{C_p(T_3 - T_2)} = 1 - \frac{T_1(T_4/T_1 - 1)}{\gamma T_2(T_3/T_2 - 1)} \qquad (1.3)$$

Where C_v and C_p are heat capacities at constant volume and constant pressure respectively.

It is important to note that the isentropic compression ratio is greater in the diesel cycle compared to the isentropic expansion ratio in Otto cycle.

1.3.3. Engine operating cycles

As mentioned at beginning of this chapter internal combustion engines can be classified as two and four stroke types in terms of realization of working cycle. For each engine cylinder the four stroke cycle requires require two crank shaft revolutions for each power stroke. To obtain a higher power output from a given engine size and a simpler valve design, the two stroke cycle was developed. The two stroke cycle is applicable to both *SI* and *CI* engines.

The present research addresses diesel engines, as a four stroke cycle engine, reciprocating internal combustion in which the piston moves back and forth in a cylinder and transmits power through crank mechanism and rod to the drive shaft (figure 1.10).

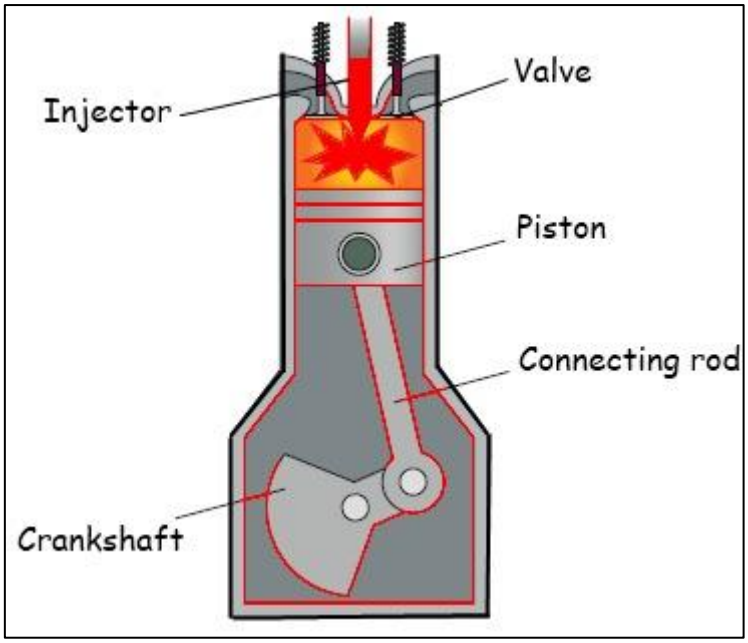

Figure (1.10): Basic geometry of the reciprocating Diesel combustion engine.

http://homeaudi.com/the-internal-combustion-engine/ 03.09.2014.

The steady rotation of the crank produces a cyclical piston motion. The piston comes to rest at *TDC* and *BDC* positions when the cylinder volume is at minimum and maximum level, respectively. The minimum cylinder volume is called the clearance volume (V_c). The difference between the maximum cylinder volume and minimum cylinder volume is the volume swept out by the piston denoted by V_d. Finally the ratio of maximum volume to clearance volume is called compression ratio r. The typical values of r are 8 to 12 for *SI* engines and 12 to 24 for *CI* engines.

The majority of reciprocating engines operate on what is known as the four stroke cycle. Each cylinder requires four strokes of its piston and two revolutions of the crankshaft to complete the sequence of events which produces one power stroke. Both *SI* and *CI* engines can use this cycle which is shown schematically in figure 1.11 .

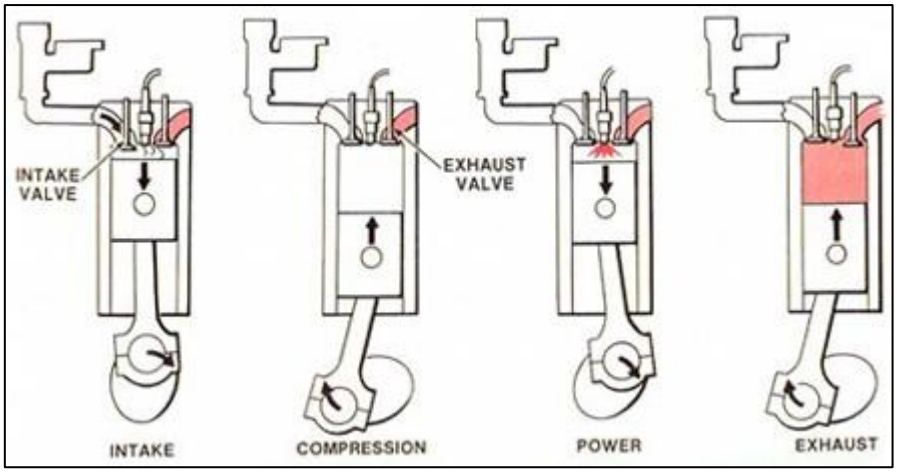

Figure (1.11): the four stroke operating cycle

The four stroke operating cycle includes the following steps:

1. An intake stroke, which starts with the piston at *TDC* and ends with the piston at *BDC*, which draws fresh air in *CI* engines and air-fuel mixture in *SI* engines into the cylinder. To increase the mass inducted, the inlet valve opens shortly before the stroke starts and closes after ends.
2. A compression stroke, when both valves are closed and the gas inside the cylinder is compressed to a small fraction of its initial volume. Injector sprays high pressure fuel into cylinder just before *TDC* and the heat produced by compressed gas starts the combustion. In *SI* engines a spark plug ignites the compressed air-fuel mixture about *TDC*. In result of the produced heat the temperature and pressure rises rapidly inside the cylinder.
3. A power stroke, (or expansion stroke), that starts with the piston at *TDC* and ends at *BDC* as the high-temperature, high-pressure, gases push the piston down and force the crank to rotate. During the power stroke, the force on the piston is about five times the force during compression. As the piston approaches *BDC* the exhaust valve opens to initiate the exhaust process and drop the cylinder pressure to close to the exhaust pressure.

4. An exhaust stroke, where the remaining burned gases exit the cylinder, because firstly the cylinder pressure may be substantially higher than the exhaust pressure and secondly they are swept out by the piston as it moves toward *TDC*. As the piston approaches *TDC*, the inlet valve opens. Just after *TDC*, the exhaust valve closes and the cycle starts again.

1.3.4. Diesel engine Advantages

Diesel engines are usually preferred to gasoline engines due to their higher efficiency and reliability.

The main advantages of diesel engines compared to petrol engines are:

- Diesel engine life time is considerably longer in comparison with a petrol engine. It also has lower maintenance costs.
- Due to a higher compression ratio compared to petrol engine, diesel engines provide higher thermal efficiency and higher torque.
- Lower fuel consumption.
- In terms of flammability, diesel engine is considered a safer engine because diesel fuel is safer than gasoline.
- Absence of high voltage wires and electrical ignition system, results in a safer and simpler system with no noise emission which can cause interference with communication and navigation systems.

1.3.5. Diesel engine disadvantages

According to evidence in the literature, diesel engine is substantially responsible for air pollution as well as noise pollution [8] as diesel engines are an important source of particulate emission. In fact product of combustion in diesel engine is a complex mixture of pollutants in gas and particulate form. Investigations on diesel engine combustion show that about 0.2 to 0.5 percent of the fuel mass is emitted as small (~0.1 μm diameter) particles [3]. Previous studies have revealed that particulate matter (*PM*) and NO_x are the most important negative environmental impact of diesel engines [9].

Nitrogen oxide emissions contribute to environmental problems such as acid rain and ground-level ozone. This reaction happens when Nitrogen dioxide reacts with water existing in air in the form of moisture ($2NO_2+H_2O \rightarrow HNO_2+HNO_3$). Eventually Nitric acid forms in result of decomposition of the produced Nitrous acid ($3HNO_2 \rightarrow HNO_3+2NO+H_2O$). Since diesel particulates are released at levels that result in direct exposure; they can be especially harmful to human health and environment. There are two main categories of particulate matter: primary and secondary particulates. Primary particulates are formed during the fuel combustion process in the engine, and are released as exhaust from the tailpipe. Primary particulate includes soot, the soluble organic fraction which contains polycyclic aromatic hydrocarbons (*PAHs*), and sulphate. Secondary particulates are formed when sulphur dioxide (SO_2) emissions from diesel exhaust are converted to sulphate particulate in the atmosphere [10].

In order to achieve a cleaner diesel engine, many new techniques have been introduced by researchers to reduce harmful effect of Particulate matter (*PM*) and NO_x emmision from diesel engine [3,7]. High pressure common rail fuel injection system, different injection strategy [1,4-6,8,11], exhaust gas recirculation (*EGR*), boosting, and exhaust gas after

treatment [12-15] are the main strategies that are widely used by diesel engine manufacturers. Parallel to engine equipment improvements, it was revealed that the physical and chemical properties of fuel have an important impact on performance of diesel engine combustion. Therefore, bio-diesels were considered as an alternative source for fossil based diesel fuel. Studies in recent years have shown that regulated diesel engine emission can be reduced significantly by bio-fuels as well as unregulated diesel engine emmission [10,16-19].

In order to meet diesel engine emission standards, diesel engine combustion phenomena should be understood and analysed completely by diesel engine designers. Many research teams around the world have been studying the engine combustion mechanisms and identifying the process which leads to emission production. This information guides engine manufactures and designers to meet increasingly stringent emission regulation.

1.4.Lay out of dissertation

In this dissertation:

Chapter 2, *Literature Review*, contains literature review and previous study in regard to Wiebe equation, Heat release analysis and ignition delay.

Chapter 3, *Theoretical methodology*, contains the methods which were used in this study for Apparent heat release rate and In cylinder temperature along with their derivations.

Chapter 4, *Experimental set up*, contains the specifications of the engine and the measurement equipment which were used to carry out the experiments in this research.

Chapter 5, *Characterising Wiebe Equation for Heat Release Analysis based on Combustion Burn Factor (C_i)*, introduces a new dimensionless parameter called *Combustion burn factor* (C_i) and discuss the benefits of using this parameter in heat release analysis and also presents a modified version of Wiebe equation and compares with original form of Wiebe equation. The benefits of using modified version of Wiebe equation in compare to original form of Wiebe equation were discussed. Also error calculation was carried out for modified Wiebe equation and original form of Wiebe equation and the results were compared [86].

Chapter 6, *Determination of specific heat ratio and error analysis for engine heat release calculations*, discusses the heat release analysis importance and discuss the most important parameters which can affect heat release rate values. Error calculation has been carried out on heat release with respect to heat capacities ratio and in-cylinder pressure. A new technique is introduced to calculate heat capacities ratio and the results were compared to literature [138].

Chapter 7, *Characterising ignition delay correlation for diesel engine by using newly proposed analytical methods*, discuss the importance of ignition delay in diesel engine combustion analysis and also discuss the existing correlations to calculate ignition delay. New analytical techniques were introduced to calculate constants for Arrhenius type expression, which was first proposed by Wolfer. Error calculation was carried out to investigate the effect of constants on ignition duration. A new correlation was developed to calculate ignition delay by using dimensionless parameters. This correlation has no constant and ignition delay duration can be calculated in terms of combustion parameters and enhanced the accuracy of ignition delay calculation.

Chapter 8, *Conclusion*, contains the summarised conclusion of this study along with the recommendation for future work.

1.5 Motivation

Internal combustion engine has been improved in terms of performance, design and structure significantly since it was first invented in 1876 by Otto. This type of engines has been used not only in passenger cars but also in heavy industry sectors.

The increase of the oil price in last decades led the manufacturers to enhance the engine quality in terms of fuel efficiency. New more efficient engines, particularly in passenger cars, resulted in the popularity of these engines worldwide. Consequently, air quality control agencies expressed their concern regarding the high level of emission produced by the increasing number of engines. These engines also took action to control the harmful effects of emission on the environment and human beings. In this regard, stringent regulations were issued and automotive companies were forced to comply with the regulations. Moreover, many investigations were carried out at engine research centres to study the engine performance in terms of engine emission and fuel economy. These investigations were used by engine designers to improve the productivity as well as adherence to the new regulations. Following the advancement of technology, the study of engine combustion and analysing the combustion parameters became more and more important. Due to complication of combustion process, different experimental techniques were developed to study the combustion process. In fact, many parameters (including temperature, pressure, volume, gas phases, force, speed and etc.) dramatically vary during the combustion process. What makes this process even more complicated and difficult to analyse is that these parameter changes occur within a very short time.

The main motivation behind the present study was to improve the analytical methods to analyse combustion process and engine heat calculation. The objective of this research was to introduce new dimensionless parameters while introducing a new technique to calculate in-cylinder gas heat capacities ratio which affects the heat calculation significantly. Another aim was to improve the ignition delay calculation by introducing new techniques to calculate the coefficients in Wolfer correlation in addition to introducing a new correlation for calculating the ignition delay accurately.

1.6 Contribution of knowledge

In this study:

- New dimensionless parameters were introduced to facilitate combustion analysis and heat release calculations.
- A new technique was introduced to calculate coefficients in Wiebe equation analytically. Also a modified version of Wiebe equation was introduced which contains only one constant therefore improves the accuracy of calculations.
- A new technique was developed to calculate in-cylinder gas heat capacities ratio in engines.
- New techniques were introduced to calculate coefficients in Wolfer correlation analytically.
- A new correlation was developed to calculate ignition delay accurately.

Chapter 2

Literature Review

2.1 Engine Research

There are number of techniques available for performing engine combustion investigation. Unfortunately, these techniques require expensive equipment and in some cases highly skilled operators. Consequently the engine research is mostly available only to institutions and universities equipped by sophisticated experimental facilities.

Stationary engine, Optical technique and Transmission Electron Microscopy (*TEM*) are the main and most widely used methods in engine research field.

2.1.1 Stationary engines

Real size engines connected firmly on a strong stand to damp engine vibrations and equipped with number of sensors have been used by research teams extensively. An Electronic Control Unit (*ECU*) detects and analyses the signals collected by the sensors and provides the properties of the working fluids and combustion products as well as engine input and output. The sensors used in the engine are generally expensive as they should be able to withstand high temperature and pressures as high as combustion chamber. Figure 2.1 *a* and *b* show the engine control unit and four cylinder engine equipped with sensors at Brunel University which were used to carry out measurement for this study.

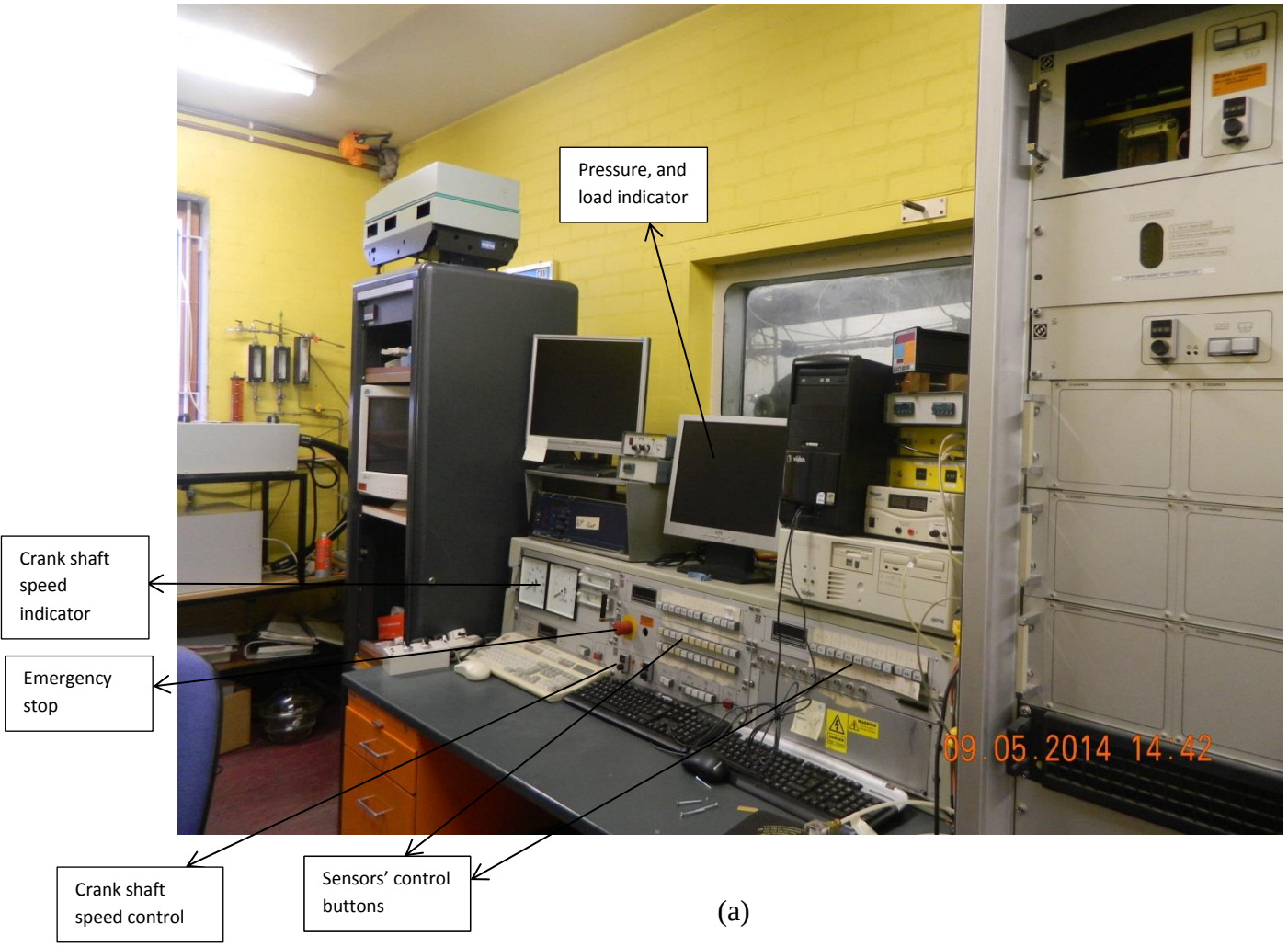
Pressure, and load indicator
Crank shaft speed indicator
Emergency stop
09.05.2014 14:42
Crank shaft speed control
Sensors' control buttons

(a)

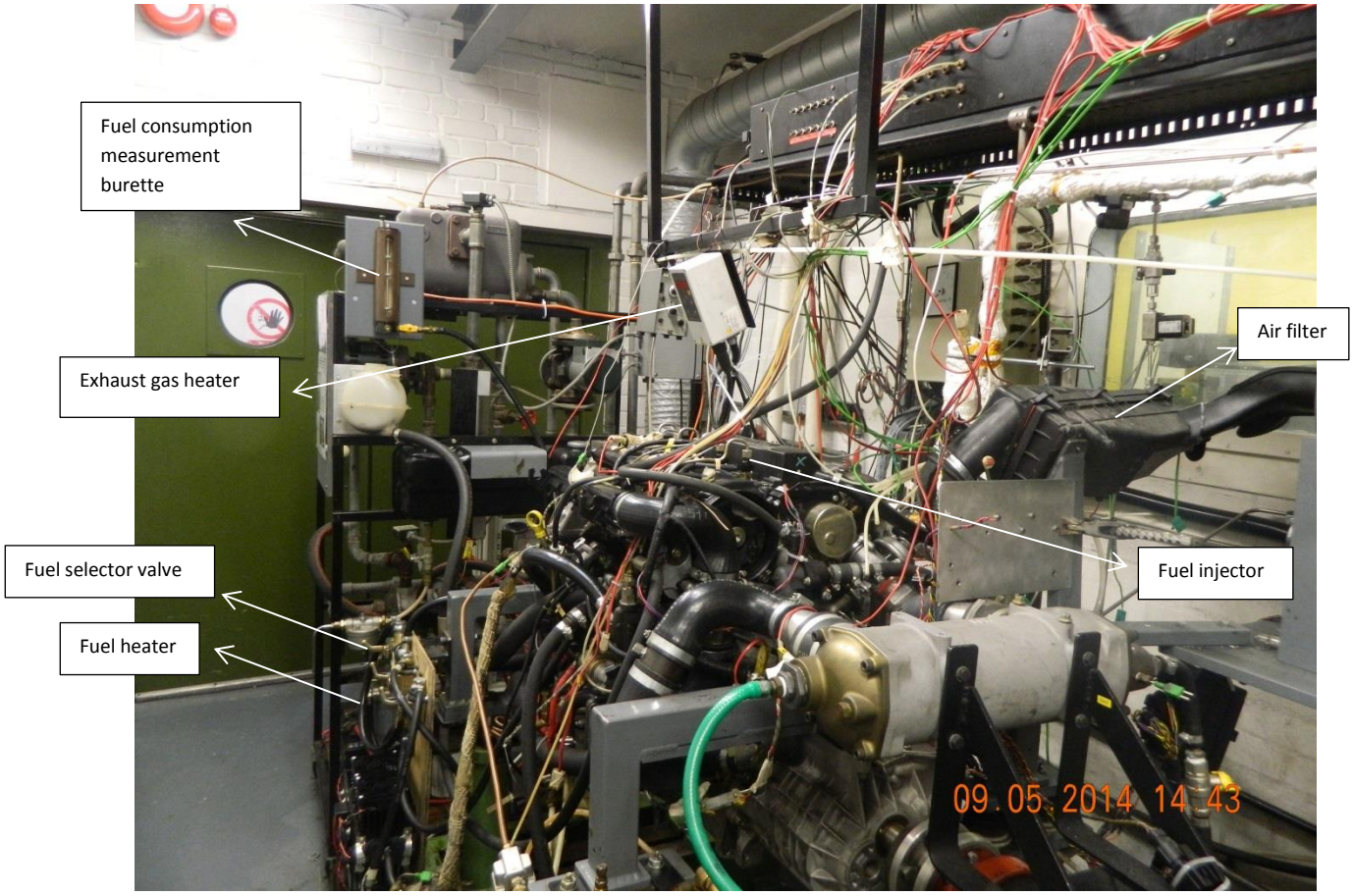

(b)

Figure (2.1): (a): Multi cylinder diesel engine control unit at Brunel University (b): Four cylinder engine equipped with sensors at Brunel University

Since the engine used is in its real size, the test engine needs to be isolated from ECU due to high level of noise. Mostly a window separates the test engine room and ECU room. The experimenters can watch the test engine through the window during the measurement and use emergency stop button when necessary. There are many ports available to access to different parts of engine for sampling and also using additional probes to use different equipment at the same time. This equipment could be *TEM* sampling, Gas analyser, Electro Mobility spectrometer (*EMS*) or any other device. Figure 2.2 shows a sample of ports.

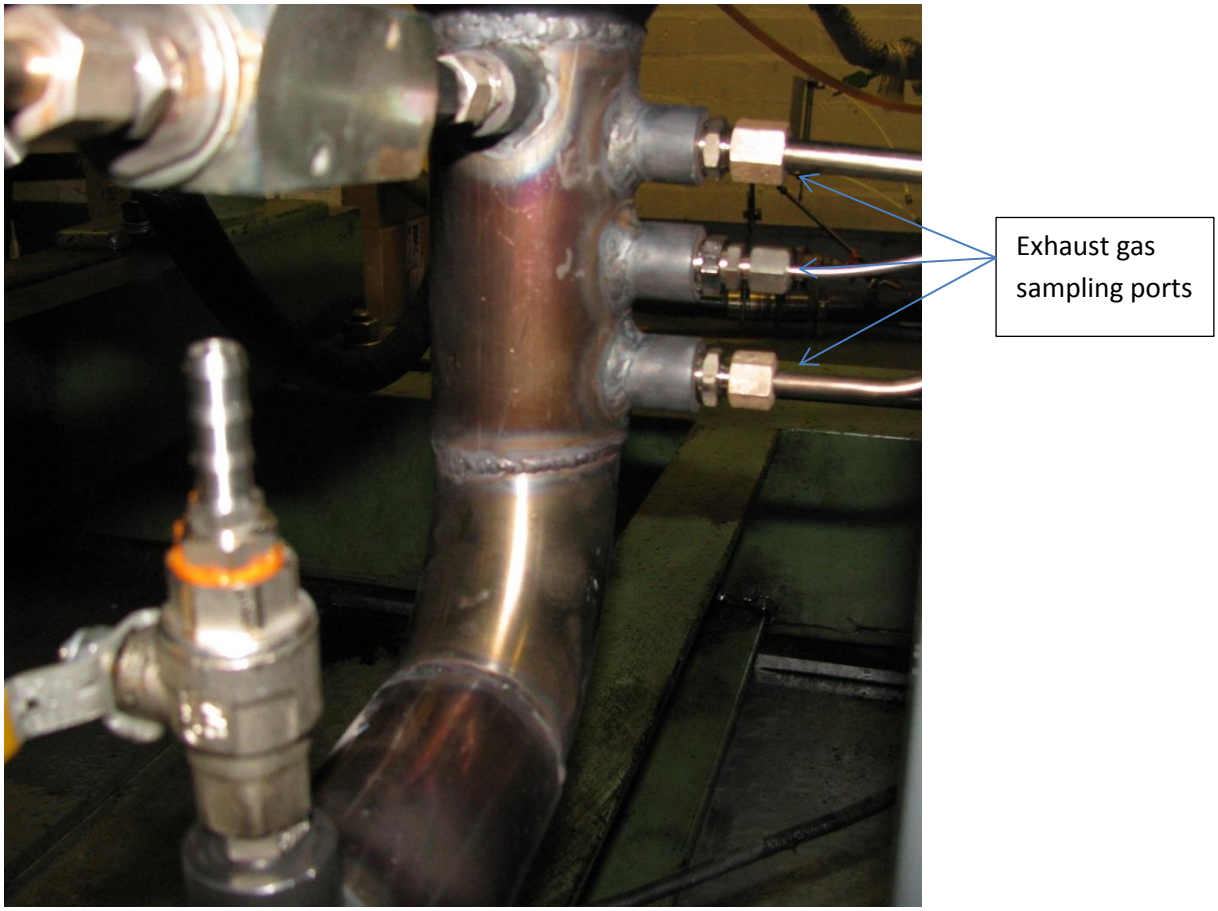

Figure (2.2): Several ports at engine exhaust for gas sampling.

The major problem in using this technique appears when several probes need to be used to carry out the measurements in a specific part of engine while the engine is running under extreme conditions. Even if the probes could be inserted to the required point, the combustion process would be disturbed by the number of sensors and the results yield unreliable measurements, therefore it needs to be considered by research team when several equipment are in use in experiments. It should be also taken into consideration that the test results may be affected due to different heat loss characteristics of stationary engine and real engine. Since the test engine is not used in its real environment, its condition is not identical to the real situation in terms of heat exchange with environment. This issue can affect the results and needs to be considered by research team too.

This technique is more available to research teams and mostly preferred to other expensive and complicated techniques.

2.1.2. Optical techniques

Optical techniques are based on the measurement of various interactions that occur between light and atoms or molecules, usually resulting in the emission of an optical signal. These emissions depend on factors such as the state of molecules and their quantity. So the information about the temperature, pressure, velocity and species content can be extracted from the region under investigation. Due to their high spatial, temporal and spectral resolutions, lasers are usually the preferred light sources [10].

Figure 2.3 a & b show a test optical engine rig at Brunel University, which is equipped with one cylinder diesel engine. The engine was equipped with sensors, for measuring and controlling the engine torque, speed, injection parameters, in-cylinder pressure and fuel consumption. Details of the engine specifications are listed in table (2.1).

Table (2.1): specification of optical engine

Type	Engine details
Bore	**86 mm**
Stroke	**87 mm**
Swept volume	**499 cm^3**
Compression ratio	**16.0:1**
Swirl Ratio	**1.4**
Number of cylinders	**1**
Type of engine	**CI**

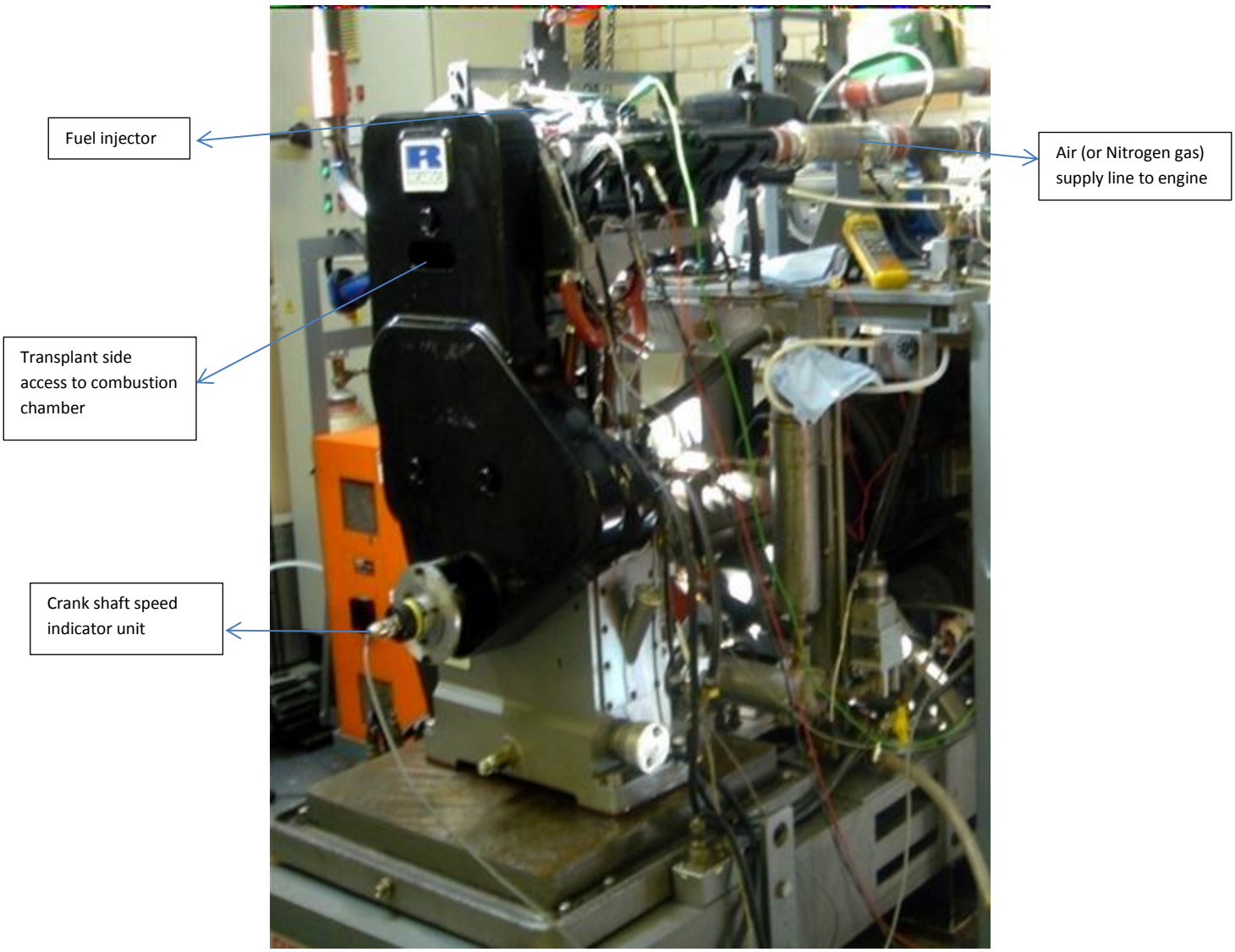
Fuel injector
Air (or Nitrogen gas) supply line to engine
Transplant side access to combustion chamber
Crank shaft speed indicator unit

(a)

(b)

Figure (2.3): (a): Ricardo Hydra optical diesel engine at Brunel University. (b): Control unit.

Single-cylinder optical engines are often used to study in-cylinder flow, combustion and pollutant formation as part of combustion system development as well as providing validation data for simulation [12]. This technique helps the researchers to study auto-ignition sites, soot formation sites and concentration, local fuel injection properties, local temperature, local air-fuel ratio, and local velocity accurately. Figures 2.4 a-f show the development of combustion in a single cylinder diesel engine for diesel fuel.

A transparent piston head is mostly used as an access to combustion chamber by using high speed camera (typically about 10000 fps) to investigate in-cylinder process visually. The major problem in using one cylinder engine is that the engine heat loss and gas leak are not identical to the real engine. This difference can cause considerable errors in measurement. Moreover as one cylinder engine is not mechanically balanced, the engine condition is not realistic compared to real engine. Due to mechanical properties of transparent materials,

unfortunately they cannot withstand high pressure and temperature. Consequently, it is very difficult to study combustion process at extreme engine operating conditions.

Mostly one optical access is sufficient to carry out a set of experiments but in some cases it is needed to have more optical accesses to combustion chamber. This can be a difficult task in internal engines especially with *IC* engines. Many different attempts have been reported in literature to use flat transparent piston head and side windows as well as existing ports used for an optical access [13-15]. These optical accesses should stand for high temperature as high as 1200 K and high pressure as high as ~100 bars without disturbing the combustion process. In some cases, an optical access needs to be transparent to ultra violet (*UV*) light as well as visible light. Once the required optical accesses are fitted, the experimenter faces another difficult task; these optical accesses have to be kept optically clean and transparent. This task can be extremely difficult especially when standard diesel or alternative fuels are under investigation at sooty engine conditions due to occurrence of misfiring in engine which produces deposits on transparent surfaces and results in serious difficulties for imaging.

It is clear that successful application of optical techniques depends on the knowledge of topics and fundamentals of techniques. The fundamentals of Laser Rayleigh Scattering (*LRS*), Spontaneous Raman Scattering (*SRS*), Laser Induced Fluorescence (*LIF*), Laser Doppler Anemometry (*LDA*), Particle Imaging Velocimetry (*PIV*) and Planar Laser-Induced Fluorescence (*PLIF*) are the main optical techniques discussed in detail in [12].

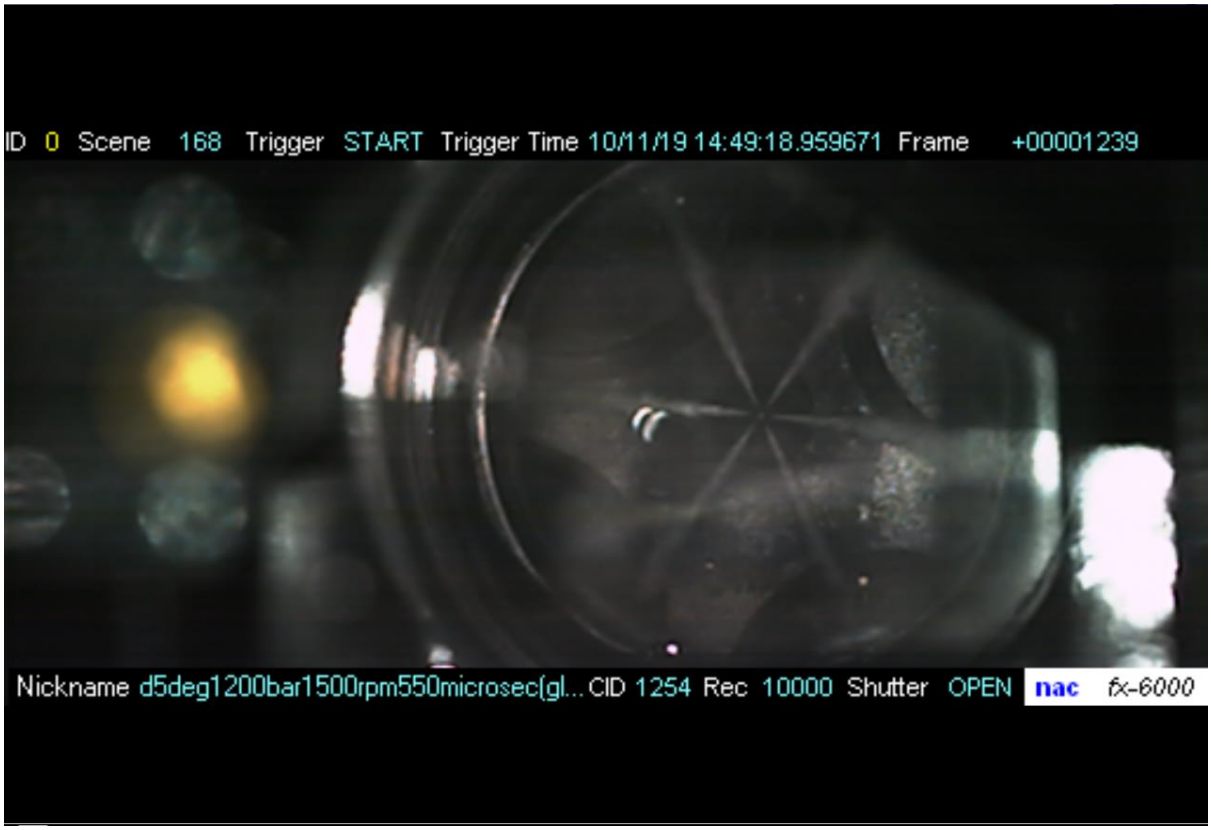
ID 0 Scene 168 Trigger START Trigger Time 10/11/19 14:49:18.959671 Frame +00001239
Nickname d5deg1200bar1500rpm550microsec(gl... CID 1254 Rec 10000 Shutter OPEN
nac fx-6000

(a)

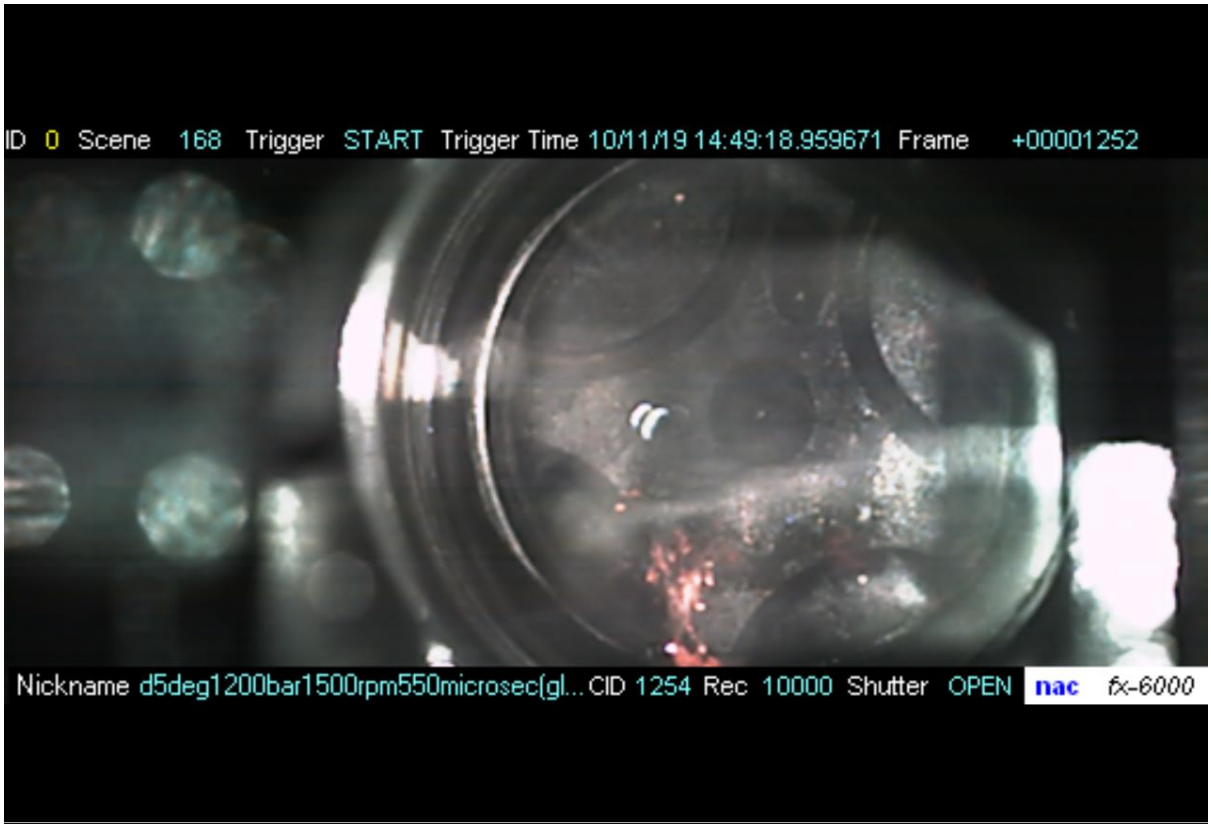
ID 0 Scene 168 Trigger START Trigger Time 10/11/19 14:49:18.959671 Frame +00001252
Nickname d5deg1200bar1500rpm550microsec(gl... CID 1254 Rec 10000 Shutter OPEN
nac fx-6000

(b)

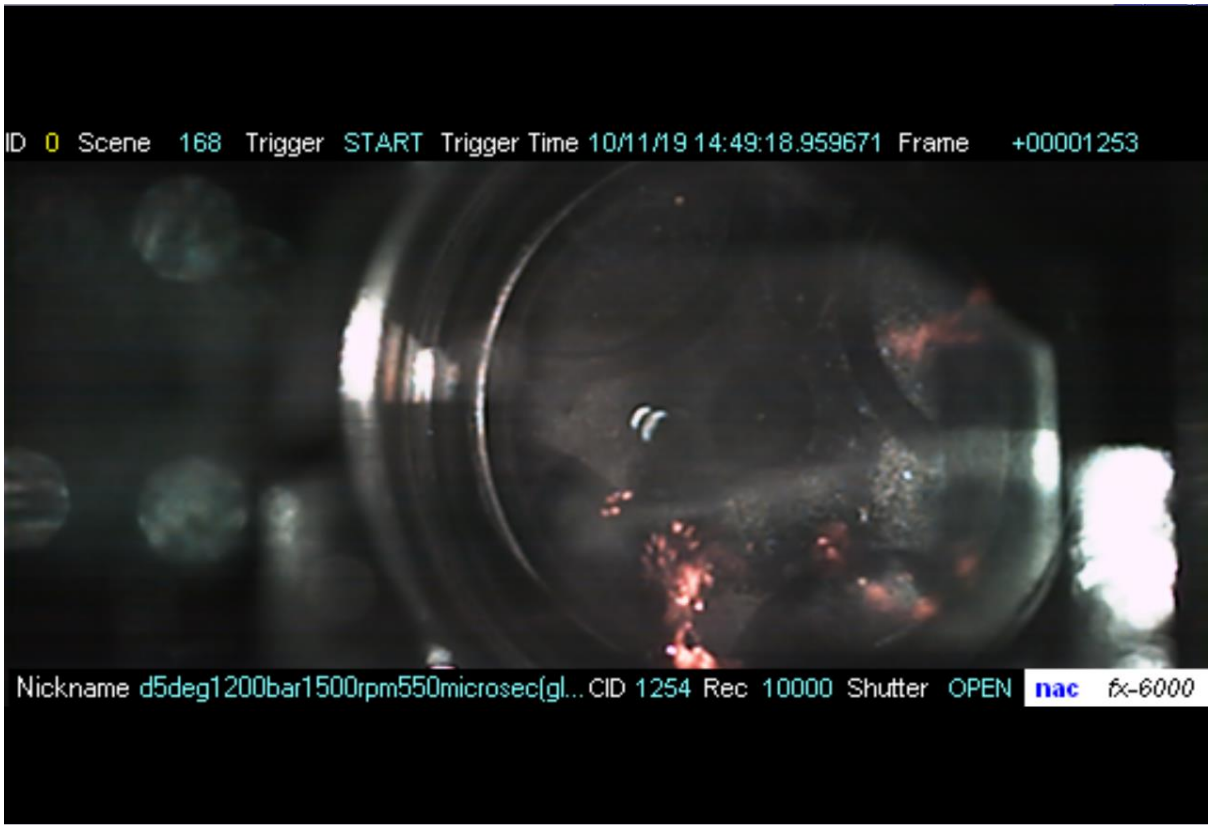
ID 0 Scene 168 Trigger START Trigger Time 10/11/19 14:49:18.959671 Frame +00001253
Nickname d5deg1200bar1500rpm550microsec(gl... CID 1254 Rec 10000 Shutter OPEN
nac fx-6000

(c)

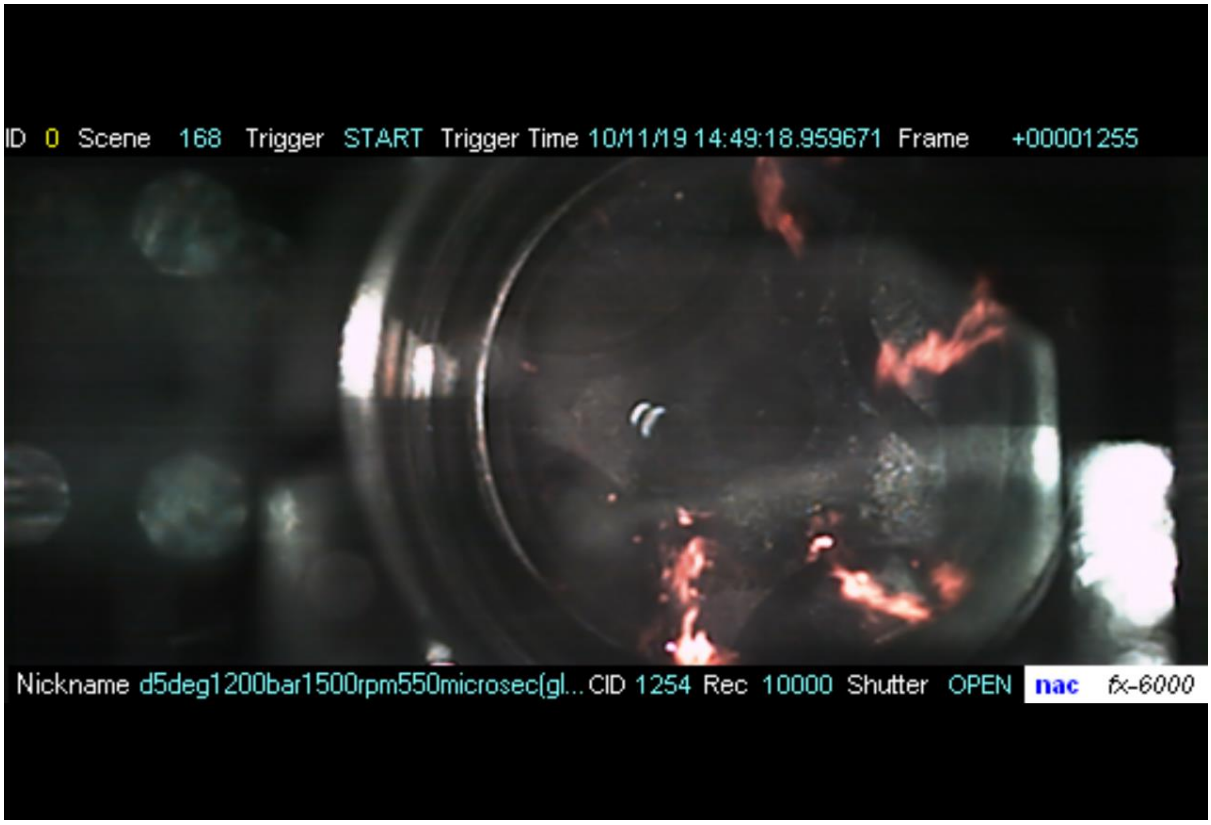
ID 0 Scene 168 Trigger START Trigger Time 10/11/19 14:49:18.959671 Frame +00001255
Nickname d5deg1200bar1500rpm550microsec(gl... CID 1254 Rec 10000 Shutter OPEN
nac fx-6000

(d)


ID 0 Scene 168 Trigger START Trigger Time 10/11/19 14:49:18.959671 Frame +00001260
Nickname d5deg1200bar1500rpm550microsec(gl... CID 1254 Rec 10000 Shutter OPEN
nac fx-6000

(e)

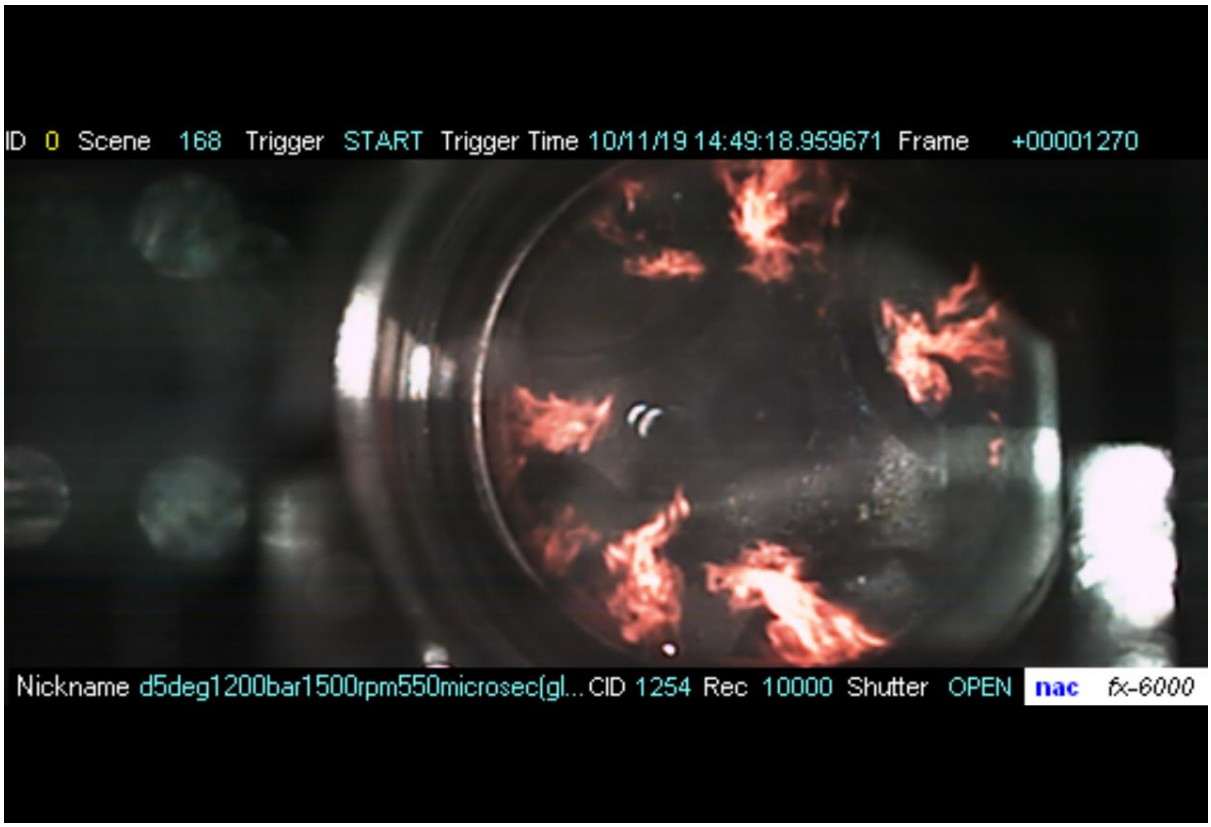
ID 0 Scene 168 Trigger START Trigger Time 10/11/19 14:49:18.959671 Frame +00001270
Nickname d5deg1200bar1500rpm550microsec(gl... CID 1254 Rec 10000 Shutter OPEN
nac fx-6000

(f)

Figure (2.4 a-f): Images of spray and combustion development in a single cylinder diesel engine using high speed camera (10000fps) for diesel fuel at engine condition: fuel injection 5 deg *BTDC*, Fuel injection pressure 1200 bar, Engine speed 1500 rpm and Fuel injection duration 550 μsec. The frame number is indicated on top right hand side for each image. Each frame number is equivalent to 10^2 μsec. Images a-f indicate the fuel spray development, spray speed and location of start of combustion as well as shape of fuel sprays.

2.1.3 Transmission Electron Microscopy (*TEM*)

2.1.3.1 Definition

The theory of Transmission Electron Microscopy (*TEM*) goes back 1927 when Hans Busch (1884-1973) showed the effect of electron beam on small particles theoretically. *TEM* and High Resolution Transmission Electron Microscopy (*HRTEM*) are commonly used to investigate the characteristics of individual and agglomerated particles [20-23]. The examination of the structure and the distribution of the carbon sheets of the primary particles and quantifying the primary particle size, the fractal dimension of the agglomerated particles provide information about reactivity and nanostructure morphology [16,24-30]. Figure 2.5 shows a typical *TEM* microscope unit.

Figure (2.5): *TEM* microscope unit at National Renewable Energy Laboratory in USA.

Morphology of the ultra-fine particles emitted by diesel engines known as diesel particulate matter has been studied extensively by using this technique. The appearance and evolution of soot particles in the cylinder has been the subject of various experimental and computational modelling studies [17-19,31-33]. There have also been several investigations of soot aggregation [34-36]. Figures 2.6 and 2.7 show images for diesel fuel and *RME* fuel respectively by using *TEM* microscope.

This technique involves collecting particles by using special copper *TEM* grids. The grids collect particles by putting them in exhaust pipe for a short time (typically 0.1 to 0.8 Sec depending on how sooty the engine operating condition is). The 3 mm grid type S160, 300 mesh from Agar scientific Ltd [37] is recommended for diesel particulate in [38]. This range of carbon films has been prepared to provide a very convenient, ready-to-use specimen support. Carbon films are thin and highly transparent to electrons, offering fine grain and low contrast that does not interfere with specimen structure.

The source of illumination is an electron beam in this type of microscopes. The specimen is loaded in a vertical cylinder. Strong pumps at several stages create vacuum condition inside

the cylinder (about absolute pressure 10^{-5} bar inside the cylinder). In order to create electron beam a high accelerating voltage (about 80 kV) is applied to the system. The electron beam directed towards the specimen which contains the collected particles on the *TEM* grid. The electron beam passes the specimen through to the space between the nano-particles. This electron beam detected and analysed behind the specimen to provide an image of the particle.

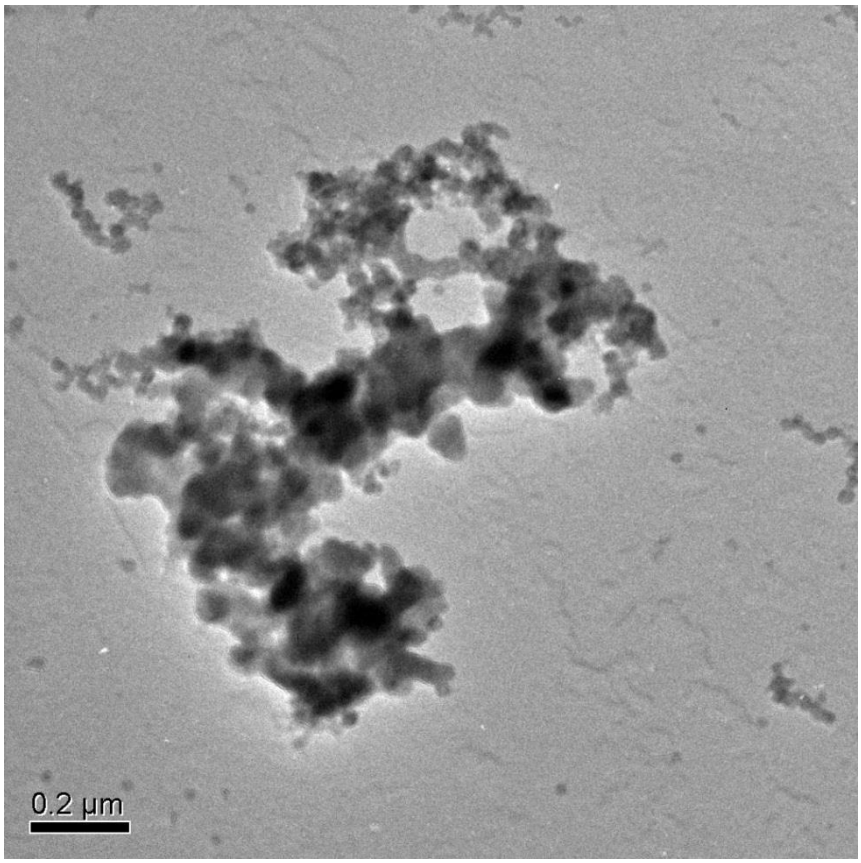

Figure (2.6): Image of diesel fuel particle by using *TEM* microscope. Engine condition: fuel injection 9 deg *BTDC*, Fuel injection pressure 800 bar, 0% *EGR*, Engine speed 2000 rpm at 2.7 bar BMEP. Multi cylinder diesel engine at Brunel University.

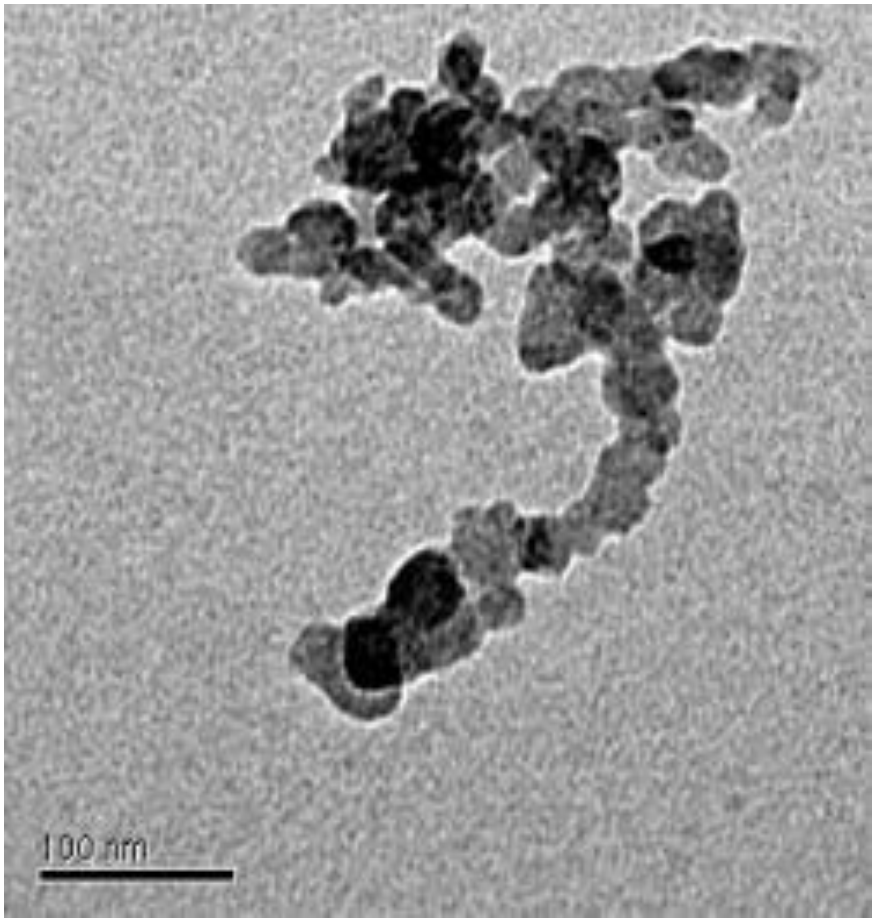

Figure (2.7): Image of *RME* fuel particle by using *TEM* microscope. Engine condition: fuel injection 9 deg *BTDC*, Fuel injection pressure 800 bar, 0% EGR, Engine speed 2000 rpm at 2.7 bar *BMEP*. Multi cylinder diesel engine at Brunel University.

2.1.3.2 Major problems using *TEM*

One of the major challenges in this technique is choosing the right acceleration voltage. Using high acceleration voltage creates a clear image of particle morphology. But if the chosen acceleration voltage is too high, the energy of electrons would be high enough to damage the morphology of particles consequently the image of particles would not reflect a true picture of the specimen morphology. The explosion of particles due to the collision of electron beam can be seen visually by using *TEM* microscope.

Also if the time between collecting the samples on the *TEM* grids and loading to *TEM* microscope is too long, the environmental conditions (mainly pressure, Temperature and humidity) can damage morphology of particles. Moreover the experimenters can interpret the results incorrectly.

Cross contamination can be another major problem. The tools at *TEM* grid sampling and loading the specimen to *TEM* microscope (tweezers and grid containers) need to be properly cleaned for each sampling. It was found that using cloth only is not sufficient to prevent cross contamination.

In addition to the above technical problems, using *TEM* is a costly and very time consuming process. Loading and unloading a single specimen to *TEM* microscope can take up to several hours; consequently many considerations need to be taken into account before choosing this technique.

2.1.4 Analytical techniques

It is clear that use of mathematical functions to analyse combustion performance analytically is extremely efficient in terms of cost and time [39]. Many computational methods and correlations were developed during last decades to predict combustion main properties i.e. in cylinder pressure and temperature, efficiency, released heat, burn rate and etc. Wiebe and Wolfer equations are good examples of correlations which are widely used to predict burn rate and ignition delay respectively. As mentioned in previous sections sophisticated laboratory equipment are used to carry out engine measurements in engine combustion research. Since these facilities are not available for many engine research teams around the world therefore analytical technique is an alternative method to study engine combustion.

In this research Wiebe and Wolfer equations were studied analytically and the results were demonstrated by using experimental measurements on multi cylinder diesel engine. Using these results new correlations were proposed to calculate burn rate and ignition delay. Furthermore, the effect of heat capacities ratio on heat release analysis was investigated analytically and new method was proposed to calculate heat capacities ratio.

2.2. Wiebe equation

Wiebe equation is the most famous function used widely by researchers. Since this function is known very well by researchers in the field of diesel engine analyses the researchers have stopped citing the source of this function. The origin of this function has been referred in several forms of Wiebe, Weibe, Veibe or Viebe by German, Russian and English researchers in international journals. First Haywood used Wiebe in his work and this form has been almost the only form which is used since then. Even though Wiebe equation is well known by engine researchers but a little is known about the person who introduced this function. Ivan Ivanovitch Wiebe was a Russian engineer and scientist from the Urals of German decent [11]. Ivan Ivanovitch Wiebe published the details of his work related to his function when he was working at 'Chilyabinsk Polytechnic Institute' in 1952. This centre in Russia is known as 'South Ural State University' now. Later he became head of International combustion engines department at South Ural State University and remained in his position until he passed away in Chilyabinsk in 1969.

2.2.1. Wiebe equation constants (*a* and *m*)

It is known that the emissions from automotive engines are one of the major sources of air pollution that affects the human health and environment [40-46]. The emission characteristics of diesel engines are strongly correlated to the in-cylinder combustion processes. The engine combustion characteristics are mainly understood through the apparent heat release rate (*AHRR*) that is determined from the measured cylinder pressure data as a function of crank angle (θ) [47-50]. The burn fraction or burn rate of a combustion process are normally characterised using Wiebe equation (2.1), which was introduced more than 60 years ago [11]. The Wiebe equation presents the relationship between the burn fraction (*f*) and the three main combustion parameters, *viz.*, (i) the instant at which heat release rate becomes positive, θ_o; (ii) instantaneous crank angle, θ; and (iii) the duration of combustion, $\Delta\theta$.

$$f = 1 - \exp[-a(\frac{\theta - \theta_o}{\Delta\theta})^{m+1}] \quad (2.1)$$

The Wiebe equation relates different phases of the combustion process. The combustion processes are usually divided into three steps, development period (ignition delay), fast burning (mostly between CA10 to CA90 or sometimes between CA5 to CA95) and quenching period (after CA90 or CA95) [11,51]. The burn fraction (f) is strongly dependent on the values of efficiency (*a*) and form (*m*) factors, so it is important to use accurate values for these constants. Different ranges of values have been suggested in the literature for *a* and *m* values, the value for *a* has been chosen arbitrarily without any physical reasoning, in most of the work the value of *a* is 5 [2,52-56] or 6.908 [57-60]. According to [2,61], the values for *a* and *m* are 5 and 2 respectively. Since Wiebe equation contains two constants, an assumption is often made with one of the constants, while the other constant is derived. Johansson *et al.* [54] has set a value of 5 for *a*, and the constant *m* was determined by fitting a

non-linear least square function between the experimentally determined cumulative heat release rate and the burn fraction of Wiebe equation, through this procedure a value of *m* = 4.29 was determined. Ravaglioli *et al.* [55] has set the values for constants as $a = 5$ and *m* = 1.4. In another published work, Rajkumar *et al.* [56] has used a value of $a = 5$ and *m* = 1.1. Cesario *et al.* [59] have discussed two set of values for *a* and *m;* for high speed combustion the value of *a* = 6.908 and *m* = 0.5 was used; and for moderate speed combustion the value of *a* = 6.908 and *m* = 2.5 was used in diesel engines. Assuming the values for the two constants *a* and *m*; or by assuming a value for either one of the constants *a* or *m* can cause error while predicting the burn fraction using the Wiebe equation [62]. Varying the values of *a* and *m* changes the predicted shape of the burn fraction significantly as these factors are placed within the exponential term of Wiebe equation [2]. Yasar *et al.* [63] studied the effects of varying the values of *m* from 0.1 to 10 and have shown that the burn fraction *f* depends mostly on *m* value, therefore the values for the constants in the Wiebe equation needs to be calculated accurately. An analytical method has been proposed in chapter 5 to calculate the accurate value of *a* and *m*.

2.2.2. Derivation of Wiebe equation

During the combustion some parts of fuel do not participate in the combustion process and leave the combustion chamber without oxidation. This product of combustion is unwanted and called *Unburned Hydro Carbon* (*UHC*). Reducing the level of *UHC* in diesel engines in order to improve the fuel economy and also emission efficiency is one of the major challenges for diesel engine researchers. *UHC* forms ineffective centres in combustion chamber and it is proportional to combustion inefficiency. On the other hand the parts of fuel which participate in the combustion process by oxidation, form effective centres which are the main part of combustion and generate heat in the engine during the combustion process.

For ideal combustion the number of molecules in effective centres is equal to total number of molecules in fuel. And in differential form at the time of *t* the equation (2.2) is expressing this relation.

$$-(\frac{dN}{dt}) = (\frac{dNe}{dt}) \tag{2.2}$$

Where N is the total number of molecules in fuel and N_e is the number of molecules in the effective centres respectively. Equation (2.2) can be written for a real combustion where some molecules do not participate in combustion process in the form of equation (2.3) which contains coefficient *n*.

$$-(\frac{dN}{dt}) = n(\frac{dNe}{dt}) \tag{2.3}$$

The density of effective centres defines as the ratio of number of molecules in effective centres and total number of molecules in the fuel and can be calculated by equation (2.4).

$$\rho = N_e \diagup N \tag{2.4}$$

The parameter ρ_r is defined by equation (2.5) and called relative density of the effective centres.

$$\rho_r = (\frac{dN_e}{dt}) \diagup N \tag{2.5}$$

Equation (2.6) determined by replacing equation (2.5) in equation (2.3).

$$-\frac{dN}{N} = n\rho_r dt \tag{2.6}$$

Integrating both sides of equation (2.6) results in equation (2.7).

$$\ln \frac{N}{N_o} = -\int_0^t n\rho_r dt \tag{2.7}$$

Where N_o is the number of molecules/moles of reactant at beginning of combustion and N is the number of molecules/moles of reactant at time t. Equation (2.7) can be rewritten as equation (2.8).

$$N = N_o e^{-\int_0^t n\rho_r dt} \tag{2.8}$$

Combustion burn fraction is defined by equation (2.9) and denoted by the notation f.

$$f = \frac{N_o - N}{N_o} \tag{2.9}$$

Substitution of equation (2.9) in equation (2.8) results in equation (2.10).

$$f = 1 - e^{-\int_0^t n\rho_r dt} \tag{2.10}$$

The relative density of the effective centres can be expressed by equation (2.11).

$$\rho_r = K_1 t^m \tag{2.11}$$

Where K_1 and m are constants and t is the time. Substitution of ρ_r in equation (2.10) results in equation (2.12).

$$f = 1 - e^{-\int_0^t nK_1 t^m dt} \tag{2.12}$$

By considering $K=nK_1$ equation (2.12) can be rewritten as equation (2.13).

$$f = 1 - e^{-\int_0^t Kt^m dt} \tag{2.13}$$

By integrating equation (2.13) f can be expressed in the form of equation (2.14).

$$f = 1 - e^{-[\frac{K}{m+1} t^{m+1}]} \tag{2.14}$$

Equation (2.14) expresses relation between f and t for the combustion period. K and m are two constants which can be obtained analytically or by fitting the experimental data (these concepts will be discussed in chapter 5. Equation (2.14) can be written for the end of combustion where $f=f_d$ and corresponding time will be denoted by t_d.

$$e^{-[\frac{K}{m+1}t_d{}^{m+1}]} = 1 - f_d \tag{2.15}$$

Similarly equation (2.14) was rearranged and resulted in equation (2.16).

$$e^{-[\frac{K}{m+1}t^{m+1}]} = 1 - f \tag{2.16}$$

Equations (2.17) is obtained by taking natural logarithm of both sides of equations (2.15) and (2.16) and dividing equation (2.15) by equation (2.16).

$$\frac{t_d^{m+1}}{t^{m+1}} = \frac{\ln(1 - f_d)}{\ln(1 - f)} \tag{2.17}$$

The *Efficiency factor* denoted by *a* and defind as $a = -\ln(1 - f_d)$. According to definition of *a*, the Efficiency factor is the function of f_d only. Replacing the value of *a* in equation (2.17) results in general form of Wiebe equation in terms of *t*.

$$f = 1 - e^{-a(\frac{t}{t_d})^{m+1}} \tag{2.18}$$

If the time is measured from start of combustion where $t=t_o$, Wiebe equation can be written as:

$$f = 1 - e^{-a(\frac{t-t_o}{t_d-t_o})^{m+1}} \tag{2.19}$$

Where t_o is the time of start of combustion. Wiebe equation also can be expressed in terms of crank angle degree which is a more useful form of Wiebe equation in comparison to equation (2.19). The crank angle degree θ at any instant is linearly related to *t* as follows:

$$\theta = \omega t \tag{2.20}$$

Where ω is the crank shaft angular velocity. Similarly $\theta_o = \omega t_o$ and $\theta_d = \omega t_d$. The crank angle corresponding to the start of combustion is denoted as θ_o. By replacing the values of t, t_o and t_d Wiebe equation can be expressed in the form of equation (2.21).

$$f = 1 - e^{-a(\frac{\theta-\theta_o}{\Delta\theta})^{m+1}} \tag{2.21}$$

Figure 2.8 shows the relation between a and f_d. According to this figure the value of a depends on value of f_d which is considered for the end of combustion. In some works, CA90 was considered for the end of combustion (corresponding to f_d=0.9) and in some others CA95 and CA99 were considered. According to this figure a is a positive value varies between 2.303 and 6.908 corresponding to f_d =0.9 and 0.999 respectively. Also considering higher f_d results in higher a. The values of a varies significantly in the range of f_d>0.98. The effect of a on calculation of f will be discussed in chapter 5.

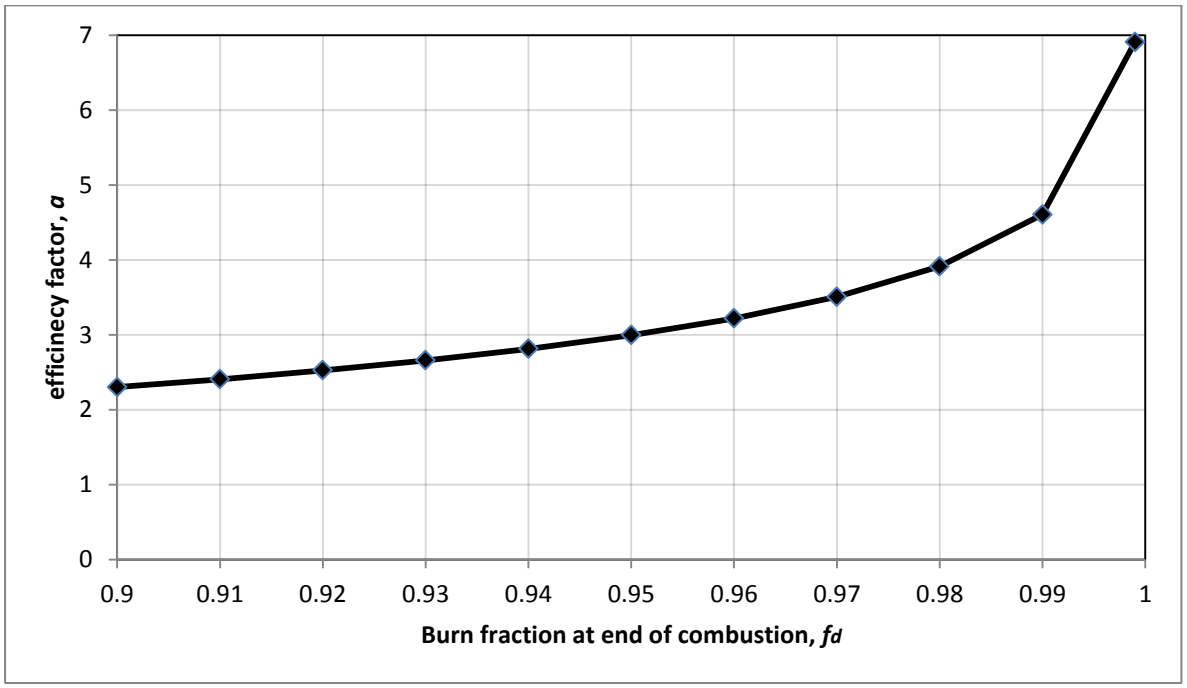

Figure (2.8): Variation of efficiency factor (a) against Burn fraction at end of combustion (f_d).

The constans a and m of Wiebe equation can affect the value of f significantly. Figures 2.20 and 2.21 present the variation of f with respect to variation of a and m respectively.

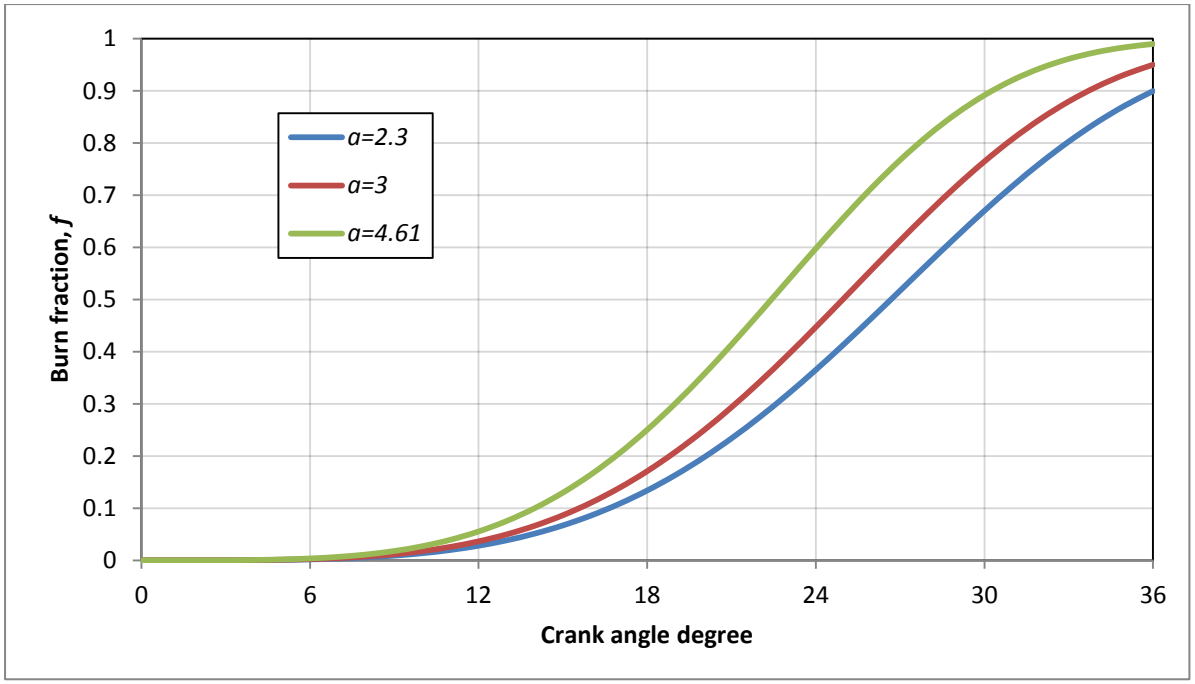

Figure (2.20): Variation of Burn fraction (*f*) with respect to *a*.

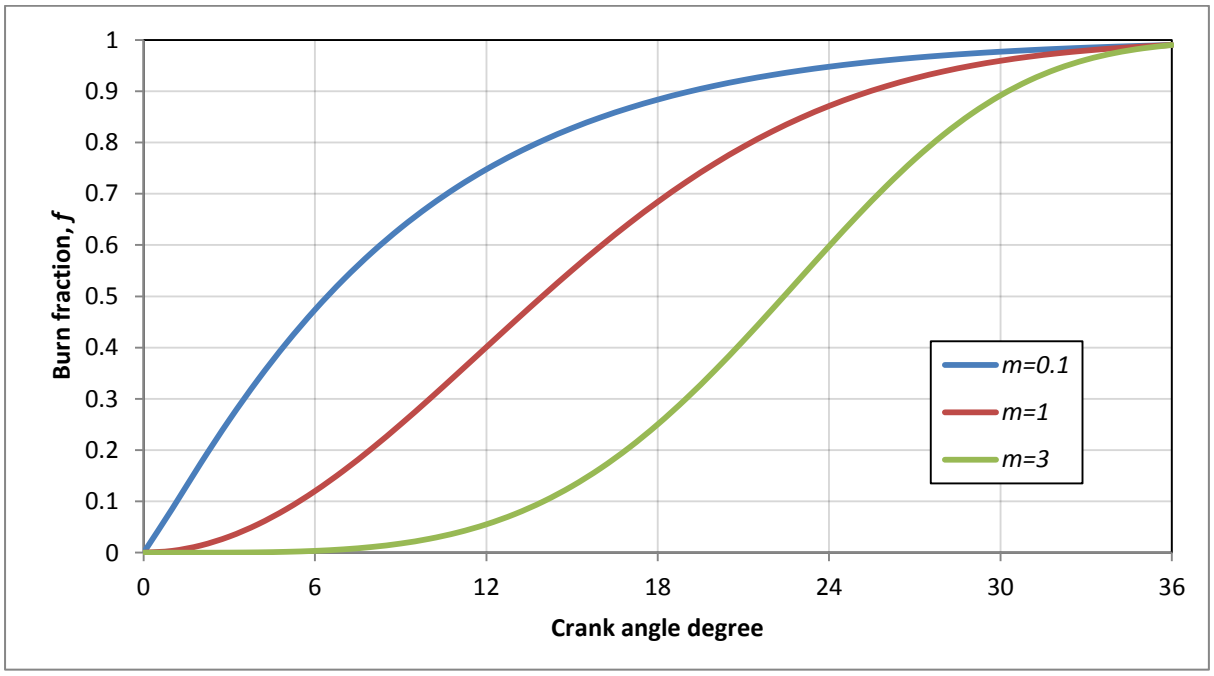

Figure (2.10): Variation of Burn fraction (*f*) with respect to *m*.

According to figures 2.9 and 2.10 the variation of *m* can affect *f* significantly more in comparison to *a*. The variation of *f* with respect to *a* and *m* will be discussed and compared in chapter 5.

The parameter called *Burn rate*, denoted by ω, can be calculated by using equation (2.19).

$$\omega = \frac{df}{dt} = a(\frac{m+1}{t_d})(\frac{t-t_o}{t_d})^m e^{-a(\frac{t-t_o}{t_d})^{m+1}} \quad (2.22)$$

Similarly, ω can be calculated in terms of crank angle by differentiating equation (2.21).

$$\omega = \frac{df}{dt} = a(\frac{m+1}{\Delta\theta})(\frac{\theta-\theta_o}{\Delta\theta})^m e^{-a(\frac{\theta-\theta_o}{\Delta\theta})^{m+1}} \quad (2.23)$$

The location of the instant which corresponds to maximum ω can be calculated by differentiation ω and equating to zero.

$$\frac{d\omega}{dt} = a(\frac{m+1}{t_d})\{\frac{m}{t_d}(\frac{t-t_o}{t_d})^{m-1} - (\frac{m+1}{t_d})(\frac{t-t_o}{t_d})^{2m}\}e^{-a(\frac{t-t_o}{t_d})^{m+1}} = 0 \quad (2.24)$$

By solving equation (2.24), the time corresponding to maximum ω can be obtained.

$$t_m = t_o + t_d K_2 \quad (2.25)$$

Where

$$K_2 = e^{-\frac{\ln\frac{a}{m}(m+1)}{m+1}} \quad (2.26)$$

a and *m* in equation (2.26) are constants. According to this equation there is always one value for t_m and the value of t_m is dependent on t_o and t_d. The difference between t_o and t_d is called combustion duration, consequently the value of t_m is related to combustion duration linearly. Similar results can be obtained by solving the equation (2.23) in terms of θ.

$$\frac{d\omega}{d\theta} = a(\frac{m+1}{\theta_d})\{\frac{m}{\theta_d}(\frac{\theta-\theta_o}{\theta_d})^{m-1} - (\frac{m+1}{\theta_d})(\frac{\theta-\theta_o}{\theta_d})^{2m}\}e^{-a(\frac{\theta-\theta_o}{\theta_d})^{m+1}} = 0 \quad (2.27)$$

$$\theta_m = \theta_o + \theta_d K \quad (2.28)$$

Figure 2.11 indicates the location of θ_m corresponding to different values of *m*.

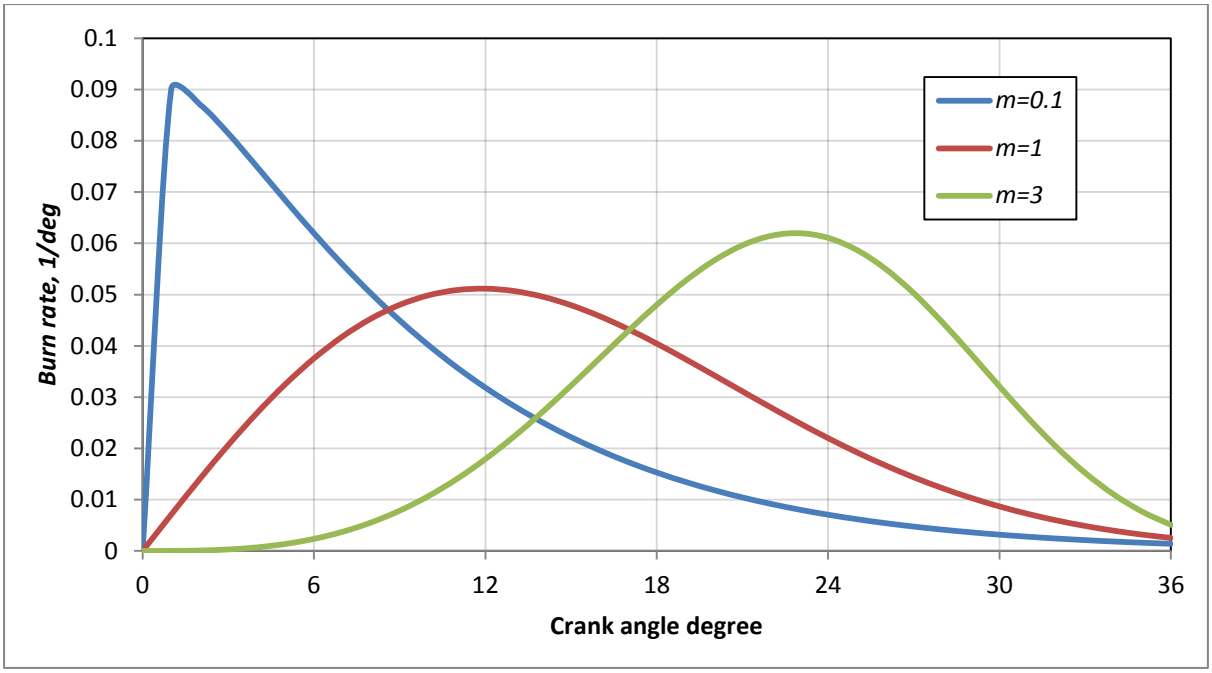

Figure (2.11): Variation of Burn rate (ω) with respect to Form factor (m) at $\Delta\theta$=36 and a=4.61.

By replacing the value of t_m from equations (2.28) and value of K_2 from equation (2.29) in equation (2.22), the corresponding Burn fraction f_m can be calculated.

$$f_m = 1 - e^{\frac{-m}{m+1}} \qquad (2.29)$$

According to equation (2.29), the value of f_m is a function of m only and it is not affected by value of a.

2.2.3. Forms of Wiebe equation

Depending upon the type of analysis, Wiebe equation can be used in several forms. Equation (2.21) is known as original form of Wiebe equation. But Wiebe equation can be expressed in different forms depending on the nature of study. Equation (2.30) is the Wiebe equation which is expressed in terms of f_m by using equation (2.29).

$$f = 1 - e^{(-a(\frac{\theta-\theta_o}{\Delta\theta})^{\frac{1}{\ln e(1-f_m)}})} \quad (2.30)$$

Where e is Napier's constant (e ≈2.718). Equation (2.30) has been obtained by eliminating m in equation (2.29) and f_m was replaced in original Wiebe equation.

Similarly equation (2.28) can be used to eliminate $\Delta\theta$ in equation (2.21). Equation (2.31) results in by replacing $\Delta\theta$ in terms of θ_m.

$$f = 1 - e^{-a(\frac{K(\theta-\theta_o)}{\theta_m})^{m+1}} \quad (2.31)$$

Where K_2 has been defined as $K_2 = e^{-\frac{\ln\frac{a}{m}(m+1)}{m+1}}$.

Wiebe equation can also be expressed in terms of location of centre of combustion (θ_{50}). It was found that the location of θ_{50} can provide valuable information about the combustion performances in terms of emission and heat release. A new methodology is presented to calculate Heat capacities ratio (γ) by using the location of θ_{50} in chapter 6. Equation (2.32) expressed Wiebe equation in terms of θ_{50}. Where $C_i = \frac{\theta-\theta_o}{\theta_{50}-\theta_o}$ and θ_o is the crank angle corresponding to the start of combustion. The derivation of Wiebe equation in terms of θ_{50} along with the benefits of expressing Wiebe equation in terms of θ_{50} will be discussed in chapter 5.

$$f = 1 - \exp[(\ln 0.5)C_i^{m+1}] \quad (2.32)$$

2.2.4. Applications of Wiebe equation

Wiebe mentioned in his presentation in 1954 that his equation was applicable for both *CI* and *SI* engines. Since then, many researchers have used Wiebe equation to express Burn rate for direct and indirect injection. Shipinski et al. used Wiebe equation to express heat release rate in a direct injection diesel engine [64] as follows:

$$Ahrr = (LHV).m^{o}.\frac{df}{d\theta} \tag{2.33}$$

Where *LHV* is the lower heating value of the fuel in *kJ/kg* and m^{o} is the mass of injected fuel in a cycle in *kg*. Equation (2.34) presents the value of $\frac{df}{d\theta}$ which is calculated by differentiating equation (2.21) respect to θ.

$$\frac{df}{d\theta} = \frac{a(m+1)}{\Delta\theta}(\frac{\theta-\theta_o}{\Delta\theta})^{m} e^{-a(\frac{\theta-\theta_o}{\Delta\theta})^{m+1}} \tag{2.34}$$

Equation (2.35) expresses *AHRR* in terms of *a* and *m* and combustion parameters (θ, θ_o, $\Delta\theta$,). Equation (2.35) results by replacing the value of $\frac{df}{d\theta}$ from equation (2.34) in equation (2.33).

$$Ahrr = (LHV).m^{o}.\frac{a(m+1)}{\Delta\theta}(\frac{\theta-\theta_o}{\Delta\theta})^{m} e^{-a(\frac{\theta-\theta_o}{\Delta\theta})^{m+1}} \tag{2.35}$$

If the combustion duration is considered CA5 to CA95, equation (2.35) can be rewritten as equation (2.36).

$$Ahrr = 3(LHV).m^{o}.\frac{(m+1)}{\Delta\theta}(\frac{\theta-\theta_o}{\Delta\theta})^{m} e^{-3(\frac{\theta-\theta_o}{\Delta\theta})^{m+1}} \tag{2.36}$$

Where *a*=3 is considered in equation (2.36).

Equation (2.35) can be used to calculate location of the crank angle which is corresponding to maximum *AHRR* . This point denoted with $\theta_{\max}$ and it can be found as follows:

$$\frac{dAhrr}{d\theta} = (LHV).m^{o}.\frac{a(m+1)}{(\Delta\theta)^{2}}(\frac{\theta-\theta_o}{\Delta\theta})^{m-1} e^{-a(\frac{\theta-\theta_o}{\Delta\theta})^{m+1}} [m - a(m+1)(\frac{\theta-\theta_o}{\Delta\theta})^{m+1}] = 0 \tag{2.37}$$

$$\theta_{\max} = [\frac{m}{a(m+1)}]^{\frac{1}{m+1}}.\Delta\theta + \theta_o \tag{2.38}$$

Equation (2.38) indicates that location of $\theta_{\max}$ is proportional to $\Delta\theta$. The value of $[\frac{m}{a(m+1)}]^{\frac{1}{m+1}}$ is a positive value consequently a longer combustion duration results in larger $\theta_{\max}$. Equation (2.37) can be solved in terms of *m* and results in equation (2.39).

$$m - a(m+1)(\frac{\theta_{\max} - \theta_o}{\Delta\theta})^{m+1} = 0 \qquad (2.39)$$

Equation (2.39) is an implicit equation with respect to *m*. In heat release analysis, the value of $\theta_{\max}$, θ_o and $\Delta\theta$ can be calculated by using in-cylinder pressure data, so by assuming the value of *a* ,value of *m* can be calculated.

2.3.Heat capacities ratio (γ)

Investigations in the field of internal combustion engines have revealed that diesel engine is responsible for number of environment issues which are affecting human life significantly [65-69]. In order to reduce the harmful effect of diesel engine combustion, new strategies were employed by engine manufacturers. Particularly fuel injection strategy has been improved significantly during the last decade. Using high injection pressure as high as 300 bars along using common rail system resulted in remarkable achievements [70-75]. In addition to fuel injection strategy using Diesel Particulate Filter (DPF) and catalysts to remove particles in exhaust along with EGR and boosting are other developed solutions by automotive companies to meet the emission regulations [76-80]. In terms of fuel chemical structure, new fuels with high oxygen content and fuel additives were introduced by fuel companies which resulted in improving diesel engine performance significantly [81-85]. The engine exhaust emission characteristics are strongly correlated to the in-cylinder combustion processes. The combustion characteristics in engines are mainly understood through the

apparent heat release rate (*AHRR*) that was determined from the first law of thermodynamics [3]. The *AHRR* model without heat exchange to cylinder walls is shown in equation (2.40).

$$\left(\frac{dQ}{d\theta}\right) = \frac{\gamma}{\gamma-1} p \frac{dV}{d\theta} + \frac{1}{\gamma-1} V \frac{dp}{d\theta} \tag{2.40}$$

Where Q is the total released heat in J and θ is the instantaneous crank angle in degree, γ is the ratio of specific heat (C_p/C_v), p is the measured cylinder pressure in Pa and V is the cylinder volume in m^3. The derivation of equation (2.40) can be found in section (3.1).

The *AHRR* is strongly related to engine operating conditions, engine specifications as well as physical and chemical properties of fuel. Moreover, the *AHRR* provides information about ignition delay (the time interval between the start of injection and the start of combustion while, the start of combustion is determined as the time instant when the *AHRR* data crosses the time-axis after the start of injection), level of premixed and diffusion burn characteristics of the combustion process, that are useful for the understanding of exhaust soot and NO_x emissions. By considering equation (2.43), it is clear that p and γ are the main parameters that influence the value of *AHRR*. The effect of p and γ along with the heat loss to the cylinder walls on the heat release analysis were discussed in [87-89]. It was found that γ significantly affects the magnitude of heat release rate (peak value) and the shape of the cumulative heat release rate. It has been shown that specific heat ratio (γ) is the most important thermodynamic property that is used for heat release analysis in engines [90,91]. It is well known that γ is a function of charge temperature and charge composition and it varies during the complete combustion period. The variation of γ at each crank angle position for the entire combustion period has been discussed in [87,90,92,93]. Several correlations have been proposed to calculate γ in terms of charge temperature [90,92,93]. Using the instantaneous value of γ can reduce error in heat release rate calculations. It has also been

revealed that the effect of varying γ during a cycle is relatively small and it is more important to use correct value of γ for the overall combustion process [87]. The effects of temperature and equivalence ratio on γ have been investigated and it has been shown that the relation between γ and temperature is almost linear [95]. Similarly, the variation with equivalence ratio is significant but much smaller than the effect of temperature [87]. Horn et al. [91] and Asad et al. [94] have considered constant value of γ for their heat release calculations for the entire combustion period. Brunt et al. [87] have calculated the error induced on the *AHRR* due to temperature and γ value, and found that the maximum error on the *AHRR* were mainly due to the use of incorrect value of γ. It was concluded that the effect of γ on *AHRR* was more significant when compared to temperature and it was also revealed that the effect of pressure on *AHRR* was not that significant.

2.4. Ignition delay (τ)

The combustion processes in diesel engines are significantly influenced by the rate at which the fuel is mixed with air inside the combustion chamber during the ignition delay (τ) period. Ignition delay is defined the time interval between the start of injection and start of combustion in a diesel engine. The duration of ignition delay influences the premixed burn fraction, heat release rate, as well as engine noise and pollutant formation. Due to importance of ignition delay many correlations have been proposed. The ignition delay correlation proposed by Hardenberg and Hase [96] is one of the well-established correlations which is based on the in- cylinder pressure, temperature, mean piston speed, activation energy together with some adjustable coefficients.

Another most widely reported correlation that has been used over the years for predicting τ in diesel engines and in diesel like environment is an Arrhenius type expression, which was

first proposed by Wolfer [97] in 1938. The pressure and temperature dependence on the proposed Arrhenius based correlation is shown in equation (2.41).

$$\tau = Ap^{-n} \exp \frac{C}{T} \tag{2.41}$$

Where τ is the ignition delay, p and T are the in-cylinder pressure and temperature; A is the pre-exponential factor and n is the experimentally determined, which are dependent on the properties of the fuel (to some extent, the injection and air-flow characteristics). The constant C is dependent on the activation energy, which can be calculated as $C = \frac{E_A}{R}$ .Where R is the universal gas constant (8.314 J/mol.K), and E_A is the apparent activation energy of the fuel that initiates the auto-ignition process, the effect of E_A on τ for diesel fuel was investigated in [82,98].Following Wolfer's work in 1938, several investigations have been carried out to explore the ignition process in a constant volume chamber, Rapid Compression Machines (*RCM*) and in engines. Previous investigations have revealed that the charge temperature, pressure and fuel properties are the most important factors, which affects the magnitude of τ [3,99-106]. Nevertheless, the τ is also influenced by the factors such as equivalence ratio [107] injection pressure, engine speed, injection timing, swirl ratio, engine load, nozzle hole diameter, and nozzle type [108].

Watson [109] developed an empirical correlation to predict τ, while proposing a constant value of 2100 for C and 3.45 for A. The correlation coefficients were mainly dedicated for diesel as the molecular structure, chemical composition and physical properties such as viscosity, surface tension and density are different for different fuels. Many recent investigations have shown that τ for bio-diesel is shorter than diesel for a given operating condition due to their different properties such as high Cetane number (*CN*). Besides fuel composition, the in-cylinder peak pressures, the mean in-cylinder temperature and pressure

during the delay period are relatively lower for bio-diesel than diesel [84,85,110-118]. The correlation proposed by Assanis [100] is a function of in-cylinder pressure, temperature and equivalence ratio (ϕ), with A=2.4 and C=2100 as shown in equation (2.42). In general the pre-exponential coefficient was found to vary from 2.6 to 3.8 in the literature.

$$\tau = 2.4 p^{-1.02} \phi^{-0.2} \exp \frac{2100}{T} \tag{2.42}$$

In another study, Alkhulaifi [101] proposed a new correlation similar to Assanis [100] by including the engine load factor. The newly included term was defined as the Brake Power fraction (BP) which is shown in equation (2.43).

$$\tau = 2.05(BP)^{-0.4} p^{-1.05} \exp \frac{2100}{T} \tag{2.43}$$

Watson [109] and Assanis [100] used an average value for the in-cylinder pressure during the ignition delay period but Alkhulaifi [101] used the instantaneous in-cylinder pressure at the start of combustion in their correlation, and discussed the benefits of their approach. In all the ignition delay correlations [98,100,101] discussed so far, the accuracy of predictions for a given in-cylinder conditions are mainly influenced by the values of the constants (A, n and C) used in the correlation. Wide range of variations in the A and n values can be seen in [100,101,119,120]. The values for A, n and C are mostly calculated by curve fitting [100,101,121] and this method can affect the accuracy of the correlation significantly depending on the limits set to fit a curve, and also the assumptions made for fitting the data.

Calculating the values of constants A, n and C analytically can improve the accuracy of the correlation due to the exact solution that can be obtained without any assumptions. In this study, it has been demonstrated through theoretical analysis and experiments how the values of A, n and C can be calculated. The values of A, n and C obtained by different methods are

compared and a new correlation incorporating only the engine operating parameters without any tuning constants have been proposed and discussed in chapter 7.

Chapter 3

Theoretical methodology

Cylinder pressure data versus crank angle over the compression and expansion strokes of the engine operating cycle can be used to obtain quantitative information on the progress of combustion. Suitable methods of analysis which yield the rate of release of fuel's chemical energy or rate of fuel burning through the diesel engine combustion process will now be described by using the first law of thermodynamics [3].

In this chapter in section 3.1 the calculation of Apparent Heat Release rate (*AHRR*) by using in-cylinder pressure will be described. In section 3.2 the calculation of in-cylinder temperature will be discussed and compared with other existing methods.

3.1. Heat release calculation

For a diesel engine over power stroke of the engine operating cycle, the content of cylinder can be considered as an open system (compressed fuel and air at high temperature and pressure). The first law of thermodynamics for this open system can be applied as follows:

$$\frac{dQ}{dt} - p\frac{dV}{dt} + \sum m_i^o h_i = \frac{dU}{dt} \qquad (3.1)$$

Where *dQ/dt* is the heat transfer rate across the system boundary into the system, *p(dV/dt)* is the rate of work transfer done by the system due to system boundary displacement, m^o is the mass flow rate into the system across the system boundary at location *i* (flow out of the system would be negative), h_i is the specific enthalpy of flux *i* entering or leaving the system,

and U is the energy of the material contained inside the system boundary. Equation (3.1) can be rearranged and expressed in form of equation (3.2).

$$\frac{dQ_n}{dt} = \frac{dQ_{ch}}{dt} - \frac{dQ_{ht}}{dt} = p\frac{dV}{dt} - m_{cr}^{o}h_{cr} - m_f^{o}h_f - \frac{dU}{dt} \qquad (3.2)$$

Where the apparent net heat release rate, dQ_n/dt, which is the difference between the apparent gross heat release rate dQ_{ch}/dt and the heat transfer rate to the walls dQ_{ht}/dt,equals the rate at which work is done on the piston plus the rate of change of sensible internal energy of the cylinder contents and also effect of mass flow rate in and out of the system. During the power stroke while the intake and exhaust valves are closed the only mass flows across the system boundary are the fuel and the crevice flow.

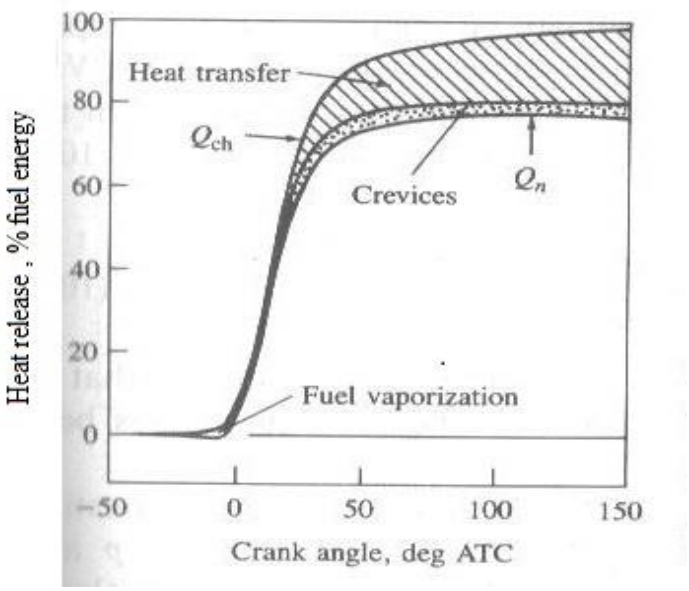

Figure (3.1): Gross and net heat release profile during combustion, for a turbocharged *DI* diesel engine in mid load and mid speed range, showing relative magnitude of heat transfer, crevice, and fuel vaporization and heat up effects. Figure from [3] page 511.

Figure 3.1 shows the effect of heat exchange with the system boundary and crevice flow [3]. This figure also indicates that the effect of heat exchange is greater than the effect of crevice flow therefore the crevice flow effects will be omitted in equation (3.2).

$$\frac{dQ_n}{dt} = \frac{dQ_{ch}}{dt} - \frac{dQ_{ht}}{dt} = p\frac{dV}{dt} - m_f^o h_f - \frac{dU}{dt} \tag{3.3}$$

There were several approaches made by research teams to calculate engine heat loss during the combustion [122-126].

The effect of heat loss is not considered in this work therefore the equation (3.3) can be simplified and expressed in form of equation (3.4).

$$\frac{dQ_n}{dt} = \frac{dQ_{ch}}{dt} - \frac{dQ_{ht}}{dt} = p\frac{dV}{dt} - \frac{dU}{dt} \tag{3.4}$$

If the content of cylinder is assumed as an ideal gas, equation (3.4) becomes

$$\frac{dQ_n}{dt} = p\frac{dV}{dt} - mC_v\frac{dT}{dt} \tag{3.5}$$

From the ideal gas law, $pV=mRT$, with R assumed constant during the combustion period, it follows that

$$\frac{dp}{p} + \frac{dV}{V} = \frac{dT}{T} \tag{3.6}$$

Equation (3.6) can be used to eliminate T from equation (3.5) results in equation (3.7).

$$\frac{dQ_n}{dt} = (1+\frac{C_v}{R})p\frac{dV}{dt} + \frac{C_v}{R}V\frac{dp}{dt} \tag{3.7}$$

Equation (3.7) can be expressed in terms of heat capacities ratio $(\Upsilon=C_p/C_v)$ as follows.

$$\frac{dQ_n}{dt} = \frac{\gamma}{\gamma - 1} p \frac{dV}{dt} + \frac{1}{\gamma - 1} V \frac{dp}{dt} \tag{3.8}$$

According to [3] an appropriate range for γ for diesel heat release analysis is 1.3 to 1.35. A new technique developed to calculate γ value in combustion heat release analysis is proposed in chapter 6.

The value of the combustion chamber volume *V*, at any crank position θ can be calculated by using geometrical properties of reciprocating engine in equation (3.9).

$$V = V_c \left\{ 1 + \frac{1}{2}(r-1)[R + 1 - \cos\theta - (R^2 - \sin^2\theta)^{\frac{1}{2}}] \right\} \tag{3.9}$$

Where the following parameters define the basic geometry of a reciprocating engine as it is shown in figure 3.2 :

1. Compression ratio:

$$r = \frac{V_d + V_c}{V_c} \tag{3.10}$$

Where V_d is the displaced or swept volume and V_c is the clearance volume.

2. Ratio of cylinder bore to piston stroke:

$$R_{bs} = \frac{B}{L} \tag{3.11}$$

3. Ratio of connecting rod length to crank radius:

$$R = \frac{l}{a} \tag{3.12}$$

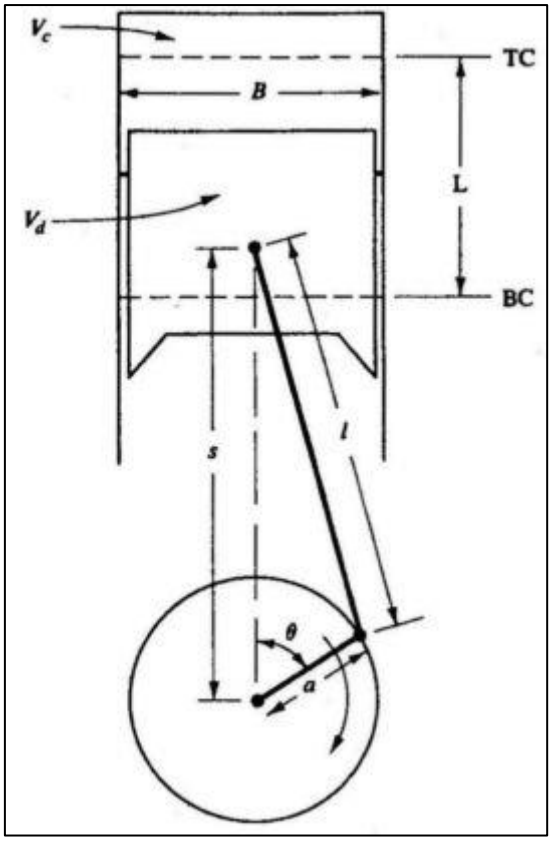

Figure (3.2): Basic geometry of the reciprocating Diesel combustion engine.

3.2. Calculation of in-cylinder temperature

In-cylinder temperatures can be measured by thermocouples or can be calculated by using the pressure data. Thermocouples are very sensitive in terms of the location of sensor and the way it is placed on the engine to detect the correct temperature.

In-cylinder temperature was measured by a thermocouple with a compensation circuit in [102,122].The compensation circuit with an operation amplifier was designed to compensate for the first order time lag due to the thermal inertia of the thermocouple. Along with the measured temperatures the in-cylinder temperatures were calculated by using the equation (3).

$$T_c = T_i(V_i / V_c)^{m-1} \qquad (3.13)$$

Where T_c and V_c are the in-cylinder temperature and volume and T_i and V_i are the known temperature and volume at a crank angle and m is polytropic index. To obtain calculated values from equation (3.13) the inlet air temperature or cylinder temperature can be considered for T_i . Figure 3.3 indicates in-cylinder temperatures using T_i=295.15 K (intake air temperature) and T_i=353.15 K (wall temperature) for diesel fuel at injection timing 6 deg *BTDC*, injection pressure= 800 bar, *BMEP*=2.7 bar and 2000 rpm. According to [103] cooling water temperature can be considered as wall temperature. According to figure 3.3, considering higher value for T_i results in overestimating of in-cylinder temperature calculation for entire combustion period. Figure 3.4 indicates variation of T_c against T_i at same operating engine conditions as figure 3.3. It was observed that T_c value is linearly related to T_i. According to [102] the slope of the line in figure 3.4 is not affected by engine speed for a given condition, but in-cylinder temperature value at the start of combustion is increasing at higher speed. Comparing calculated values for T_c by using intake air temperature and cylinder temperature for T_i with measured in-cylinder temperatures revealed that using cylinder temperature for T_i provides more accurate in-cylinder temperatures [102].

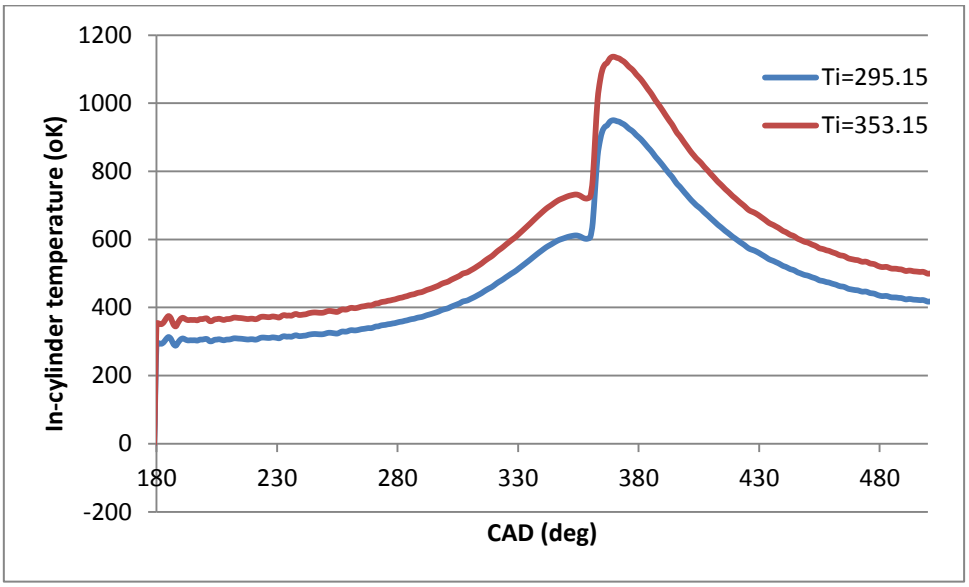

Figure (3.3): Variation of in-cylinder temperature at different intake air temperatures for diesel fuel at injection timing 6 deg *BTDC* , injection pressure= 800 bar , *BMEP*=2.7 and 2000 rpm.

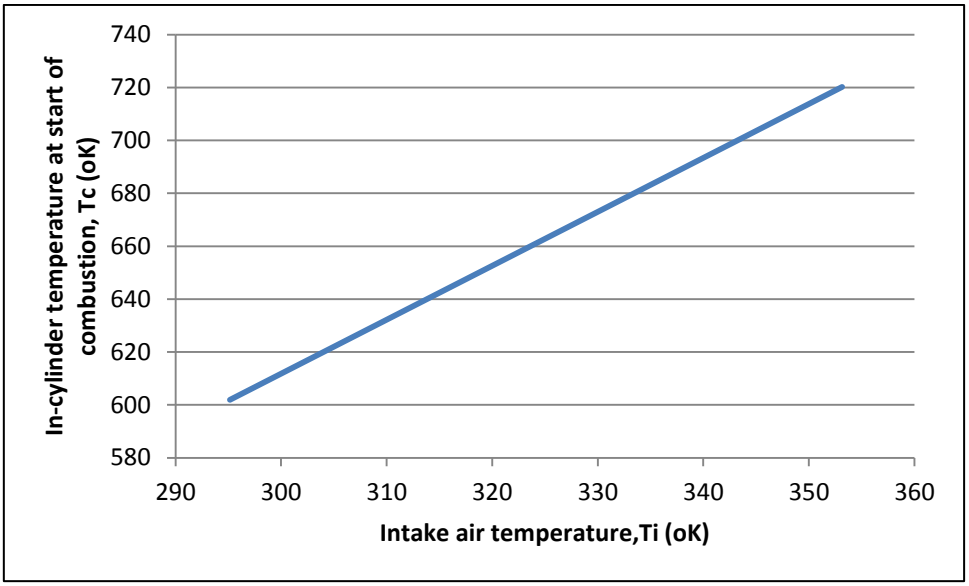

Figure (3.4): variation of in-cylinder temperature at start of combustion at different intake air temperature for diesel fuel at injection timing 6 deg *BTDC* , injection pressure= 800 bar , BMEP=2.7 and 2000 rpm.

Apart from T_i, an incorrect value for *polytropic index* can affect accuracy of T_c value. Using an appropriate technique can provide an accurate value for *m*. Experimental data and correlations can be used to calculate *m*. Equation (3.14) developed by Hardenberg and Hase, can be used to calculate *m* value for entire diesel combustion [96].

$$m = \gamma - \frac{\gamma - 1}{f.S_p + 1} \qquad (3.14)$$

Where γ is the ratio of specific heat (C_p/C_v), f= 1.1 is a constant and S_p is the mean piston velocity. Higher value for S_p corresponds to lower heat transfer in engine as less absolute time is available for each cycle. Figure 3.5 indicates variation of *m* against S_p.

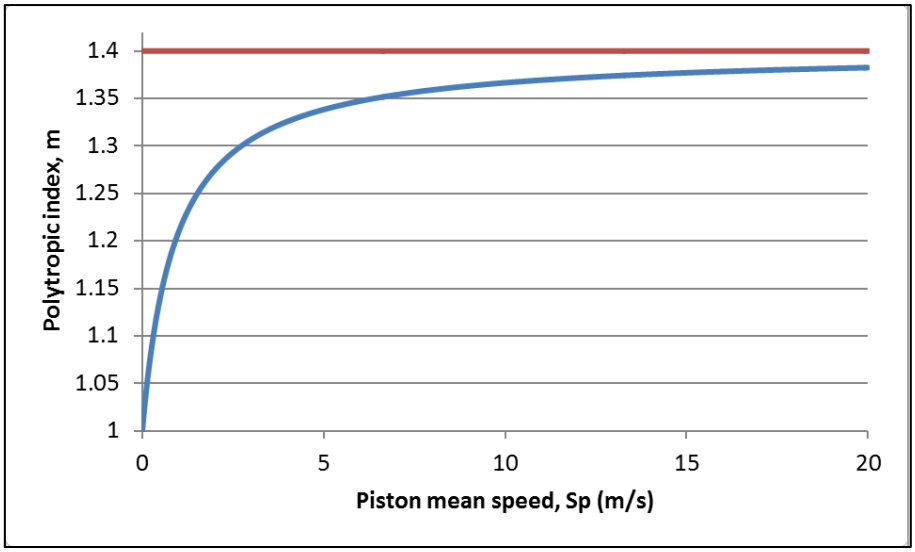

Figure (3.5): Variation polytropic index (*m*) against piston mean speed for diesel fuel.

According to figure 3.5 as piston mean speed increases, the *m* value tends to be a constant value. This condition corresponds to engine heat loss reduction per each cycle. In other word higher piston mean speed can result in a stable value for *m*. Using an accurate value for *m* and *Ti* can provide an accurate T_c.

Kwon *et al*. found that one of the difficulties in ignition delay study is to define the cylinder temperature at the time of ignition [102]. In-cylinder temperature can be calculated by using ideal gas law. In this technique in-cylinder mixture is assumed an ideal gas and the fuel mass and heat loss were neglected. Equation (3.15) can be used to calculate T_c.

$$T_c = T_i . \frac{p_c v_c}{p_i v_i} \tag{3.15}$$

The first law of thermodynamic also can be used to calculate T_c. In this technique the cylinder content is assumed an ideal gas and the values of R and γ were considered during the combustion period. Equation (3.16) can be used to calculate T_c.

$$\left(\frac{dQ}{d\theta}\right)_i = p_i \frac{(V_{i+1} - V_i)}{(\theta_{i+1} - \theta_i)} + \frac{p_i V_i}{T_i} . \frac{1}{\gamma - 1} . \frac{(T_{i+1} - T_i)}{(\theta_{i+1} - \theta_i)} \tag{3.16}$$

Where $(\frac{dQ}{d\theta})_i$ can be calculated by using equation (3.18) at a known crank angle position. In this equation the only unknown parameter is T_{i+1} . Figure 3.6 indicates in-cylinder temperature by using equations (3.13), (3.15) and (3.16).

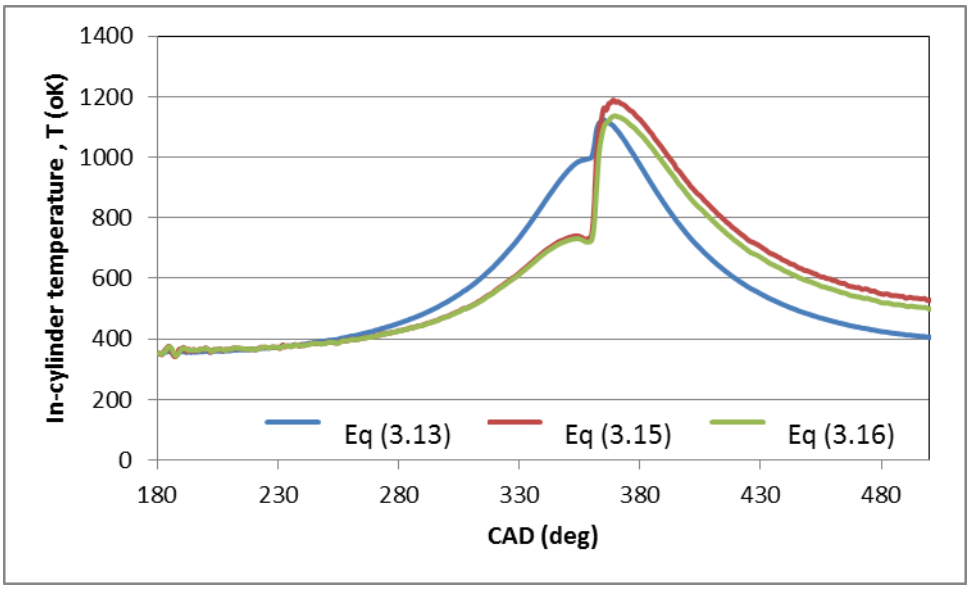

Figure (3.6): variation of in-cylinder temperature using three different methods for diesel fuel at injection timing 6 deg *BTDC* , injection pressure= 800 bar , *BMEP*=2.7 and 2000 rpm. Cylinder wall temperature was considered for T_i for three sets of data.

Equation (3.16) was used to calculate in-cylinder temperatures which provides realistic in cylinder temperature values in comparison to equations (3.13) and (3.15).

Chapter 4

Experimental set up

A four cylinder 2 litre Ford Puma Zetec 16 valves High Speed Direct Injection (HSDI), naturally aspirated diesel engine was employed to carry out these investigations. The pressure data was acquired using a fast response piezo-resistive pressure transducer (Kistler 6125A), and the data was acquired over 100 cycles to minimise the error due to cycle to cycle fluctuation. The average coefficient of variation was found to be less than 1%. Investigations were carried out using diesel which was tested for two engine loads, at different injection timings and at different injection pressures while the engine speed was kept constant at 2000 rpm for all conditions. A gas analyser type Horiba, Model MEXA 7170 was connected to intake and engine exhaust to provide the analysis of intake gas and exhaust gas accurately. The Horiba gas analyser shown in figure 4.1 is a programmable unit as shown in figure 4.2 is able to measure all regulated emissions. Horiba gas analyser can be programmed to provide reading for certain elements as well as displaying the readings. A sample reading has been shown for *EGR, CO, HC,* NO_x, O_2 and CO_2 in figure 4.3 . *NO* and NO_2 can be measured by using this analyser individually.

Figure (4.1): Horiba Mexa-7170 gas analyser.

Figure (4.2): Horiba MEXA-7170 control system.

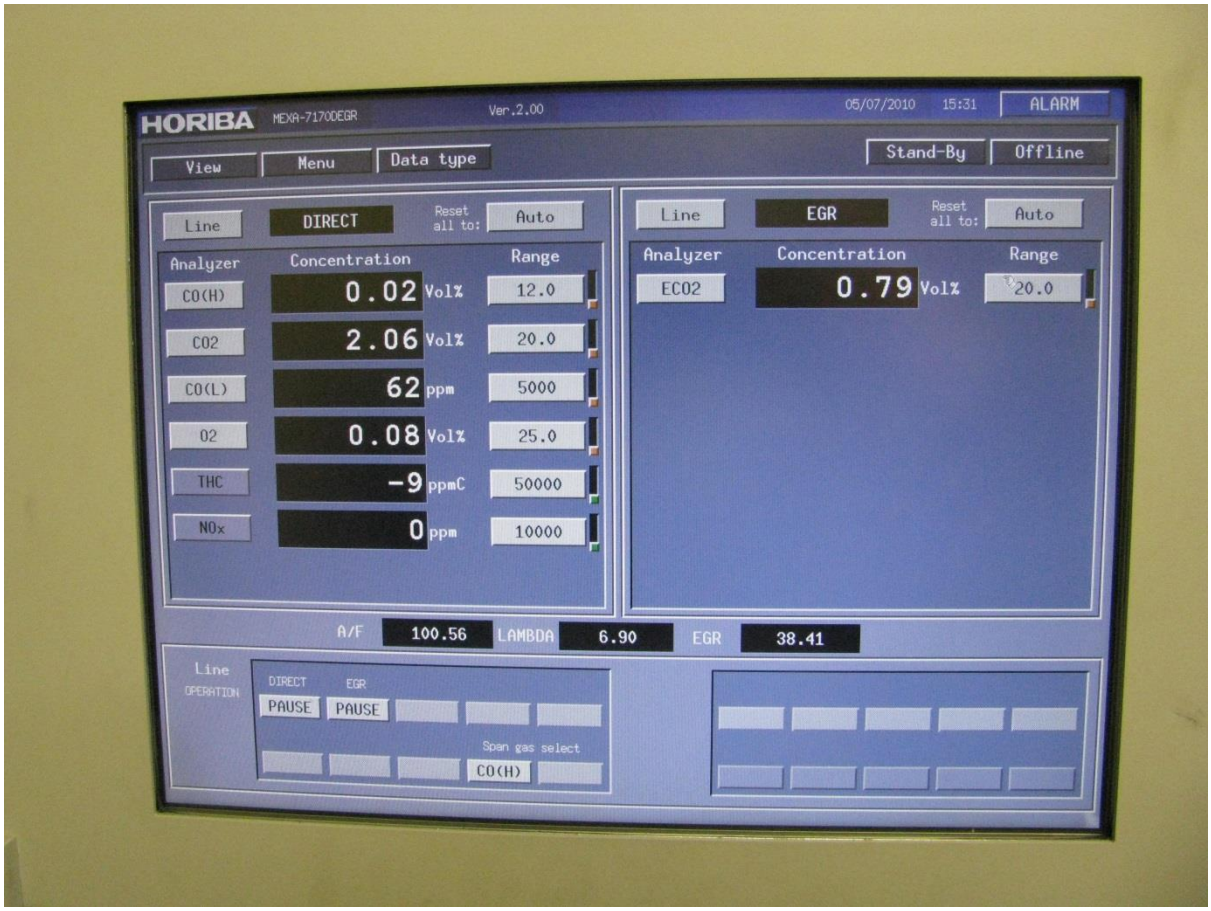

Figure (4.3): A sample reading by gas analyser type: Horiba MEXA-7170.

The engine was equipped with sensors, to measure and control the engine torque, speed, injection parameters, cylinder pressure and fuel consumption. Figure 4.4 shows the engine in the engine lab. Details of the test matrix are presented in a table in chapters 5, 6 and 7. The engine specifications are listed in table (4.1).

Table (4.1): Specification of engine.

Number of cylinders	4	
Cylinder bore	86	mm
Crankshaft stroke	86	mm
Swept Volume	1998.23	cm^3
Compression Ratio	18.2	
Con-Rod Length	155	mm
V_c	29.04404	cm^3

The engine has an ability to have intake air either naturally aspirated or supercharged to engine. In this work all test were on naturally aspirated condition. The possibility of connecting EGR as well exists but in this investigation the effect of EGR was not considered.

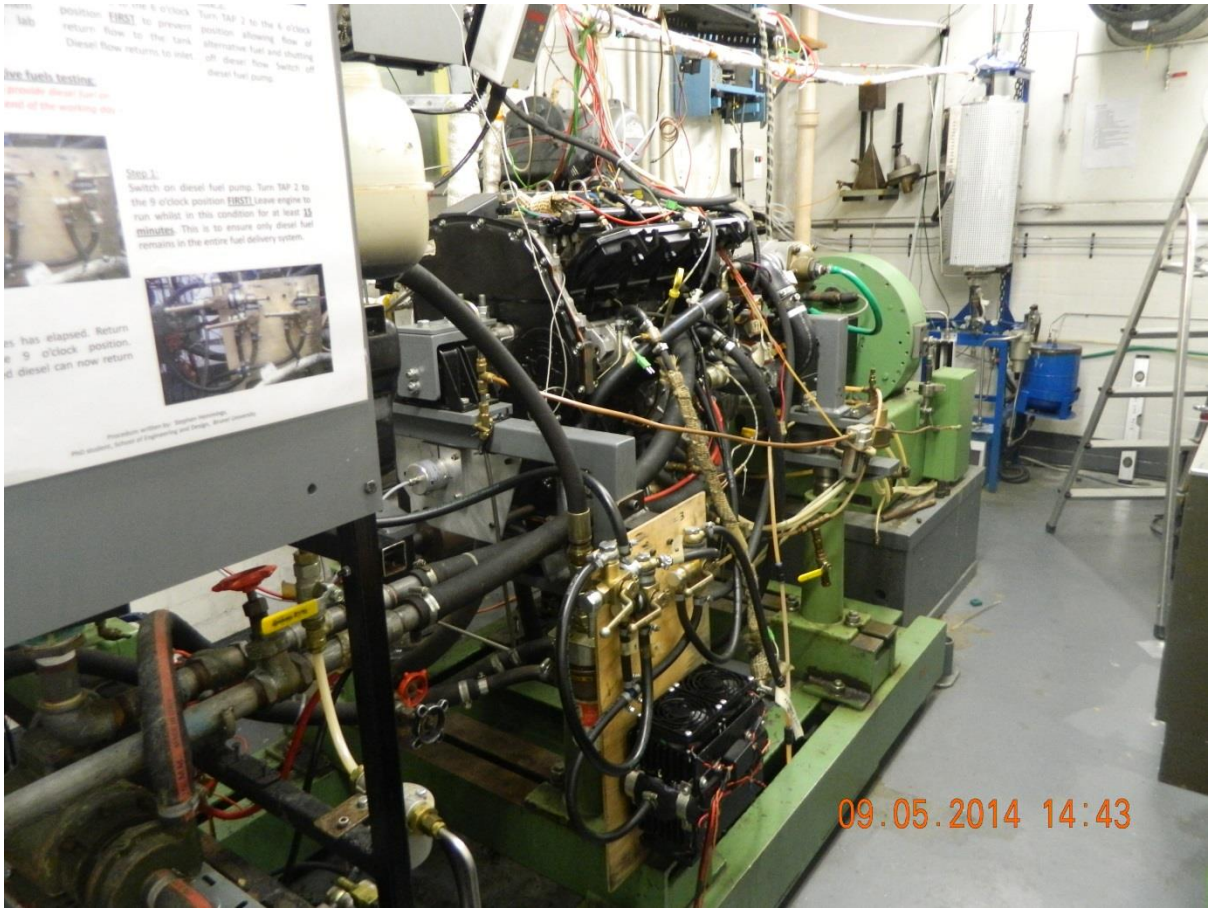

Figure (4.4): four cylinder 2 litre Ford Puma Zetec 16 valves High Speed Direct Injection (*HSDI*) diesel engine at Brunel University engine lab.

Chapter 5

Characterising Wiebe Equation for Heat Release Analysis based on Combustion Burn Factor (C_i)

5.1 Introduction

There is no doubt that the existing correlations in engine combustion analysis are very useful for engine research teams in terms of better understanding of engine chemical and physical processes. Wiebe and Wolfer equations are good examples of correlations which were studied in this chapter and chapter 7. Correlations can help researchers to understand the physical relation between the parameters and enable them to categorize the parameters in several groups which results in reducing of number of experiments and also cost of engine combustion research.

Dimensionless parameters which are ratio of several physical parameters can be used along with correlations to provide double benefit of using correlations. Due to the complication of combustion process and also number of the parameters which are involved during the combustion process, in some cases it is almost impossible to analyse the engine combustion without using dimensionless parameters. Consequently dimensionless parameters not only facilitate engine research but also enable researchers to extract more results from experiment data.

Dimensionless parameters are well known in thermodynamics and have been used extensively in different subject areas but not many correlations exist in engine heat release analysis. It could be associated to complication of engine combustion process which cause research teams to consider experimental approaches only rather than analytical solutions.

In this work an analytical approach was considered to discuss and also highlight the benefits of using Wiebe equation. This correlation has been used as a strong tool to calculate Burn fraction (*f*) in diesel engine combustion for more than 60 years since Ivan Ivanovitch Wiebe published his function in 1952.

Correlations are characterized by number of coefficients which are the constants and need to be calculated prior to calculation. The main problem arises when the value of these constants have not been calculated accurately. The effect of using inaccurate value of constants can be significant and result in incorrect calculation. In this work the effect of constants in Wiebe equation were studied and compared. New methods were proposed to calculate accurate value for constants. A new modified form of Wiebe equation was proposed and the benefits of using this form is compared to original form of Wiebe equation were discussed. A dimensionless parameter called Combustion burn factor (C_i) was introduced and the benefits of using C_i was discussed. It was also concluded that Wiebe equation is function of C_i only [86].

5.2.Modified Wiebe Equation

The Wiebe equation in general form in terms of crank angle degree is as follows:

$$f = \exp[-a(\frac{\theta-\theta_o}{\Delta\theta})^{m+1}] \qquad (5.1)$$

The crank angle corresponding to 50% of cumulative amount of heat released during combustion process corresponds to the condition of $f = 0.5$ and $\theta = \theta_{50}$ so equation (5.1) can be rewritten as:

$$0.5 = \exp[-a(\frac{\theta_{50} - \theta_o}{\Delta\theta})^{m+1}] \tag{5.2}$$

Equation (5.2) applies to the centre of combustion, taking natural logarithm to both sides of Equation (5.2) results in Equation (5.3).

$$\ln 0.5 = -a(\frac{\theta_{50} - \theta_o}{\Delta\theta})^{m+1} \tag{5.3}$$

Rearranging equation (5.1) and taking natural logarithm on both sides results in equation (5.4)

$$\ln(1 - f) = -a(\frac{\theta - \theta_o}{\Delta\theta})^{m+1} \tag{5.4}$$

Dividing equation (5.4) by equation (5.3) and further simplification results in the proposed modified version of Wiebe equation (5.5), where the burn fraction f is expressed in terms of θ, θ_o, θ_{50} and m.

$$f = 1 - \exp[(\ln 0.5)(\frac{\theta - \theta_o}{\theta_{50} - \theta_o})^{m+1}] \tag{5.5}$$

The modified version of the Wiebe equation has only one constant compared to the original Wiebe equation, and this constant can be determined against experimentally measured cylinder pressure data.

5.3.Determination of Instantaneous Form (*m*) and Efficiency (*a*) Factors

The cumulative heat release based on the first law of thermodynamics was obtained for all the engine operating conditions A1 to A30 shown in table (5.1).

Table (5.1): Engine operating conditions A1 to A30.

Experiment No.	Injection Timing degree bTdc	Injection pressure(Pa) $x10^5$	BMEP (Pa) $x10^5$	Θ_o ,Crank angle degree
A1	9	800	2.7	356.4
A2	9	1000	2.7	355.12
A3	9	1200	2.7	354.8
A4	6	800	2.7	358.09
A5	6	1000	2.7	358.05
A6	6	1200	2.7	357.4
A7	3	800	2.7	361.11
A8	3	1000	2.7	360.72
A9	3	1200	2.7	360.34
A10	0	800	2.7	363.98
A11	0	1000	2.7	363.72
A12	0	1200	2.7	363.37
A13	-2	800	2.7	367.08
A14	-2	1000	2.7	366.53
A15	-2	1200	2.7	365.91
A16	9	800	5	355.16
A17	9	1000	5	355.02
A18	9	1200	5	354.72
A19	6	800	5	357.97
A20	6	1000	5	357.75
A21	6	1200	5	357.3
A22	3	800	5	360.81
A23	3	1000	5	360.56
A24	3	1200	5	360.21
A25	0	800	5	363.62
A26	0	1000	5	363.34
A27	0	1200	5	363.22
A28	-2	800	5	366.23
A29	-2	1000	5	365.83
A30	-2	1200	5	365.44

The value of *m* was determined analytically at each time instant of the experimentally measured data by using the modified Wiebe equation (which has only one unknown *m* in equation (5.5)). By substituting the value of the determined '*m'* in equation (5.1), the unknown value, '*a'* was calculated for each time instant of the combustion period for a given experimental data. Thus it can be seen that the values for *a* and *m* in this work are determined differently without making any assumption as proposed in [3,52, 54- 56,59]. These values for *a* and *m* are actual values, thus they are denoted as *a(ac)* and *m(ac)* for subsequent analysis.

Besides the above described procedure, the value for *m* was also obtained through the fitting procedure described earlier in [54,62,127,128] by fixing the value of *a* to be 5 in equation (5.1) as proposed in [51,54,129,130]. The values of *a* and *m* obtained through this procedure will be denoted as *m(f)* and *a** respectively for subsequent analysis.

The values of *m(ac)* calculated using equation (5.5) at each crank angle position for condition A2 have been plotted against $\frac{\theta - \theta_o}{\Delta\theta}$ in figure 5.1 .

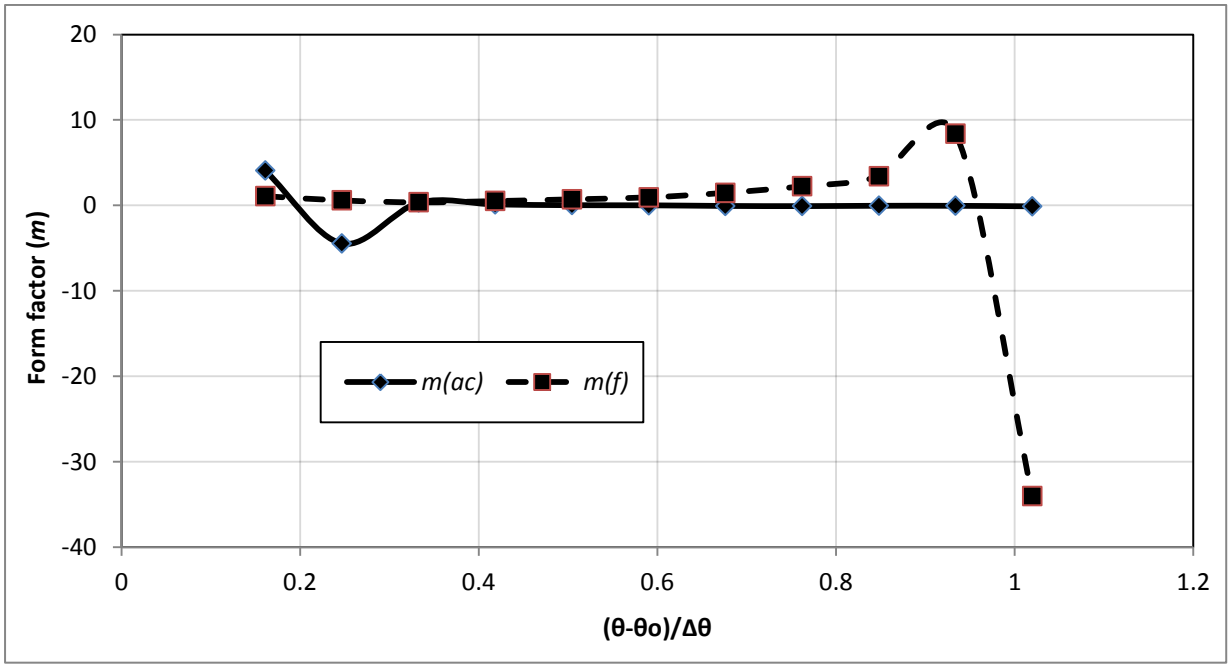

Figure (5.1): Variation of actual Form factor *m(ac)* and fitted value *m(f)* versus $(\theta-\theta_o)/\Delta\theta$ for the engine operating condition A2.

On the other hand the values of *m(f)* determined by the described fitting procedures for a constant value of a =5 are also plotted against $\frac{\theta-\theta_o}{\Delta\theta}$ in figure 5.1 . The assumed a^* value and the calculated values of *a(ac)* at each crank angle position for the condition A2 are plotted against $\frac{\theta-\theta_o}{\Delta\theta}$ in figure 5.2 .

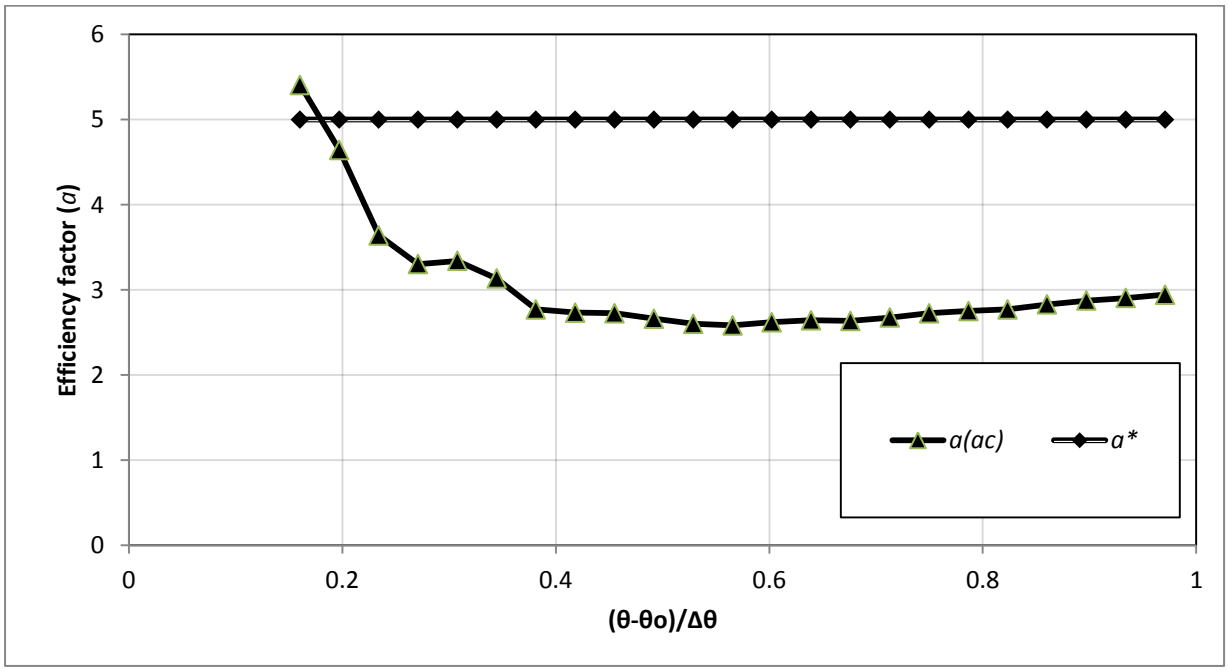

Figure (5.2): Variation of actual Efficiency factor *a(ac)* and chosen value a^* versus $(\theta-\theta_o)/\Delta\theta$ for the engine operating condition A2.

Figures 5.1 and 5.2 indicate that the variation in the actual values of $a(ac)$ and $m(ac)$ tend to become steady during the later stages of combustion, and this can be attributed to the effects of fluctuations in ignition at the beginning of combustion process. The value of *a(ac)* shows some fluctuations during the early stages of combustion and attain almost a constant value for the rest of combustion. In contrast the values of *m(f)* shows no fluctuation in the beginning, but at later stages of combustion, *m(f)* varies significantly compared to the *m(ac).* This large

difference between *m(f)* and *m(ac)* may be attributed to fixing the value of *a**. Since the value of *a** is fixed to a constant value, *m(f)* undergoes fluctuations to match the experimental data with the theoretical burn fraction curve. Similar trends were observed for all other engine operating conditions. These differences between *m(f)* and *m(ac),* and also between *a(ac)* and *a** shows the deviation of *m(f)* and *a** with respect to the actual value that is required by the combustion and this results in an error on the calculated value of *f*.

5.4.Determination of Overall Form and Efficiency Factors for entire combustion

By having accurate values for *a* and *m* at each time instant during combustion process, it is also possible to obtain one value for *a* and *m* for the entire combustion period. The overall value for *m* for the entire combustion period can be elucidated using equation (5.6), which is obtained by rearranging the modified Wiebe equation (5.5).

$$\ln\left(\frac{\ln(1-f)}{\ln(0.5)}\right) = (m+1)\ln\left(\frac{\theta-\theta_o}{\theta_{50}-\theta_o}\right) \qquad (5.6)$$

Equation (5.6) is of the form of a straight line with a slope of *m+1* with zero y intercept. The variation of $\ln\left(\frac{\ln(1-f)}{\ln(0.5)}\right)$ against $\ln\left(\frac{\theta-\theta_o}{\theta_{50}-\theta_o}\right)$ is shown in figure 5.3 .

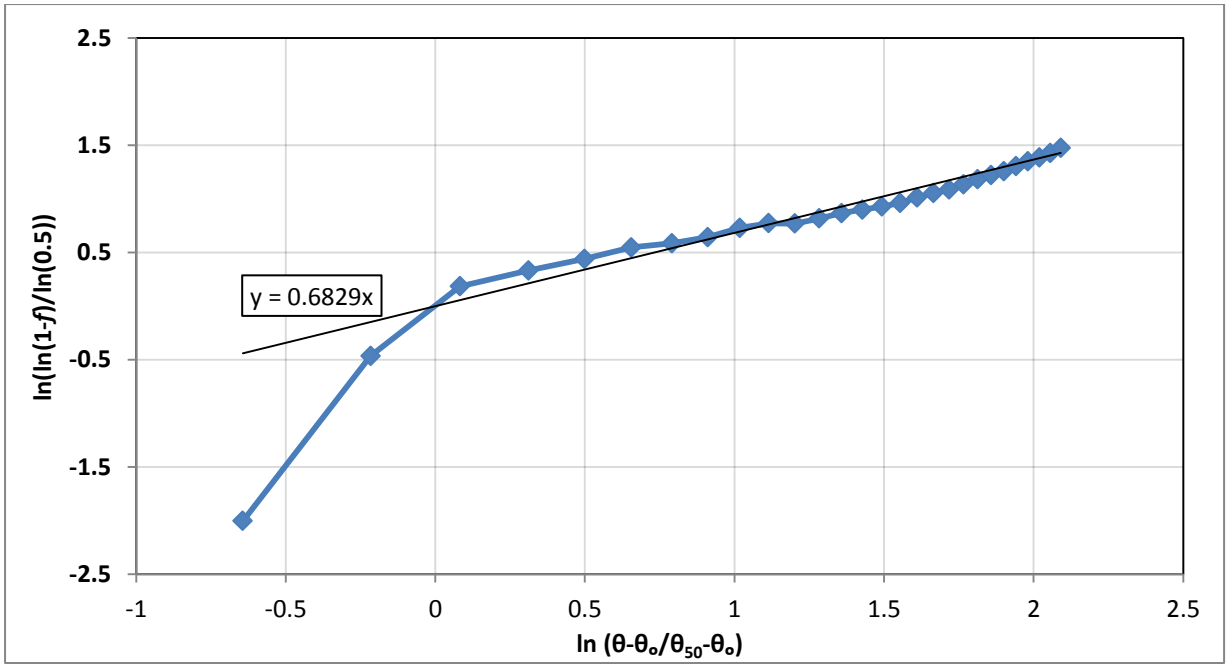

Figure (5.3): Determination of one overall value of the form factor by taking the slope of $\ln(\frac{\ln(1-f)}{\ln(0.5)})$ and $\ln(\frac{\theta-\theta_o}{\theta_{50}-\theta_o})$.

For a given operating condition of (A2), the slope of 0.68 was obtained and this corresponds to the value of $m=-0.32$. Similarly the overall value for *a* can be obtained by rearranging Wiebe equation, to express it in a linear form with *a* as the slope of equation (5.7) and zero Y intercept.

$$-\ln(1-f)=a(\frac{\theta-\theta_o}{\Delta\theta})^{m+1} \qquad (5.7)$$

Plotting the values of $-\ln(1-f)$ and $(\frac{\theta-\theta_o}{\Delta\theta})^{m+1}$ provides the value for *a* as shown in figure 5.4 , the overall value for *a* corresponding to the A2 condition was found to be 2.9.

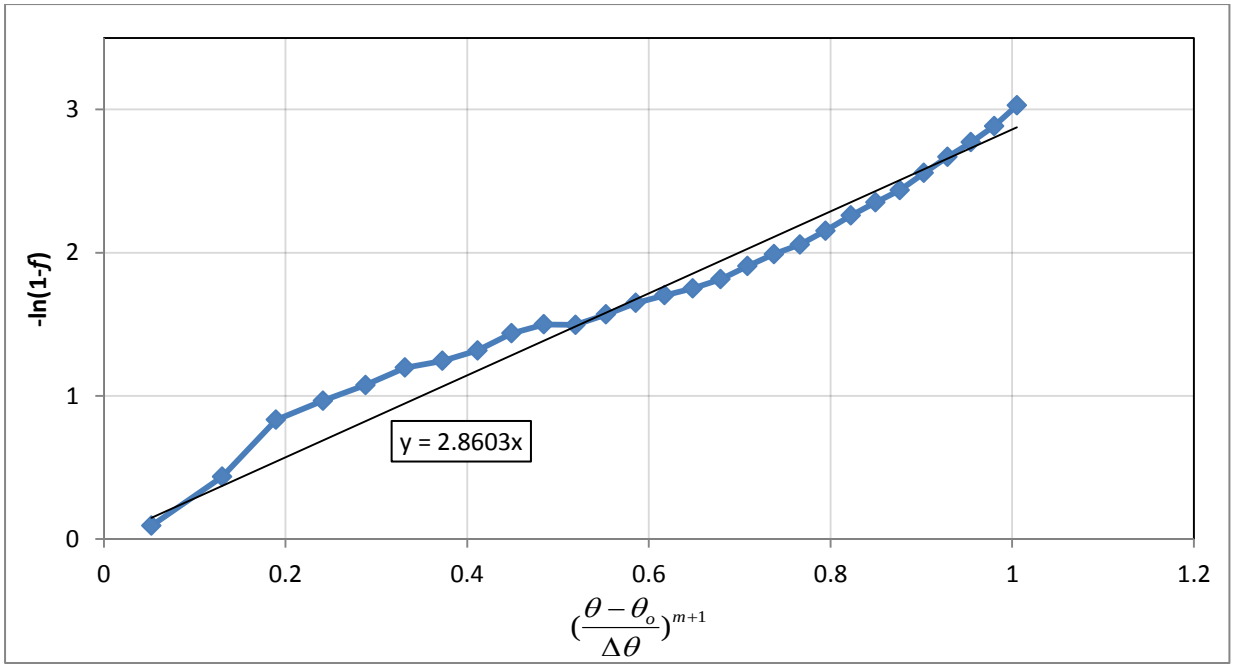

Figure (5.4): Determination of one overall value of the efficiency factor by taking the slope of $-\ln(1-f)$ and $(\frac{\theta-\theta_o}{\Delta\theta})^{m+1}$.

5.6.Comparison of theoretical models

Figure 5.5 presents the comparison of the experimental data against four sets of theoretically determined *f* obtained through different methods.

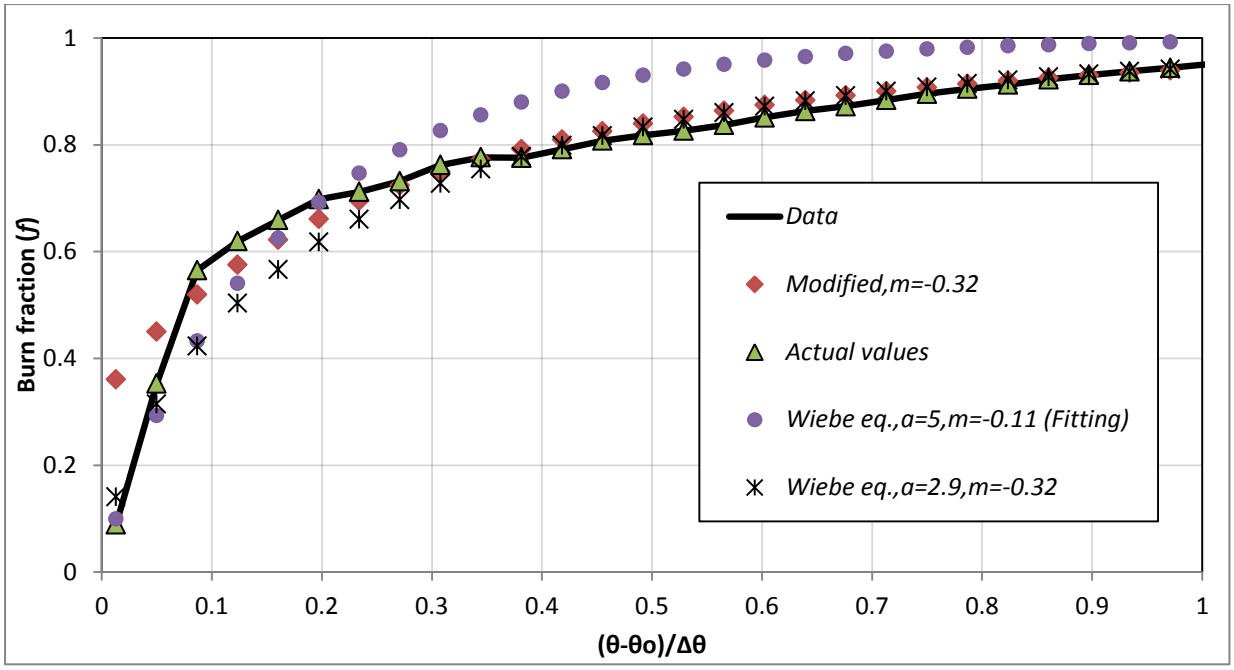

Figure (5.5): Variation of *f* against $\frac{\theta-\theta_o}{\Delta\theta}$, for four set of data along with experimental data, for the engine operating condition A2.

It can be seen that the Wiebe equation with the actual values fits the experimental data with a difference of less than 1% at each time instant for the entire combustion period. The modified Wiebe equation provides an average difference of 3.3% between the calculated burn fraction and experimental data beyond the range $\frac{\theta-\theta_o}{\Delta\theta} > 0.05$. For the early stages of combustion when $\frac{\theta-\theta_o}{\Delta\theta} < 0.05$ large differences were found between calculated values and experimental data and it could be due to fluctuations in ignition and unsteady nature of early flame development process. Wiebe equation with one overall value (*m=-0.32* and *a=2.9*) obtained from figure 5.3 and figure 5.4 fits the experimental data well for the combustion phase $\frac{\theta-\theta_o}{\Delta\theta} > 0.4$ and $\frac{\theta-\theta_o}{\Delta\theta} < 0.05$. The calculated values deviated from experimental data in the region between $0.06 < \frac{\theta-\theta_o}{\Delta\theta} < 0.4$ and the average difference between theoretical and

experimental data was found to be 6.45% for entire combustion period. The theoretical values of *f* obtained from the Wiebe equation using the fixed value of *a** and with the one overall value for form factor *(m=-0.11)* obtained by fitting procedure provides an underestimation of *f* in the region $\frac{\theta-\theta_o}{\Delta\theta} < 0.2$ and overestimation of *f* in the region $\frac{\theta-\theta_o}{\Delta\theta} > 0.2$ and the average difference between theoretical and experimental data was found to be 10.16% for the entire combustion period. In summary, the Wiebe equation with actual values fits better with experimental data, followed by modified Wiebe equation, Wiebe equation with (*m=-0.32* and *a=2.9*) and Wiebe equation with (*m=-0.11* and *a*=5*).

The error induced on the theoretical determined *f* due to the values of *a* and *m* that were obtained through two different procedures will be analysed and compared in the next section.

5.7.Burn Fraction Error Analysis

The error induced in the obtained values of *a* and *m* and their effects on the theoretical calculation of *f* has been be analysed and discussed in this section by differentiating equation (5.1), with respect to *a* and *m*, which results in equation (5.8) and (5.9) respectively.

$$df/da = \left(\frac{\theta-\theta_o}{\Delta\theta}\right)^{m+1}\left(e^{-a\left(\frac{\theta-\theta_o}{\Delta\theta}\right)^{m+1}}\right) \tag{5.8}$$

$$df/dm = \left(a.\ln\left(\frac{\theta-\theta_o}{\Delta\theta}\right)\right)\left(\frac{\theta-\theta_o}{\Delta\theta}\right)^{m+1}\left(e^{-a\left(\frac{\theta-\theta_o}{\Delta\theta}\right)^{m+1}}\right) \tag{5.9}$$

$$\frac{df/dm}{df/da} = \frac{\left(a.\ln\left(\frac{\theta-\theta_o}{\Delta\theta}\right)\right).\left(\frac{\theta-\theta_o}{\Delta\theta}\right)^{m+1}\left(e^{-a\left(\frac{\theta-\theta_o}{\Delta\theta}\right)^{m+1}}\right)}{\left(\frac{\theta-\theta_o}{\Delta\theta}\right)^{m+1}.\left(e^{-a\left(\frac{\theta-\theta_o}{\Delta\theta}\right)^{m+1}}\right)} = a.\ln\left(\frac{\theta-\theta_o}{\Delta\theta}\right) \tag{5.10}$$

Equation (5.10) is obtained by dividing equation (5.9) by equation (5.8), which shows that the error on f with respect to *m* divided by error on f with respect to *a* at each point is not a function of *m* and this value in equation (5.10) is called *error fraction (Er).*

The value of $\frac{\theta-\theta_o}{\Delta\theta}$ ranges between 0 and 1, and it is equal to ≈0 at the start of fast burning and equal to ≈1 at the end of fast burning. The value of $\ln\left(\frac{\theta-\theta_o}{\Delta\theta}\right)$ is a negative value and *a* is a positive value so the *error fraction (Er)* in equation (5.10) is a negative value, which consequently indicates that equation (5.8) and equation (5.9) will always have opposite signs. The negative sign indicates that the error on f with respect of *a* and *m* have opposite effect, consequently they have no additional effects on f which can cause to reduce the net error. This effect has been shown in figure 5.6 where it clearly indicates the induced error on f with respect to the variations of *a* and *m* values are positive and negative respectively.

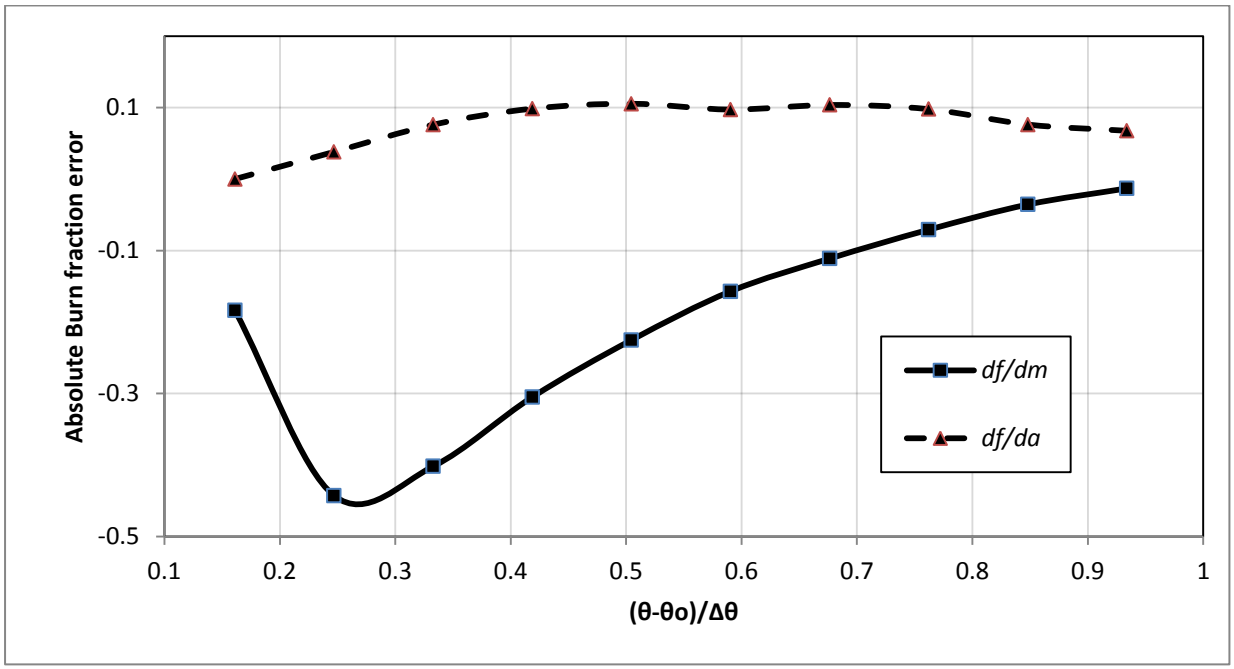

Figure (5.6): Variation of *f* for different value of $(\theta-\theta_o)/\Delta\theta$ with respect to *a* and *m* for the engine operating condition A2.

The positive error on *a* results in an overestimation of f and the positive error on *m* results in an underestimation of f. According to figure 5.6 the absolute value of error on f with respect to *m* is greater than *a*, consequently the value of f is more affected by the variation of *m* compared to *a*. This indicates that the value of *m* needs to be calculated precisely. This is one of the reasons for assuming the value for *a* and fitting the heat release data to get the value for *m* in the published literatures [51,52,54,129,130].

The *Error function (E)* calculates the total error induced on f with respect to *a* and *m* values as shown in equation (5.11). This total error is equal to the sum of equation (5.8) and equation (5.9).

$$E = [1 + a.\ln(\frac{\theta - \theta_o}{\Delta\theta})].[(\frac{\theta - \theta_o}{\Delta\theta})^{m+1}[e^{-a(\frac{\theta-\theta_o}{\Delta\theta})^{m+1}}] \qquad (5.11)$$

The effect of total error induced on f due to *a* and *m* values of equation (5.11) are shown in figure 5.7 and these values are plotted against $\frac{\theta - \theta_o}{\Delta\theta}$.

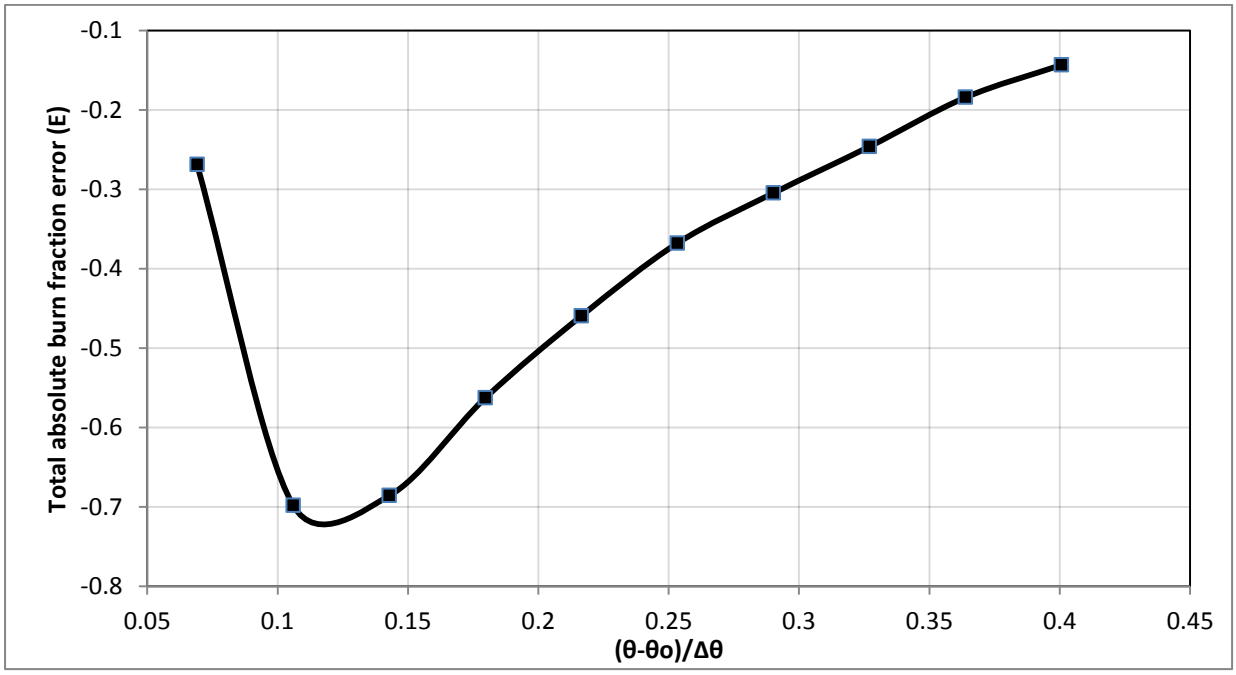

Figure (5.7): Total absolute Burn fraction (E) for different value of $(\theta-\theta_o)/\Delta\theta$ with respect to a and m for the engine operating condition A2.

According to figure 5.7 there is only one maximum absolute error value and this value is a function of a and m. The values of E were calculated for different values of a and m and the maximum absolute error value (E_{max}) for each set of a and m values were plotted against m in figure 5.8 .

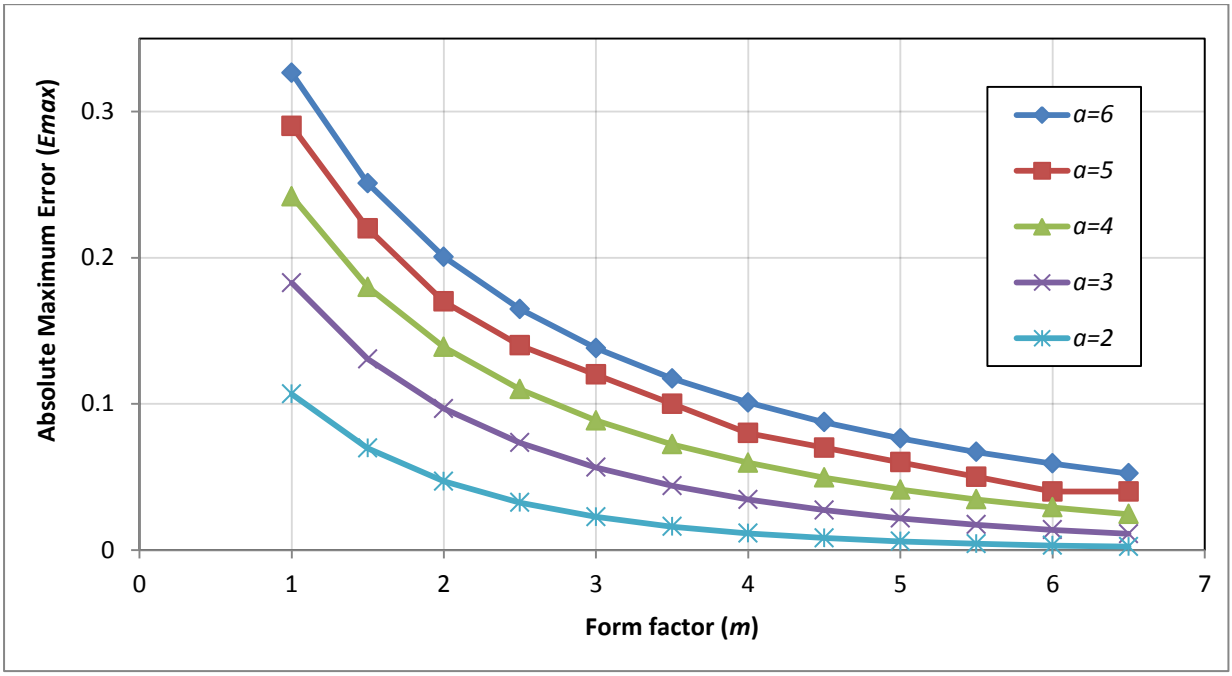

Figure (5.8): Variation of E_{max} for different values of a and m.

The magnitude of E_{max} was found to be the highest for a combination of high values of a and for low values of m. The magnitude of E_{max} was also found to be the lowest for a combination of high m values and low a values. The variation of E_{max} with respect to m is larger than a, therefore m can influence E_{max} significantly compared to a.

Figure 5.6 also indicates that over estimation of a and m values results in underestimation of f due to significant effect of m with respect to a and vice versa. The analysis presented in

figures 5.6 and 5.8 indicate that the values of the burn fraction are affected more by the value of *m* compared to the value of *a*.

Similar to the error function of Wiebe equation (5.11), the error function has also been obtained for the modified Wiebe equation, equation (5.12).

$$E = -(\ln(0.5)).(\ln(\frac{\theta-\theta_o}{\theta_{50}-\theta_o})).(\frac{\theta-\theta_o}{\theta_{50}-\theta_o})^{m+1}.\exp(((\ln(0.5)).(\frac{\theta-\theta_o}{\theta_{50}-\theta_o})^{m+1}) \qquad (5.12)$$

The modified Wiebe equation is not a function of *a*, consequently for a given *m* value, the error function for all values of *a* is a constant value. Figure 5.9 presents the variation of E_{max} against *m* values ranging from 1 to 6.5, and for two typical values for *a* (5 and 6.908), which were mentioned earlier in this work.

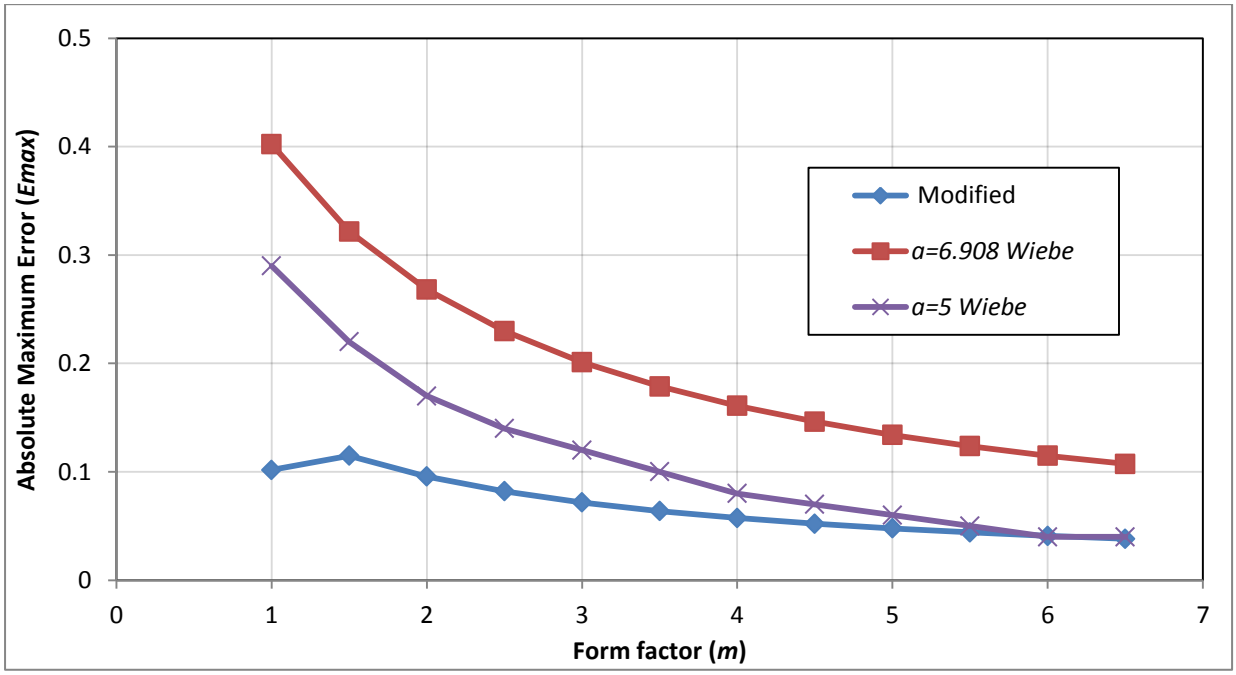

Figure (5.9): Variation of E_{max} against *m* for *a*=5 and *a*=6.908 for Wiebe equation and modified Wiebe equation.

Figure 5.9 indicates that the modified Wiebe equation produces less error when compared to Wiebe equation with the most commonly assumed values of *a*. The differences between the

error values of Wiebe equation and the modified version of Wiebe equation is more significant for lower *m* values and the error difference minimises as the *m* value increases.

5.8.Combustion burn factor (C_i) and heat release rate analysis

The exponential term of the modified Wiebe equation contains parameters such as θ, θ_o *and* θ_{50} and these parameters are combined to be expressed in the form of a non-dimensional parameter $\frac{\theta-\theta_o}{\theta_{50}-\theta_o}$. This new non-dimensional parameter is called the *combustion burn factor* in the subsequent text, and this factor represents the combined effects of θ_o, θ_{50} and θ of each combustion condition and it is denoted by the notation C_i. Substitution of this *combustion burn factor* C_i in the modified Wiebe equation results in equation (5.13), and it can be seen that the burn fraction f is only a function of C_i.

$$f = 1 - \exp[(\ln 0.5)C_i^{m+1}] \tag{5.13}$$

Equation (5.14) can be used to calculate the value of C_i at the start (where $f = 0.05$) and the end (where $f = 0.95$) for fast burning in terms of *m* as:

$$C_i = \left(\frac{\ln(1-f)}{\ln(0.5)}\right)^{\frac{1}{m+1}} \tag{5.14}$$

At the end of fast burning the value of C_i can be expressed as $C_i = (4.32)^{\frac{1}{m+1}}$ and the corresponding value of C_i for the start of fast burning can be expressed as $Ci = (0.07)^{\frac{1}{m+1}}$.

Since the newly defined non-dimensional parameter *combustion burn factor (C_i)* is the only parameter that affects the burn fraction and it will be a valuable parameter to study the heat release rate analysis. Several details about the combustion process can be obtained when the heat release rate is plotted against the non-dimensional combustion burn factor C_i.

Many investigations have been carried out to study the effects of combustion and emission process with respect to θ_o and θ_{50} independently. In this work the combination effect of these parameters on diesel engine combustion will be considered. The benefits of using C_i for the heat release analysis have been discussed in the subsequent section. Figure 5.10 shows the variation in *AHRR* plotted against instantaneous crank angle for three different engine operating conditions A4, A7 and A10.

Since these three conditions have different injection timing, the difference between θ_o and θ_{50} for each condition are different, and the corresponding start of combustion and the end of combustion are different for each of these conditions. Consequently it makes difficult to compare the curves for different conditions. Using the non-dimensional C_i to construct *AHRR* instead of instantaneous crank angle (θ) can produce another form of apparent heat release chart (figure 5.11), which provides more information about the combustion and it is easier to compare the data from different operating conditions.

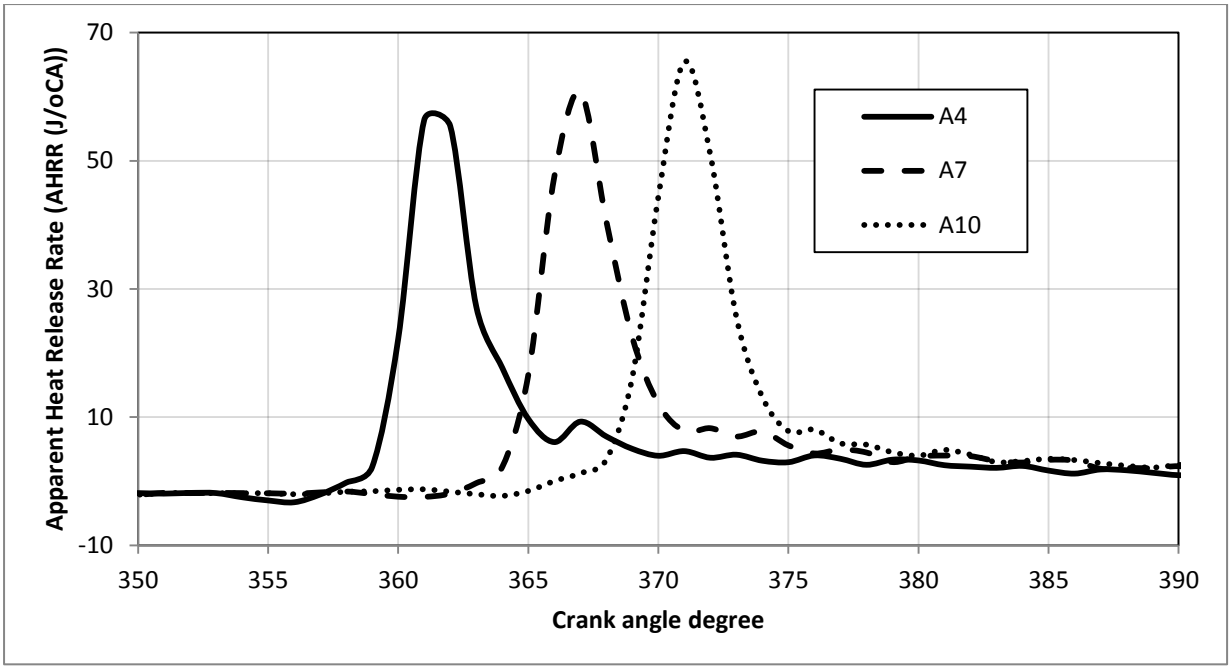

Figure (5.10): Apparent heat release rate against instantaneous crank angle *(θ)* at different engine operating conditions A4, A7 and A10.

In figure 5.10 , it is not clear where the centre of combustion is and the exact location where the combustion is taking place with respect to centre of combustion. These aspects can be viewed in figure 5.11 by plotting *AHRR* against C_i. At any instant on the *AHRR-Ci* chart it is possible to extract information about where the temporal location of combustion is with respect to the start of combustion, the end of combustion and the centre of combustion. As described below:

- $C_i=0$ corresponds to start of combustion so all the *AHRR-Ci* charts are corrected automatically to have the same starting point and it makes easier to compare the charts at any time in terms of apparent heat release rate.
- C_i = 1 corresponds to centre of combustion of the *AHRR-Ci* chart. The apparent heat release rate value at the centre of combustion can be read directly from this chart. Any temporal location on the *AHRR-*C_i chart can be identified with respect to start of combustion, end of combustion and centre of combustion.

- C_i corresponding to end of fast combustion is known (end of fast combustion is based on CA95), consequently the value of apparent heat release rate is known at the end of fast combustion.

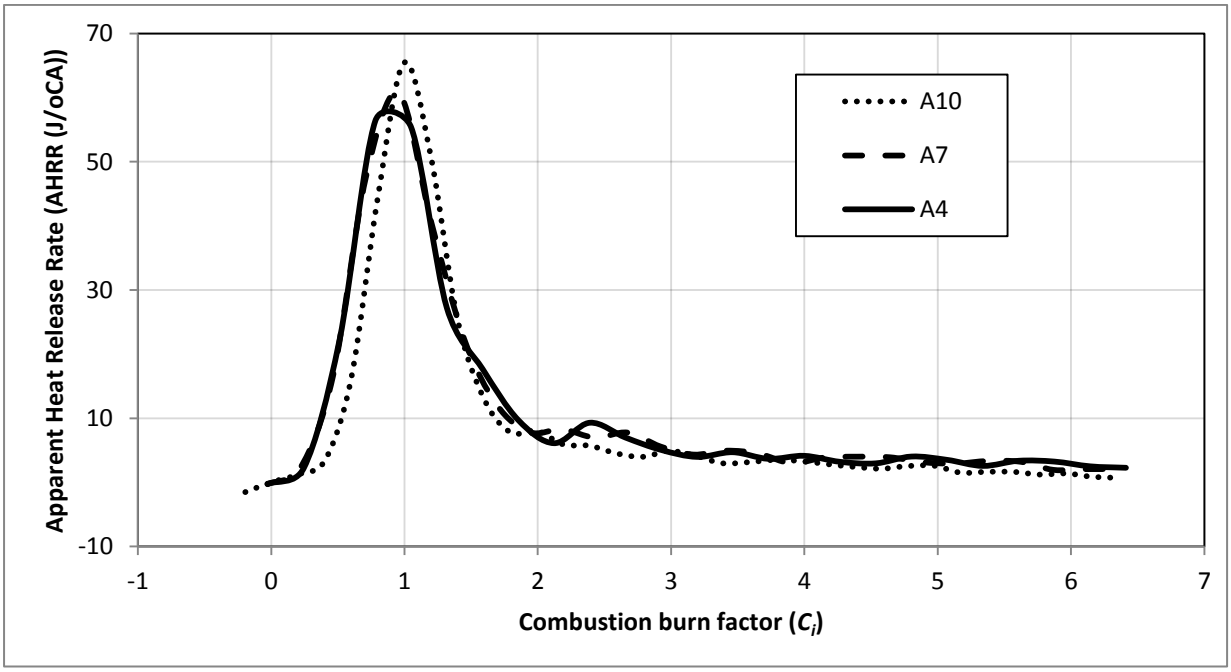

Figure (5.11): Apparent heat release rate expressed in terms of non-dimensional combustion burn factor *(C_i)* at conditions A4, A7 and A10.

Since the value of C_i corresponding to any value of f is known, the magnitude of apparent heat release rates can be determined directly from the chart for any specific location of combustion and the heat release rate values can be compared against different engine operating conditions. The raising slope of the *AHRR-C_i* chart provides information about the relative level of pre-mixing in the combustion process when compared against different engine operating conditions. This helps with the understanding of the variation in NO_x and soot emissions under different engine operating conditions.

5.9.Conclusions

A new method was proposed to determine the accurate values of the *form factor* (*m*) and *efficiency factor (a)* of the Wiebe equation analytically. This method results in good accuracy of estimating the burn fraction. The maximum absolute error induced on *f* due to these constants was found to be the lowest for a combination of high *m* values and low *a* values.

A modified form of Wiebe equation has been developed in this work, and this equation is benefitted by having only one constant, *form factor* (*m*). The constant *m* was calculated directly by comparing the modified version of Wiebe equation against the experimentally determined heat release data.

The development of the modified Wiebe equation resulted in the identification of a new non-dimensional parameter, *combustion burn factor* C_i. The burn fraction f was found to be dependent only on C_i. The value of C_i at the start of combustion, centre of combustion and end of combustion were found in terms of *m*. The raising slope of the *AHRR*-C_i is related to the level of pre-mixing in the combustion process, which can help with the understanding of NO_x and soot formation process in diesel engines.

Chapter 6

Determination of specific heat ratio and error analysis for engine heat release calculations

6.1.Introduction

Heat release analysis has been used as a solid tool to study engine combustion by engine research community [131-135]. Heat release analysis generally starts by measuring instantaneous in-cylinder pressure by accurate pressure transducers and plotting in-cylinder pressure against the crank angle. A typical measurement system which is almost similar system that was used in this work is shown in figure 6.1 .

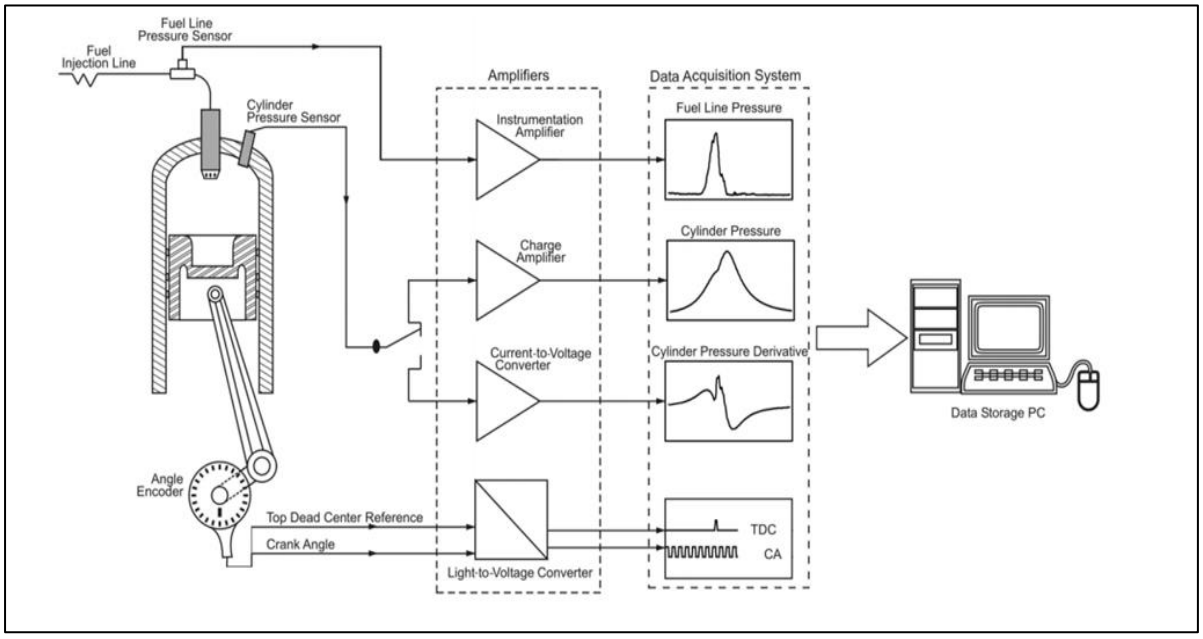

Figure (6.1). A typical engine measurement system.

Pressure transducers technology was improved over the years since the internal engine was invented. Parallel to development of engines and in result of that increase the running engine

speed, the analogue transducers were not able to measure pressure data accurately. Piezoelectric pressure transducers were developed to collect accurate in-cylinder instantaneous pressure measurements in high speed engines in mid-seventies. This generation of pressure transducers were enhanced the accuracy of pressure measurements significantly. A typical Piezoelectric pressure transducer is shown in figure 6.2.

Figure (6.2): Pressure transducer type: Kistler 6125A.

The benefits of using modified Wiebe equation was discussed in chapter 5. It was shown that the exponential term of the modified Wiebe equation contains parameters such as θ, θ_0 and θ_{50} and these parameters are combined to be expressed in the form of a non-dimensional parameter. This non-dimensional parameter was called the combustion burn factor (C_i) and it represents the combined effects of θ_0, θ_{50} and θ of each combustion condition. It was concluded that C_i in equation (6.1) is the only parameter that affects the burn fraction and it would be a valuable parameter to study the heat release rate analysis.

$$f = 1 - \exp[(\ln 0.5)C_i^{m+1}] \qquad (6.1)$$

The benefits of using C_i for heat release analysis have been shown in chapter 5. It was found that C_i variation does not follow the variation of other two parameters θ_o and θ_{50} but it

simultaneously represents the effect of those parameters on the engine combustion and performance.

By considering the relation of C_i, it is evident that the only parameters which affect the value of C_i are θ_0 and θ_{50}. To calculate the location of θ_0 and θ_{50}, the values of *AHRR* for complete combustion period need to be calculated precisely. The error in determining the parameters θ_0 and θ_{50} can result in an error on C_i calculation. Therefore any error in the calculation of the *AHRR* results in an error in the determination of C_i.

In this chapter the errors associated with the determination of *AHRR* and the cumulative heat release (*Cum.Hrr*) from the measured cylinder pressure data and the assumed specific heat ratio (γ) was determined and compared. It is discussed that the value of γ affected the calculated *AHRR* more than the cylinder pressure. Overestimation of γ resulted in an underestimation of the peak value of the *AHRR* and vice versa, this occurred without any shift in the combustion phasing. A new methodology has been proposed to determine the instantaneous and mean value of γ for a given combustion. This new methodology has been applied to determine γ for a wide range of engine operating conditions and for different fuels [138].

6.2.Theory and Results

6.2.1.Determination of γ

The values of γ are normally obtained from the logarithmic plot of pressure and volume as discussed in figure 6.3 .

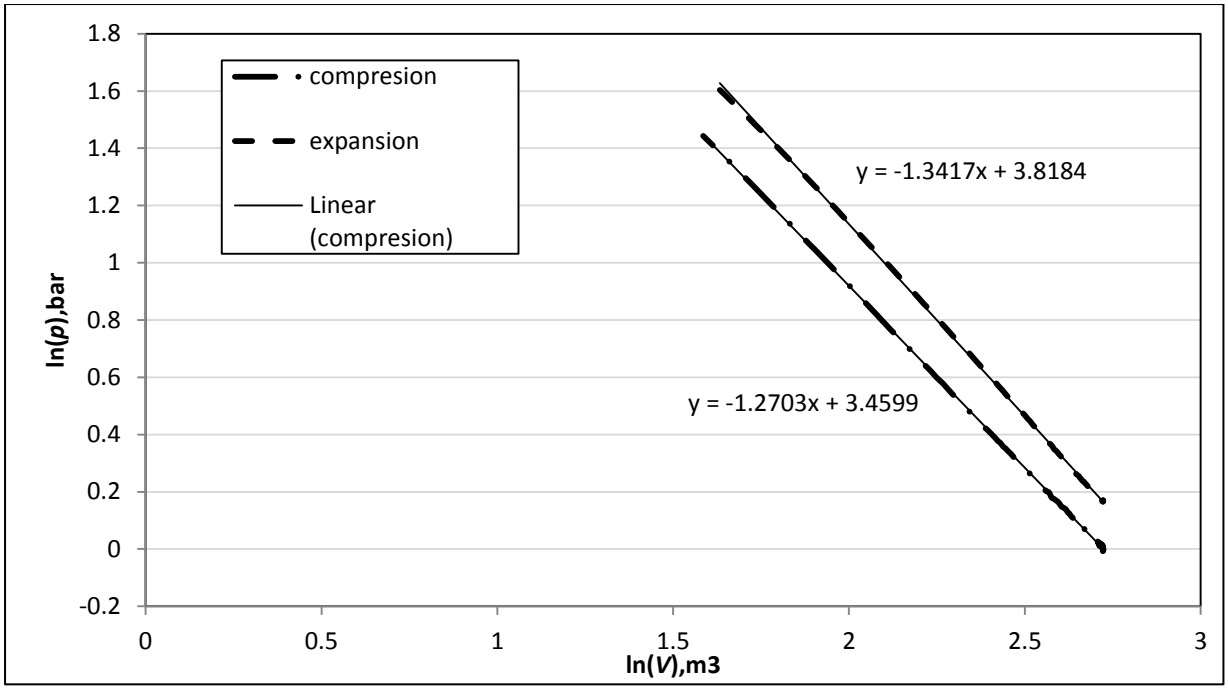

Figure (6.3): Variation of in-cylinder pressure against combustion volume. The average of the slope of compression and expansion line provide γ value (*pV* diagram).

This figure presents measured cylinder pressure versus cylinder volume on a logarithmic plot. The slope of two linear parts of chart during expansion and compression presents γ value for expansion and compression processes respectively; the average of the two provides appropriate γ value that can be used for heat release rate equations. The average γ values for all the experimental data have been presented in figure 6.4 . Engine operating conditions A1-A15 are listed in table (6.1).

Table (6.1): Engine operating conditions A1 to A15.

Condition	Injection Timing,BTDC (deg)	Injection Pressure (bar)	IMEP (bar)
A1	9	800	2.7
A2	9	1200	2.7
A3	6	1000	2.7
A4	6	1200	2.7
A5	3	800	2.7
A6	3	1200	2.7
A7	0	1200	2.7
A8	9	800	5
A9	9	1000	5
A10	9	1200	5
A11	6	800	5
A12	6	1000	5
A13	6	1200	5
A14	3	800	5
A15	0	800	5

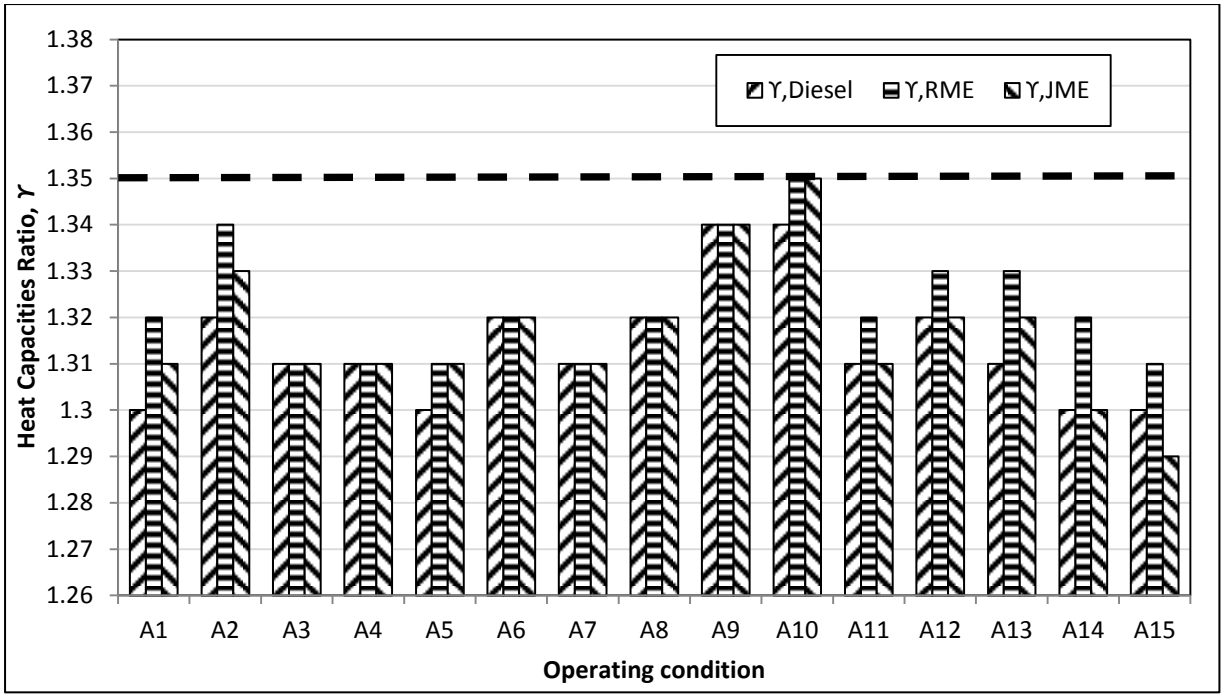

Figure (6.4): The value of specific heat ratio ϒ obtained using logarithmic *pV* diagram for the engine operation conditions A1-A15 described in table (6.1). The most commonly used value in literature ϒ=1.35 is plotted by dotted line.

As it was expected the data indicates that the average values of γ obtained for different fuels under different engine operating conditions were different. The difference in γ values are mainly related to variation in heat exchange and chemical composition of charge within the cylinder. These factors result in different cylinder pressure and temperature in the combustion chamber. Consequently the values for γ were different depending upon the operating condition. If the combustion duration is considered differently (CA5-CA90 or CA5-CA95) consequently this technique provides different values for γ. Also the calculated values of γ during compression and expansion periods are different as seen in figure 6.3 .

A new methodology has been proposed to determine the value of γ from the pressure and volume variations based on the centre of combustion location. The apparent heat release rate equation (3.8) for the centre of combustion can be rewritten as:

$$Ahrr_{50} = \frac{\gamma}{\gamma - 1}(p\frac{dV}{d\theta})_{50} + \frac{1}{\gamma - 1}(V\frac{dp}{d\theta})_{50} \quad (6.2)$$

Equation (6.2) can be re-arranged to determine the values of γ as described in equation (6.3).

$$\gamma = \frac{Ahrr_{50} + (V\frac{dp}{d\theta})_{50}}{Ahrr_{50} - (p\frac{dV}{d\theta})_{50}} \quad (6.3)$$

Substituting γ from equation (6.3) in equation (3.8), the *AHRR* can be expressed in terms of $AHRR_{50}$ and K_1 and K_2 as:

$$Ahrr = Ahrr_{50}.K_1 + K_2 \quad (6.4)$$

Where:

$$K_1 = \frac{V\frac{dp}{d\theta} + p\frac{dV}{d\theta}}{(V\frac{dp}{d\theta})_{50} + (p\frac{dV}{d\theta})_{50}} \quad (6.5)$$

and

$$K_2 = \frac{(V\frac{dp}{d\theta})_{50}.(p\frac{dV}{d\theta}) - (p\frac{dV}{d\theta})_{50}.(V\frac{dp}{d\theta})}{(V\frac{dp}{d\theta})_{50} + (p\frac{dV}{d\theta})_{50}} \quad (6.6)$$

The *AHRR* on the left hand side of equation (6.4) and the $AHRR_{50}$ term on the right hand side of equation (6.4) can be calculated by using equations (3.8) and (6.2) respectively. Substituting the values of *AHRR* from equation (3.8) in equation (6.4), the best instantaneous or mean value of γ can be obtained for each crank angle or for the entire combustion by minimising the residual value (*Residual Function)* of equation (6.7).

$$RF = [(\frac{\gamma}{\gamma - 1} p \frac{dV}{d\theta} + \frac{1}{\gamma - 1} V \frac{dp}{d\theta}) - (Ahrr_{50}.K_1 + K_2)] \quad (6.7)$$

Figure 6.5 indicates the variation of sum of square value of *RF* ($\sum RF^2$) plotted against different γ values for three fuels at the operating condition A3.

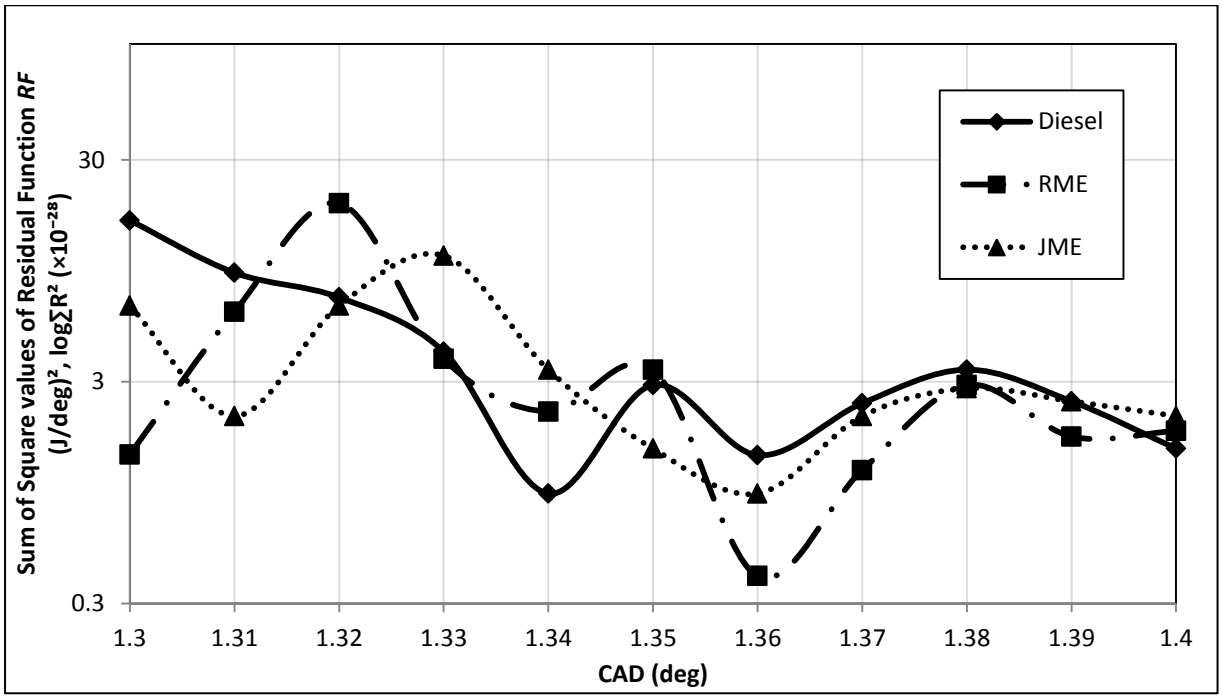

Figure (6.5): Variation of sum of square value of Residual Function (*RF*) for three fuels (diesel, Rapeseed Methyl Ester (*RME*) and Jatropha Methyl Ester (*JME*)) at operating conditions A3. The absolute minimum of each curve provide the best γ value.

It can be seen that according to figure 6.5 the value of γ =1.34 provides a minimum value for $\sum RF^2$ for diesel, and 1.36 for *RME* and *JME* at the corresponding engine operating condition. It was found that different values of γ did not influence the location of end of combustion. The obtained values for γ by using θ_{50} position of *AHRR* are plotted in figure 6.6.

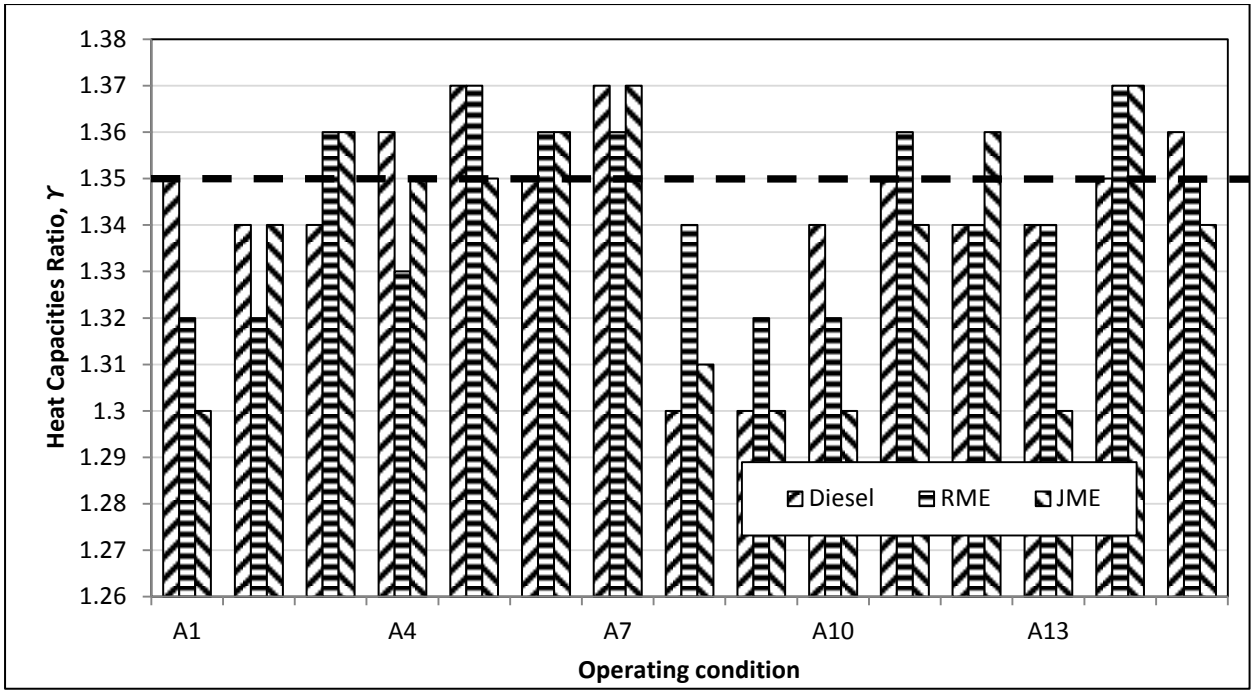

Figure (6.6): The values of γ obtained using the method based on centre of combustion (θ_{50}) position for the engine operating conditions A1-A15. The most commonly used value in literature ϒ=1.35 is plotted by dotted line.

Comparing two sets of values for γ using the proposed new method and the logarithmic *pV* diagram shows that by using the proposed method the value for γ is relatively higher for most of operating conditions as can be seen in figures 6.7a-c for diesel, RME and JME fuels respectively.

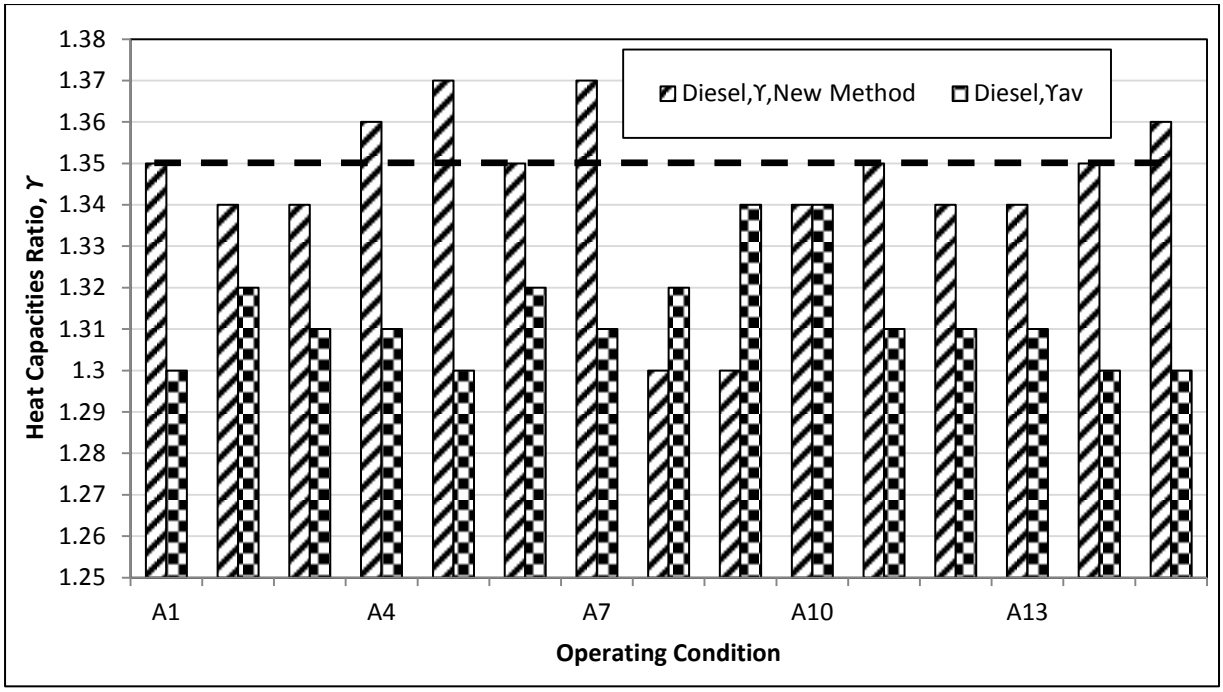

Figure (6.7a): Diesel fuel

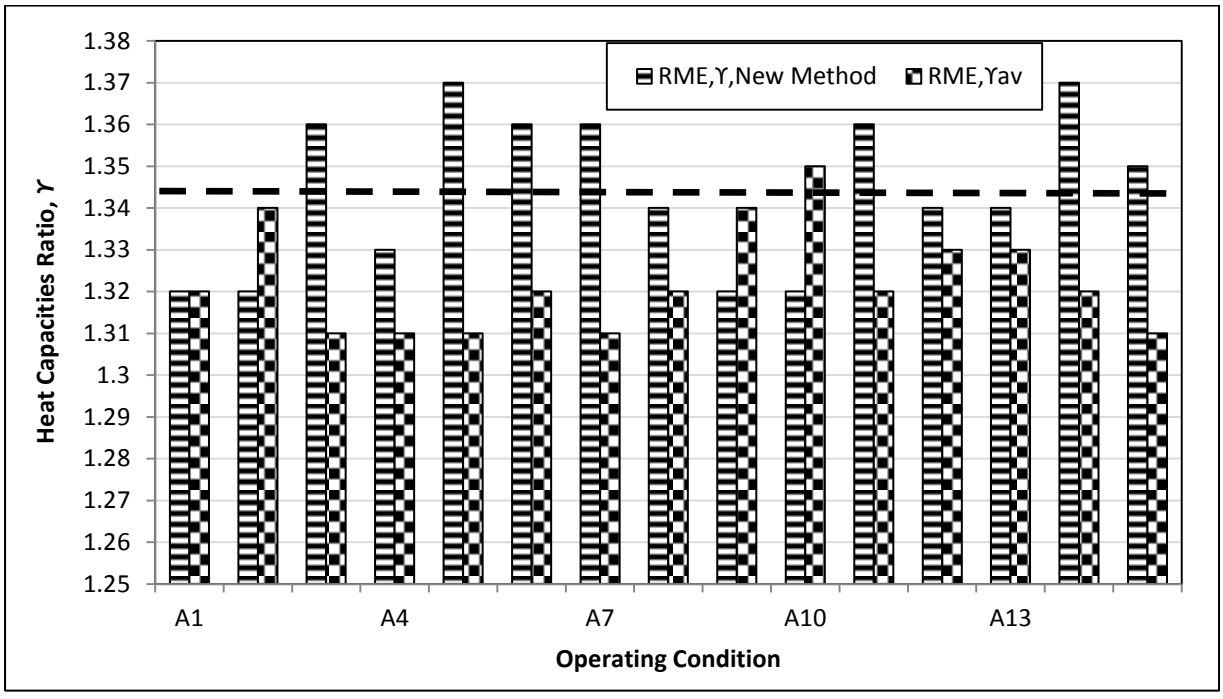

Figure (6.7b): *RME*

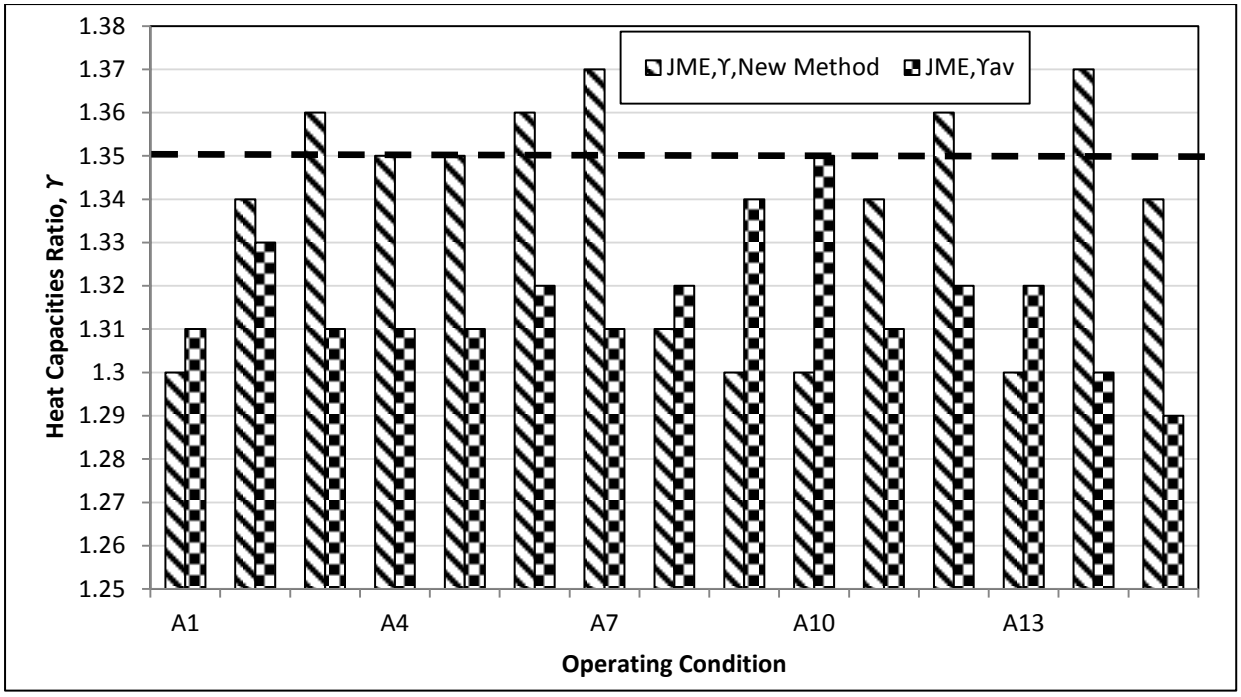

Figure (6.7c): *JME*

Figure (6.7a, 6.7b, 6.7c): The value of γ for the engine operating conditions A1-A15 for diesel fuel , RME and JME using the method based on centre of combustion (θ_{50}) position (new method) and *pV* diagram. The most commonly used value in literature γ =1.35 is plotted by dotted line. γ_{av} corresponds to average value of heat capacities ratio during expansion and compression periods.

Using logarithmic *pV* diagram revealed that γ values during the expansion period is higher than γ value during the compression period. But the proposed method is based on the calculated heat release rate and the centre of combustion during the combustion period; therefore the calculated values of γ are relatively higher compare to that which was obtained by using the logarithmic *pV* diagram. In general the calculated γ values from the proposed method are comparable to γ values obtained from the expansion period using logarithmic *pV* diagram and similar results were observed for *RME* and *JME*.

6.2.2.Error associated with pressure on *AHRR* and *γ*

The error associated with pressure measurements and its effect on the calculated *AHRR* will be discussed in the following section. If p_m is the measured pressure at each crank angle and if the actual pressure is p_a then the error associated with the pressure measurements can be expressed by a coefficient delta (δ), so the actual pressure can be expressed as:

$$p_a = \delta . p_m \tag{6.8}$$

Substituting the correct pressure value in the *Ahhr* equation (3.8) results in heat release rate expression $\left(\frac{dQ}{d\theta}\right)_a$ that is corrected for the errors associated with pressure measurements which is expressed as:

$$\left(\frac{dQ}{d\theta}\right)_a = \frac{\gamma}{\gamma - 1} p_a \frac{dV}{d\theta} + \frac{1}{\gamma - 1} V \frac{dp_a}{d\theta} \tag{6.9}$$

The subscript *a* is referred to actual value of heat release rate that has been corrected for pressure. Equation (3.8) and equation (6.9) can be combined to show that the actual value of heat release rate that is corrected for errors from pressure measurements can be expressed as the product of coefficient δ and the heat release rate from the uncorrected pressure data.

$$\left(\frac{dQ}{d\theta}\right)_a = \delta \left(\frac{dQ}{d\theta}\right)_m \tag{6.10}$$

The equation (6.10) shows that the *AHRR* data and the cumulative heat release follow the accuracy of measured pressure values.

The measured pressure data shows that the variation of *AHRR* and the cumulative heat release due to pressure is only in the range of $\pm$ 0.2%. This finding is in a good agreement with [87].

The other parameter that affects the calculated apparent heat release rate is the specific heat ratio γ. As it was discussed in the previous sections the specific heat ratio γ are normally

calculated by using the logarithmic slope of the *pV* diagram [91,93] and the value of γ can be obtained from equation (14).

$$\gamma = \frac{\ln(P_s / P_e)}{\ln(V_e / V_s)} \tag{6.11}$$

The subscripts *s* and *e* indicate the start and the end of the adiabatic compression or expansion interval. Applying the previously discussed error coefficient δ to the specific heat ratio will result in $(p_s)_a = \delta.(p_s)_m$ and $(p_e)_a = \delta.(p_e)_m$. Further substitution in equation (6.11) will result in equation (6.12).

$$\gamma_a = \frac{\ln(\delta.(p_s)_m / \delta.(p_e)_m)}{\ln(V_e / V_s)} = \gamma_m \tag{6.12}$$

Equation (6.12) shows that the linear error on pressure data does not affect the specific heat ratio γ, this finding is in a good agreement with the work reported in [93].

6.2.3.Effect of variation of γ on *AHRR*

In order to elucidate the specific heat ratio effects on the *AHRR*, equation (3.8) has been differentiated with respect to γ and it is expressed as:

$$\frac{d}{d\gamma}(Ahrr) = \frac{-1}{(\gamma-1)^2} p \frac{dV}{d\theta} - \frac{1}{(\gamma-1)^2} V \frac{dp}{d\theta} \tag{6.13}$$

By applying *p* and *V* values for each condition and applying the most commonly used value γ =1.35 , the absolute error value at each crank angle can be obtained. The error induced on *AHRR* for a small variation of 1 % of the value of the specific heat ratio γ has been presented

in figure 6.8 as a function of crank angle for diesel, *RME* and *JME* corresponding to condition A3.

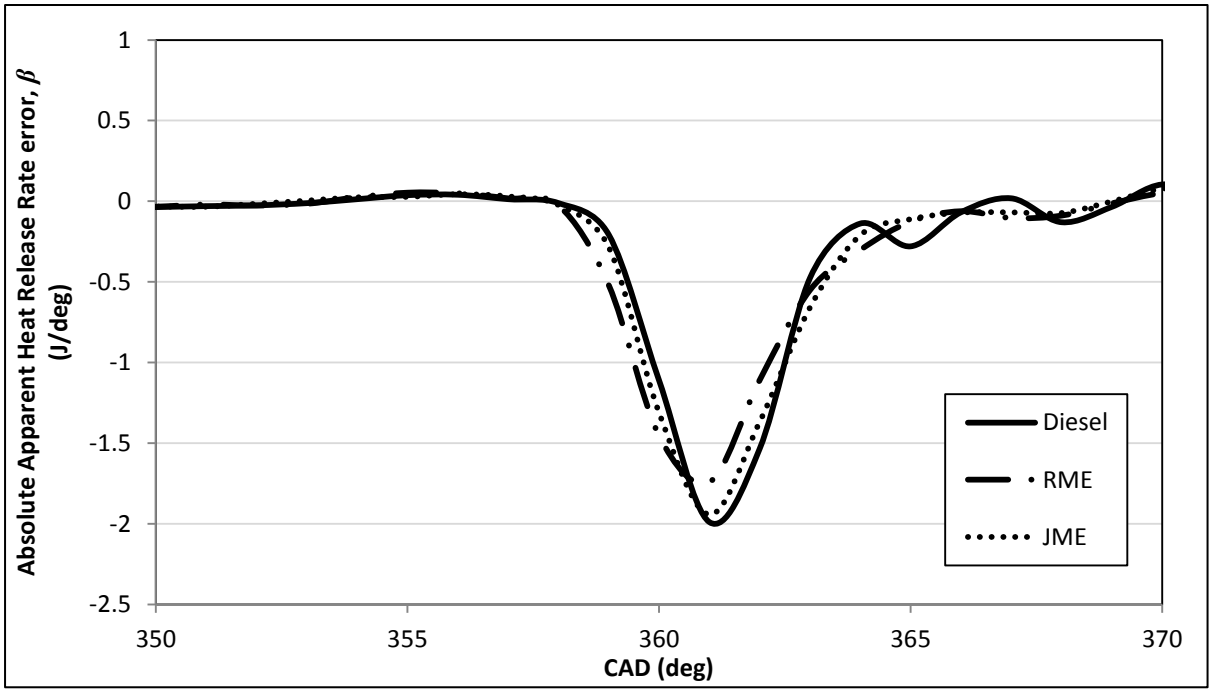

Figure (6.8): Absolute Apparent heat release rate error value, dϒ=0.01, for the engine operating condition A3.

The absolute error caused by the variation of specific heat ratio is denoted by the notation β. It is clearly evident from figure 6.8 that the maximum absolute error occurs at the crank angle where the *AHRR* has its highest magnitude. The negative value of absolute error indicates that an overestimation of γ value results in an underestimation of the *AHRR* and vice versa, this observation was in good agreement with the works presented in [93,95]. The peak value of *AHRR* varies with chemical composition of fuel and engine operating conditions, so eventually the peak value of β varies accordingly and this has been observed for the rest of the engine operating conditions as shown in figure 6.9 .

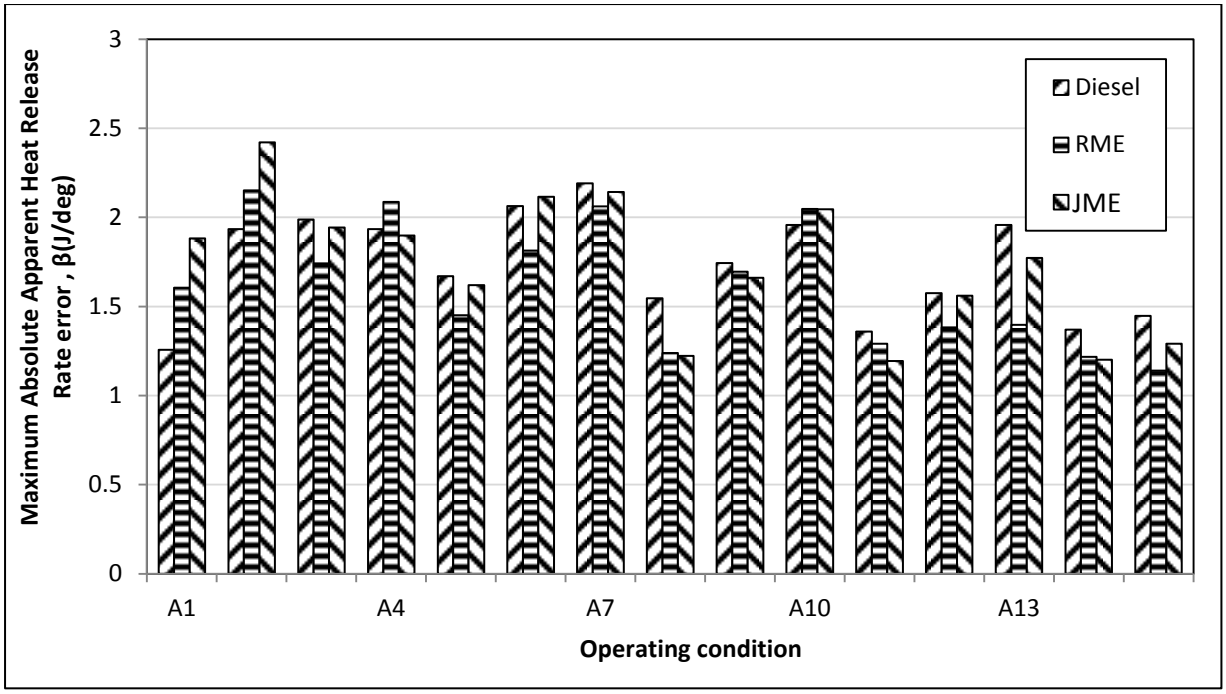

Figure (6.9): Variation of maximum absolute error (β) for Apparent Heat Release Rate for three fuels (diesel, Rapeseed Methyl Ester (*RME*) and Jatropha Methyl Ester (*JME*)) at engine conditions A1-A15.

The value of the maximum absolute error β caused by a small variation (~1%) to the specific heat ratio for condition A1-A15 was found to be 2.42 J/deg. Figure 6.10 indicates the *relative AHRR error* (α) at each crank angle.

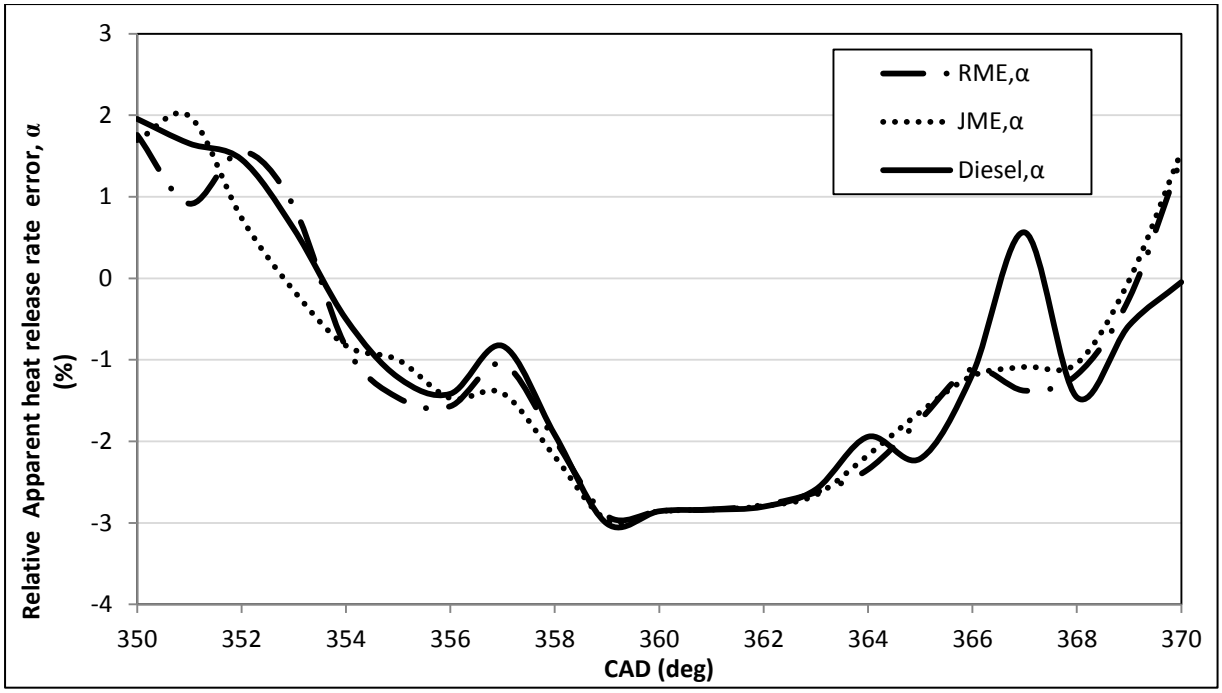

Figure (6.10): Apparent heat release rate relative error (α) for a small change in γ value, dϒ =0.01, at the engine operating condition A3.

This was determined by dividing the *absolute AHRR error* (β) by the magnitude of *AHRR* at each crank angle. The negative values for α indicates the opposite effect of γ value variation on *AHRR*. According to figure 6.11 the maximum α values for the operating conditions A1-A15 was found to be 4% which corresponds to *JME* fuel at condition A2.

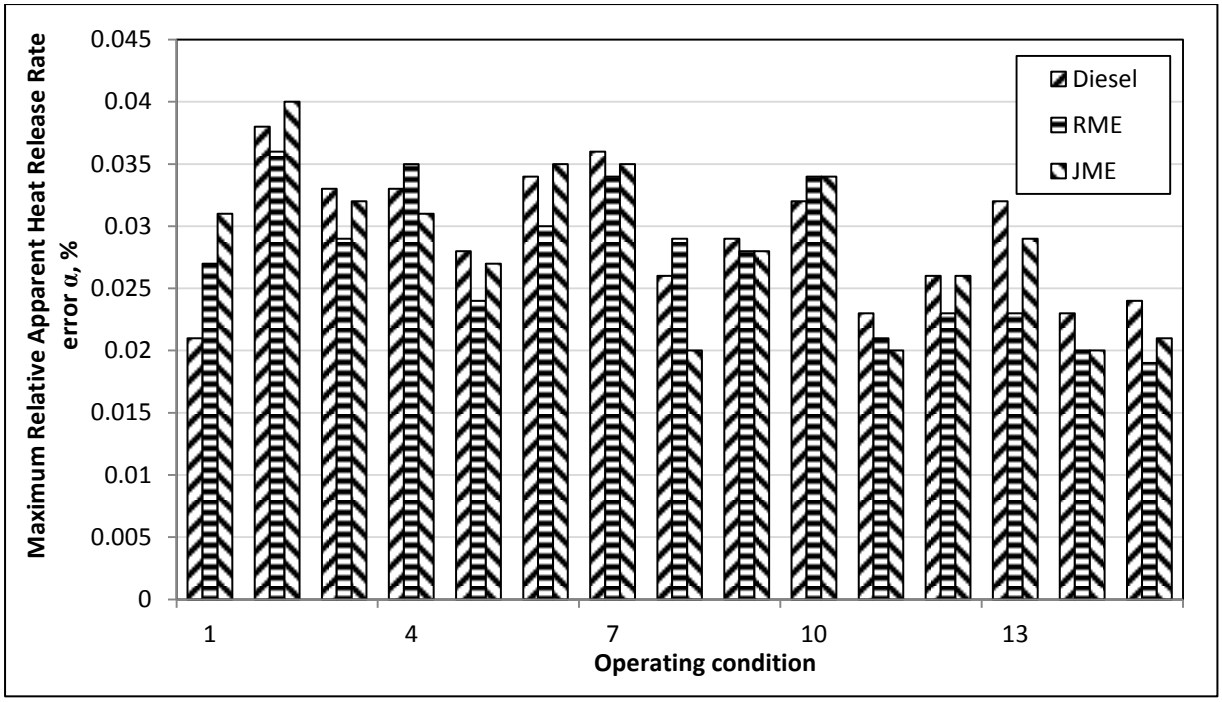

Figure (6.11): Variation of the maximum value relative Apparent Heat Release Rate error for three fuels (diesel, Rapeseed Methyl Ester (*RME*) and Jatropha Methyl Ester (*JME*)) at the engine operating conditions A1-A15.

This shows that for the chosen operating condition (A1-A15) a small change (~1%) in the value of γ can result in an uncertainty of up to ~4% of the calculated *AHRR* **.** The 4% uncertainty in the calculated values of *AHRR* did not affect the start of combustion θ_o and the location of the peak of the heat release rate (θ_{max}) .

6.2.4.Effect of variation of γ on Cumulative Heat Release

The cumulative value of the apparent heat release (*Cum.Hrr*) is constant for a given combustion. The absolute error induced on the *Cum.Hrr* due to the variation of the specific heat ratio γ can be deduced from equation (6.14). The deduction of this equation is provided in [Appendix 1]. Since the cumulative value of the apparent heat release is constant for a

given combustion the absolute error induced on the *Cum.Hrr* by the variation of γ does not depend upon the crank angle θ.

$$\frac{d}{d\gamma}(Cum.Hrr) = \frac{-1}{(\gamma-1)^2}.pV \qquad (6.14)$$

The absolute error values were calculated and it was found that the uncertainty induced on the calculated cumulative heat release corresponds to a maximum of 4% for a variation of 1% of γ value for the chosen operating condition.

6.3.Conclusion

- It has been shown that the burn fraction *f* of Wiebe equation is only a function of newly defined dimensionless parameter *combustion burn factor* (C_i), thus it improved the interpretation of heat release data.
- A new method was proposed to calculate instantaneous and mean value of γ by using the location of centre of combustion. Since the calculated value of γ was obtained based on the centre of combustion and the calculated heat release rates, the calculated value of γ is relatively higher compared to that which was obtained by using the logarithmic *pV* diagram.
- It has been shown that measured in-cylinder pressure did not affect the value of heat capacities ratio significantly. The absolute induced error on the Apparent Heat Release Rate (*AHRR*) and the cumulative heat release were found to follow the accuracy of cylinder pressure measurement.
- The absolute error on the calculated *AHRR* with respect to γ varies against the crank angle and the maximum error was observed at the peak position of *AHRR*. It was also

found that an overestimation of γ resulted in an underestimation of the peak of the *AHRR* and vice versa.

- The uncertainty in the calculated values of γ does not affect the start of combustion (θ_o) and the location of the peak of the heat release rate (θ_{max}) but the location of 50% of heat release (θ_{50}) has marginally shifted, and this shifting is larger for high load in compare to low load.
- The average variation in γ value at wide range of engine operating conditions with respect to most commonly used value of γ=1.35 was found to be less for the method based on θ_{50} position in compare to the method based on *pV* diagram for Diesel , *RME* and *JME*.
- The absolute error on *AHRR* and the cumulative heat release was found to be 4% when the value of γ was varied by 1%.

Chapter 7

Characterising ignition delay correlation for diesel engine by using newly proposed analytical methods

7.1.Introduction

Ignition delay is one the most important parameter that characterises the combustion and performance of diesel engine. The relation between ignition delay and combustion performance in terms of efficiency and emission was revealed by researchers.

Ignition delay is defined the time interval between start of fuel injection and start of combustion in diesel engine [3]. As it was discussed in section (2.6) the diesel engine combustion is affected significantly by ignition delay period. It was revealed that the duration of ignition delay is proportional to NO_x, produced by diesel engine combustion [136]. Therefore many strategies were taken to control ignition delay period to improve the combustion performance in modern engines.

Ignition delay period is consisting of physical ignition delay and chemical ignition delay. Physical ignition delay mainly refers to fuel atomisation, vaporisation and air fuel mixing. The chemical ignition delay refers to chemical reactions which take place prior to main combustion. Physical and chemical ignition delays occur after fuel injection and simultaneously.

In order to understand the concept of ignition delay, several correlations were proposed to predict the ignition delay in diesel engine. Wolfer is the main correlation which was discussed in section (2.6). This correlation can facilitate engine combustion research in terms

of cost and time significantly. Similar to Wiebe equation the accuracy of Wolfer correlation can be affected by calculation of inaccurate constants, consequently the constants in Wolfer correlation need to be calculated precisely.

In this chapter, Ignition delay period measurement and calculation for study of diesel engine combustion along with the most used correlation for ignition delay were discussed. The effect of constants on accuracy of the correlation were discussed and induced error on calculated ignition delay periods with respect to the constants were calculated and compared. New techniques were proposed to calculate the constant values directly by using the experimental data. It was found that calculated values for ignition delay periods using new techniques were matched well with experimental data. These techniques can improve the accuracy of the ignition delay correlation. Also a new correlation with no constants was introduced in this work. This correlation can be used to predict ignition delay directly by using engine parameters only. The introduced correlation provides better results in compare to Arrhenius type correlation presented by Wolfer.

7.2. Error Induced by Constants on Ignition Delay

The ignition delay correlation described in equation (2.44) shows that the ignition delay is dependent on three main parameters namely, the in-cylinder pressure, temperature and the fuel properties which are reflected in the constant *C*.

Figure 7.1 shows the effect of *A* and *n* on τ, according to this figure the accuracy of these constants can affect the accuracy of the calculated τ.

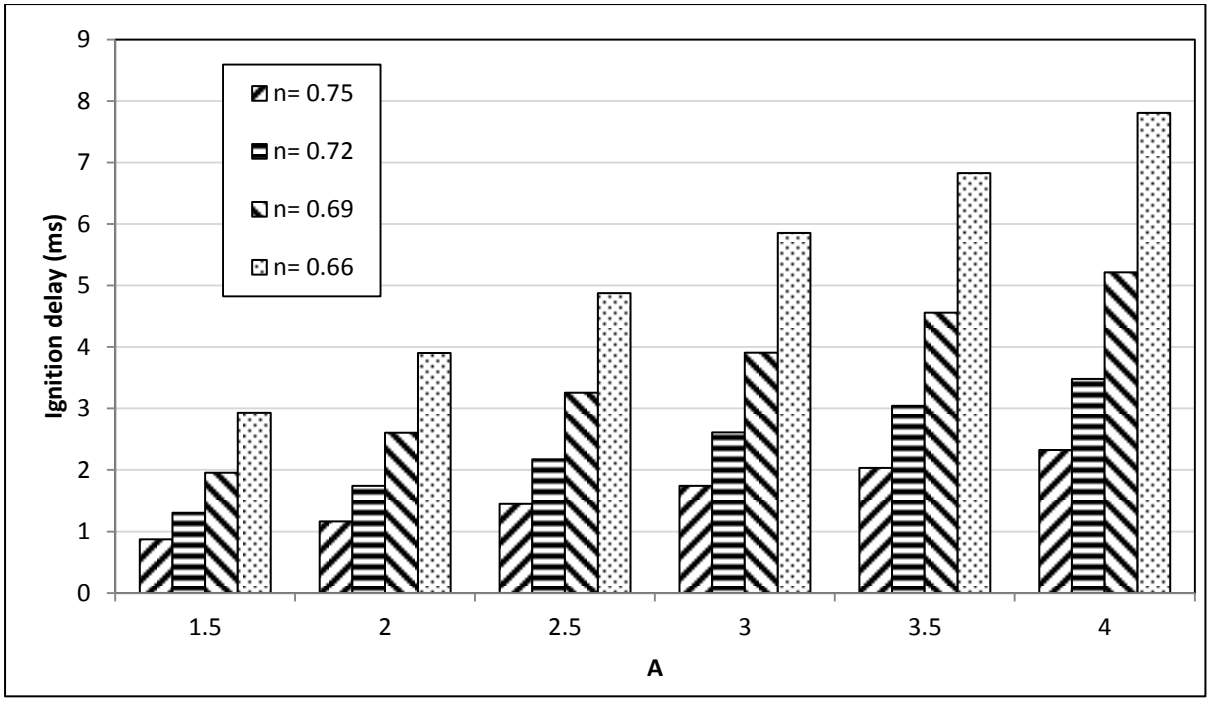

Figure (7.1): Variation of calculated ignition delay values at given condition for different values of *A* and *n.*

It is important to understand the uncertainty induced by these two constants on the calculated ignition delay. Thus the error induced on the ignition delay τ with respect to these constants *A* and *n* were determined by differentiating τ with respect to each constant *A* and *n* which are shown in equations (7.1-7.2).

$$\frac{\partial \tau}{\partial A} = p^{-n} \exp \frac{C}{T} \tag{7.1}$$

$$\frac{\partial \tau}{\partial n} = (Ap^{-n} \exp \frac{C}{T})(-\ln p) \tag{7.2}$$

Dividing equation (7.2) by equation (7.1) results in a relation which shows the proportion through which the constants *A* and *n* affect τ.

$$\frac{\left(\frac{\partial \tau}{\partial n}\right)}{\left(\frac{\partial \tau}{\partial A}\right)} = A(-\ln p) \tag{7.3}$$

The typical values for *A* and *ln(p)* are both positive and greater than one and thus the ratio described on the left hand side of equation (7.3) is greater than one therefore the absolute error induced on τ due to *n* is more than *A.* This confirms the trends discussed in the figure 7.1 where the effect of *A* and *n* on τ are shown. Also as it is demonstrated in figure 7.1 the negative sign in equation (7.3) indicates that the error induced on τ with respect to *n* and *A* do not have additional effects and their variation tends to reduce the total error on τ.

Similarly the effect of *C* on τ was determined by differentiating equation (2.44) with respect to *C* which results in equation (7.4).

$$\frac{\partial \tau}{\partial C} = (Ap^{-n} \exp \frac{C}{T})(\frac{1}{T}) \tag{7.4}$$

Dividing equation (7.4) by equation (7.1) results in a relation which shows the proportion through which the constants *A* and *C* affect τ.

$$\frac{\left(\frac{\partial \tau}{\partial C}\right)}{\left(\frac{\partial \tau}{\partial A}\right)} = A\left(\frac{1}{T}\right) \tag{7.5}$$

Where *T* is the in-cylinder temperature of the charge, by considering the typical values of *A* and *T* it can be concluded that $A\left(\frac{1}{T}\right)$ is a positive quantity and a much smaller value compared to $A(-\ln p)$ in equation (7.3). Consequently it can be concluded that the value of τ is most affected by the value of *n* compared to *A* and *C*. Thus it is essential to have *A*, *n* and *C* determined precisely to minimise the error that can be induced on the calculated values of τ.

7.3.Determination of *A*, *n* and *C*

Several methods have been proposed to determine the value of the constants *A*, *n* and *C* to improve the accuracy of predicting the ignition equation (2.44). Aligrot *et al*. [121] have used several empirical coefficients to determine the values for *A*, *n* and *C* by using empirical equations and their assumptions may result in an uncertainty on the determined values of *A*, *n* and *C*. Watson [109] proposed a constant value for *C* as 2100 for diesel fuel. Assanis [100] and Alkhulaifi [101] have also considered the value for *C* to be 2100 in their analysis based on the work of Watson. Hardenberg [96] calculated the value of *C* by using the equation (7.6).

$$C = \frac{618840}{R(CN + 25)} \tag{7.6}$$

Aghav [137] modified equation (7.6) and calculated the value of *C* using equation (7.7).

$$C = \frac{1310000}{R(CN + 25)} \tag{7.7}$$

Several works [100,101,121] have obtained the values of *A* and *n* by fitting the theoretical data obtained from the correlation against the experimentally measured ignition delay data by fixing the value of *C*. In the next sections the values for *A*, *n* and *C* are calculated analytically and also by fitting the measured and correlated ignition delay to minimise the least square error to get the best fit. The results obtained both from the analytical and fitting approaches are compared.

7.3.1. Analytical approach (Determination of *A* and *n*)

The minimum value of the in-cylinder pressure of all the engine operating conditions E1-E13 provided in table (7.1) was found to be for the condition E7 and consequently this condition was considered as the reference condition.

Table (7.1): Experimental conditions for the tests.

E	Inj. Timming(BTDC)	Inj.P(bar)	BMEP, bar
1	9	1200	2.7
2	3	1000	2.7
3	3	1200	2.7
4	0	800	2.7
5	0	1000	2.7
6	0	1200	2.7
7	-2	800	2.7
8	-2	1000	2.7
9	9	800	5
10	6	1200	5
11	3	1200	5
12	0	800	5
13	-2	800	5

The in-cylinder pressure, temperature and ignition delay at this reference condition is denoted as p_o, T_o and τ_o respectively. The ignition delay corresponding to the reference condition is given as:

$$\tau_o = A p_o^{-n} \exp \frac{C}{T_o} \tag{7.8}$$

Dividing equation (2.44) by equation (7.8) and further simplification results in equation (7.9)

$$\frac{\frac{\tau}{\tau_o}}{\exp(\frac{C}{T}-\frac{C}{T_o})}=(\frac{p}{p_o})^{-n} \tag{7.9}$$

The dimensionless terms on the left and right hand side of equation (7.9) are replaced by the notation Δ and Π respectively, thus the equation (7.9) can be expressed in terms of Δ and Π as:

$$\Delta=(\Pi)^{-n} \tag{7.10}$$

The benefits of using dimensionless parameters in combustion analysis were discussed widely in authors' recent publications [86,138]. Equation (7.10) expresses the relation between *n* and the engine in-cylinder parameters, which can be determined directly from the experimental data for a given value of *C*. The only unknown parameter is *n*, which can be calculated by using equation (7.11) as follows.

$$n=-\frac{\ln\Delta}{\ln\Pi} \tag{7.11}$$

The final value for *n* was obtained by averaging all the calculated *n* values for each engine operating conditions E1-E13. Condition E7 was the reference condition, consequently no value was calculated for *n* at condition E7. By substituting the final averaged value of *n* in equation (2.44), the values of *A* were calculated as proposed in equation (7.12).

$$A=\frac{\tau}{p^{(\frac{\ln\Delta}{\ln\Pi})}\exp\frac{C}{T}} \tag{7.12}$$

Similarly the final value for *A* was obtained by averaging all the calculated *A* values for engine operating conditions E1-E13. Thus both *A* and *n* values were obtained through this analytical approach.

7.3.2.Line fitting approach (Determination of *n*)

The value of *n* can also be determined from equation (7.11) through the line fitting procedure and this is achieved by substituting $Y = \ln\Delta$ and $X = -\ln\Pi$ results in an equation for a straight line $Y = nX$ with a slope of *n* and zero *Y* intercept. By applying the straight line fitting formula *n* can be calculated as follows.

$$n = \frac{N\sum X_i Y_i - \sum X_i . \sum Y_i}{N\sum X_i^2 - (\sum X_i)^2} \tag{7.13}$$

Where *N* is the number of measured data sets. Values for *Y* and *X* are replaced in equation (7.13) to obtain the value of *n*.

$$n = \frac{N\sum(-\ln\Pi_i).(\ln\Delta_i) - \sum(-\ln\Pi_i).\sum\ln\Delta_i)}{N\sum(-\ln\Pi)^2 - (\sum(-\ln\Pi_i))^2} \tag{7.14}$$

It is clear that the higher value for *N* can result in more accurate value for *n*. Equations (7.14) and (7.12) can be used to calculate *A* and *n* values analytically by using combustion parameters. From the previous discussion of linear expression *Y=nX* , *Y* intercept for this straight line after replacing the *X* and *Y* values as they were defined above results in equation (7.15).

$$b = \frac{\sum(-\ln\Pi_i)^2 . \sum(\ln\Delta_i) - \sum(-\ln\Pi_i).\sum(-\ln\Pi_i).(\ln\Delta_i)}{N\sum X_i^2 - (\sum X_i)^2} \tag{7.15}$$

It is expected that the value of *b* calculated from equation (7.15) equals to zero. The value of *b* calculated from equation (7.15) by using the experimental data for operating conditions E1-E13 was found -3.8E-4 which is reasonably closer to zero value.

Figure 7.2 presents the calculated values for *A* and *n* for each engine operating conditions (E1 – E13), In this figure the analytical and line fitting refer to calculation procedure explained in section 7.3.1 and 7.3.2 for *A* and *n* respectively.

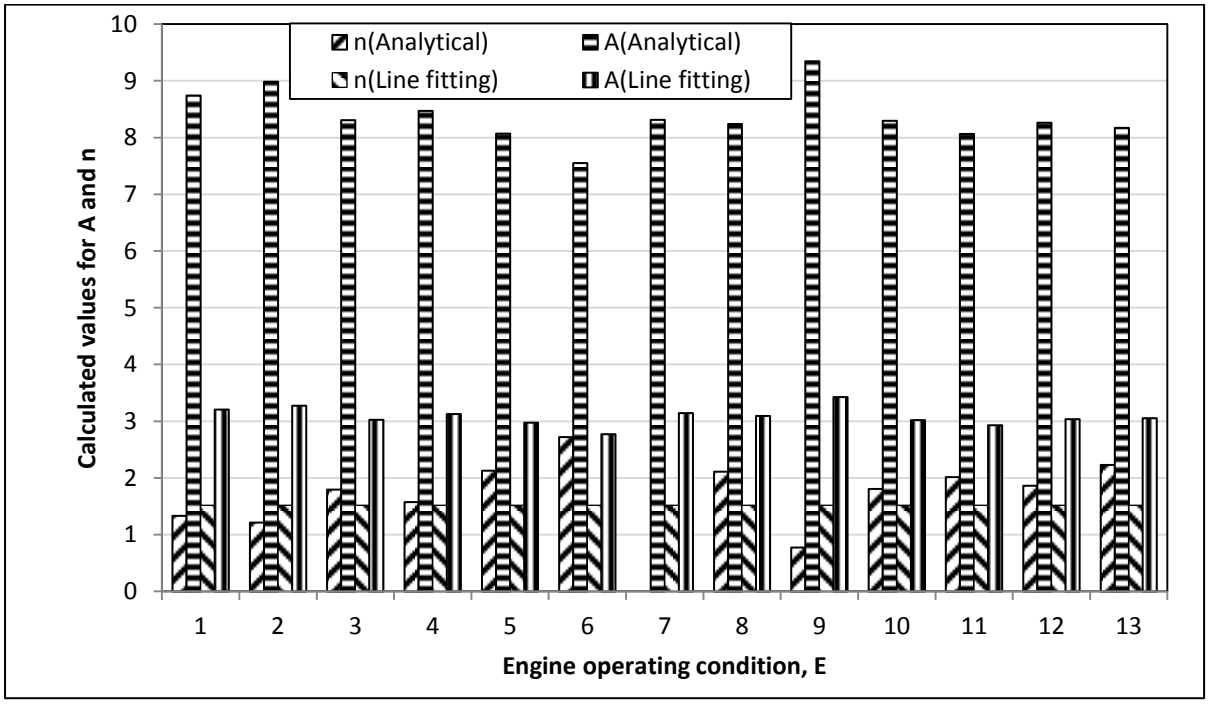

Figure (7.2): The calculated values for *A* and *n* at conditions E1-E13 by using Analytical and line fitting methods.

7.3.3. Determination of constant *C*

The value of *C* can be determined analytically by using the experimentally determined combustion parameters. By considering τ_1 and τ_2 as the measured ignition delay periods for two engine operating conditions. Applying these two conditions to equation (2.44), and taking the ratio and natural logarithm on both sides will result in an analytical expression for the constant *C* given by equation (7.16).

$$C = \frac{\ln(\frac{\tau_1}{\tau_2}) + n\ln(\frac{p_1}{p_2})}{\frac{1}{RT_1} - \frac{1}{RT_2}} \tag{7.16}$$

Equation (7.16) was further simplified by choosing the conditions from the experimental data set that had the cylinder pressures which were nearly equal ($p_1 \approx p_2$) to eliminate n from equation (7.16). All the terms on the right hand side of equation (7.17) are known to evaluate the constant C.

$$C = \frac{\ln(\frac{\tau_1}{\tau_2})}{\frac{1}{RT_1} - \frac{1}{RT_2}} \tag{7.17}$$

The constant C calculated from equation (7.17) based on the experimentally measured data corresponding to the operating conditions E1 to E13 resulted in an averaged value of C = 2208. According to Watson [109] and Assanis [100] the value of C is 2100, and according to Hardenberg [96] and Aghav [137] the values of C are 979 and 2073 respectively. According to Rothamer [139] the value of C was found to be 2287 which was determined by fitting a non-linear least square function. The value of C that was analytically calculated by equation (7.17), (C=2208) is very close to that of [100,109]. Consequently five different values for the constant C were obtained by using different techniques (C=2100, 979, 2073, 2287 and 2208). Combining the values of C with the analytical derived expressions, the values of n can be obtained using equation (7.11) and equation (7.14) respectively; similarly the value for the constant A can be obtained from equation (7.12). In addition to this the values of A and n were also determined by fitting a non-linear least square function between the experimental data and the ignition delay correlation of equation (2.44). All of these values are also summarised in table [7.3].

Table (7.2): Values determined for *A* and *n* for different values of *C* obtained from Watson & Assanis, Hardenberg , Aghav, Rothamer (fitting) , analytical calculation and Line fitting in present work.

	C	*Fitting least square function*	*Analytical, equations(7.11,7.12)*	*Line fitting, equations(7.12,7.14)*
Watson & Assanis	**2100**	**A=4.2,n=1.56**	**A=12.51,n=1.87**	**A=4.29,n=1.57**
Hardenberg	**979**	**A=4.2,n=1.31**	**A=804.77,n=2.59**	**A=131.72,n=2.08**
Aghav	**2073**	**A=4.07,n=1.54**	**A=13.83,n=1.88**	**A=4.66,n=1.58**
Rothamer (fitting)	**2287**	**A=3.71,n=1.6**	**A=6.25,n=1.75**	**A=2.42,n=1.52**
Calculation (present work)	**2208**	**A=4.15,n=1.6**	**A=8.38,n=1.80**	**A=3.08,n=1.52**

7.4.New Correlation (Determination of ignition delay)

As discussed above the experimental data was used to obtain the constants *A*, *n* and *C* and these constants are used in equation (2.44) to predict ignition delay for an operating condition. The predicted values of the ignition delay from these correlations are affected significantly by the value of the constants *A* and *n*. In order to improve the accuracy of predicting ignition delay, a new correlation has been proposed without any calibration or tuning constants. The ignition delay can be calculated directly from the main combustion parameters by using this correlation.

The value of *Y* intercept can be calculated from equation (7.15), as mentioned earlier in section 7.3.2, the straight line $Y = nX$ has zero *Y* intercept, and therefore equation (7.15) can be expressed as:

$$\sum(-\ln \Pi_i)^2 . \sum(\ln \Delta_i) - \sum(-\ln \Pi_i) . \sum(-\ln \Pi_i) . (\ln \Delta_i) = 0 \qquad (7.18)$$

Equation (7.18) expresses the relation between the parameters Δ and Π which are defined by using the main combustion parameters (*p, T and C*). Equation (7.18) has been re-written to express the Δ term in the n^{th} form as:

$$\sum_{i=1}^{n}(-\ln\Pi_i)^2.[(\sum_{i=1}^{n-1}\ln\Delta_i)+(\ln\Delta_n)]-[\sum_{i=1}^{n}(-\ln\Pi_i)].\{[\sum_{i=1}^{n-1}(-\ln\Pi_i.\ln\Delta_i)]+[(-\ln\Pi_n).(\ln\Delta_n)]\}=0$$

(7.19)

Equation (7.19) has been restructured to determine the n^{th} term of Δ, using the n^{th} term of Δ along with the definition of Δ result in a new correlation. Details of this derivation are provided in Appendix 2.

$$\tau_n=\tau_o.\exp[(\frac{[\sum_{i=1}^{n}(-\ln\Pi_i)].[\sum_{i=1}^{n-1}(-\ln\Pi_i).(\ln\Delta_i)]-[\sum_{i=1}^{n}(-\ln\Pi_i)^2].(\sum_{i=1}^{n-1}\ln\Delta_i)}{[\sum_{i=1}^{n}(-\ln\Pi_i)^2]-[\sum_{i=1}^{n}(-\ln\Pi_i)].(-\ln\Pi_n)})+C(\frac{1}{T_n}-\frac{1}{T_o})]$$

(7.20)

The equation (7.20) is the new correlation that is developed to calculate ignition delay directly by using combustion parameters (*p*,*T* and *C*). The new correlation considers the effect of all the main combustion parameters to calculate the ignition delay value directly. Ignition delay values were calculated using the new correlation for the engine operating conditions E1-E13 are plotted in figure 7.3 along with the experimental data.

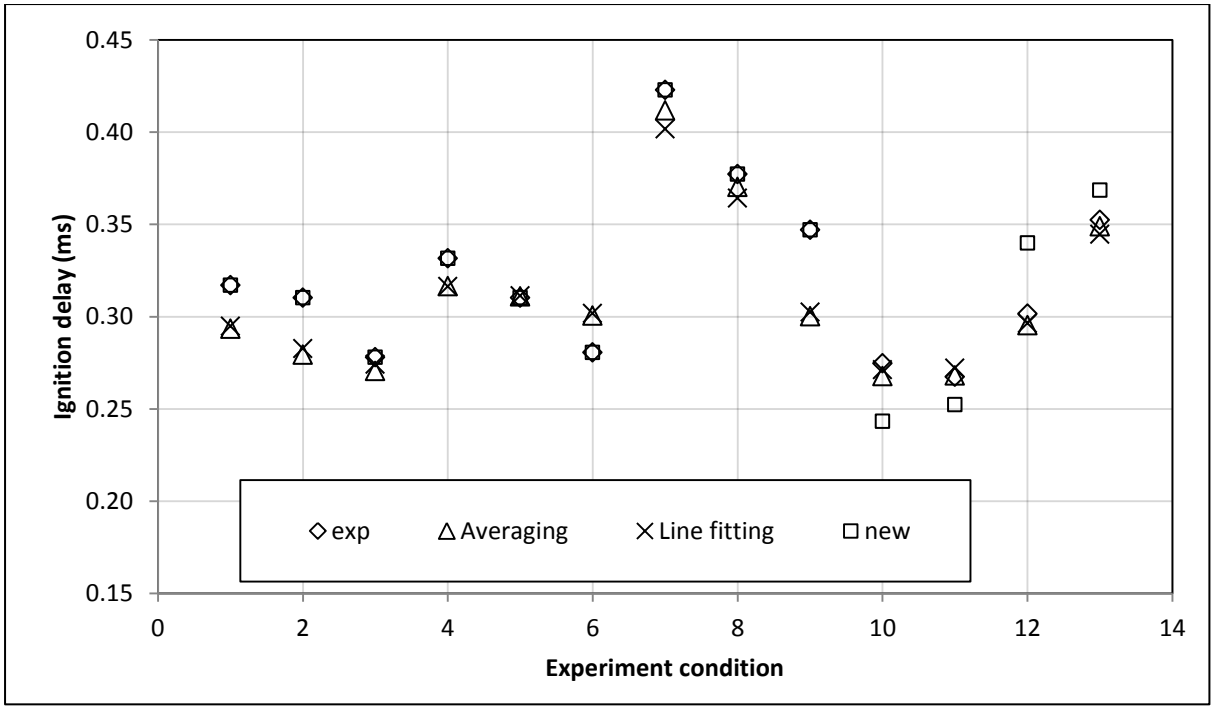

Figure (7.3): Variation of ignition delay for operating conditions E1-E13 by using three analytical techniques along with experimental data.

In addition to this the ignition delay values calculated using equation (2.44) based on the values of *A* and *n* that are obtained through analytical and line fitting approach (section 7.3.1 and 7.3.2) are also presented. The data indicates that the new correlation can improve the calculation of ignition delay considerably.

7.5.Results

7.5.1.Induced error on ignition delay with respect to *A*, *n* and *C*

Figure 7.1 presents the variation of τ with respect to the constants *A* and *n* for a given value of *C*=2100. The data shows that the effect of *n* on τ is greater when compared against *A*. The corresponding in-cylinder pressure and temperature value is 37.63 bar and 715.07 K respectively.

By using the calculated values of *A, n* and *C* from the present work, and the values of in-cylinder temperature and pressure mentioned above, it has been found that 1% error in the value of *A, n* and *C* causes an uncertainty to τ in the order of 10^{-3}, $3.61X10^{-3}$ and $3.88X10^{-4}$ *msec* due to the variation of *A, n* and *C* respectively. Comparing absolute values for these error values indicates good agreement between these findings and equations (7.3) and (7.5).

The calculated values for *A* and *n* using three different approaches (fitting, analytical and line fitting) are summarized in table (7.2).

7.5.2. Analytical approach

Equations (7.11, 7.12) were used to calculate *A* and *n* values as discussed in section 7.3.1. It was found that by using analytical approach, the calculated values for *n* were in the range 1.75-1.88 for all the five values of *C* (2100, 979, 2073, 2287 and 2208). Figure 7.4 presents the values of ignition delay calculated by using analytical approach for the operating conditions E1-E13. In this figure five set of ignition delays were produced by using the values of *C* discussed earlier, and they were plotted along with experimental data.

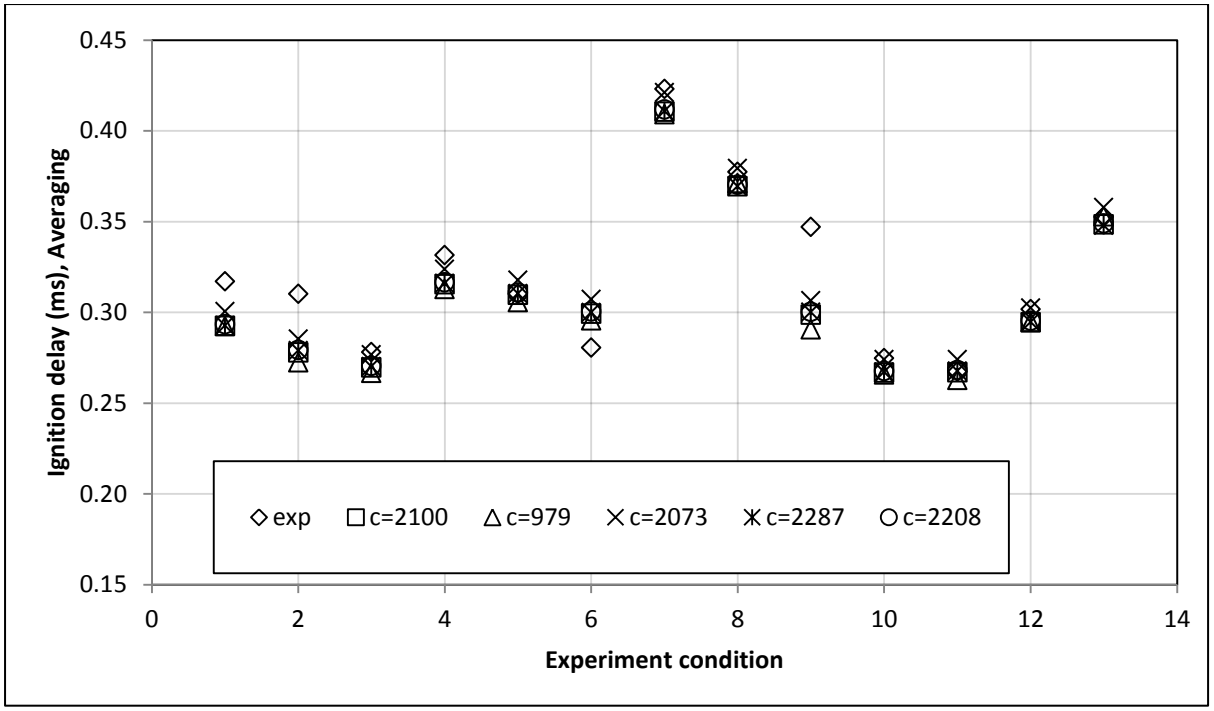

Figure (7.4): Variation of ignition delay by considering different values for constant *C* for E1-E13. *A* and *n* were calculated by analytical approach.

7.5.3.Line fitting approach

Equations (7.12) and (7.14) were used to calculate *A* and *n* values in this section. As discussed in section 7.3.2. Figure 7.5 presents the values of ignition delay calculated by using line fitting approach for operating conditions E1-E13 along with experimental data.

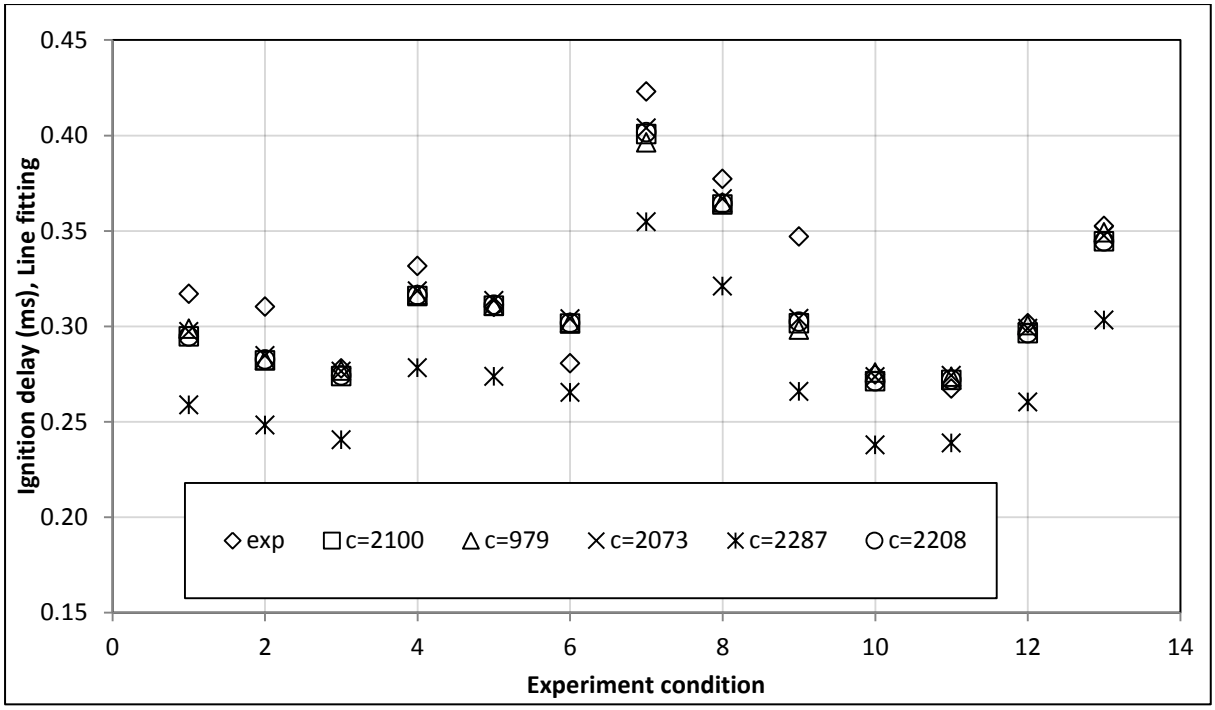

Figure (7.5): Variation of ignition delay by considering different values for constant *C* for operating conditions E1-E13. *A* and *n* were calculated by line fitting approach.

7.5.4.Fitting least square function

In addition to values of *A* and *n* discussed in section 7.5.2 and 7.5.3, the values of *A* and *n* were calculated through the fitting a least square function. Figure 7.6 presents the values of ignition delay calculated by using fitting least square function technique for operating conditions E1-E13 along with experimental data.

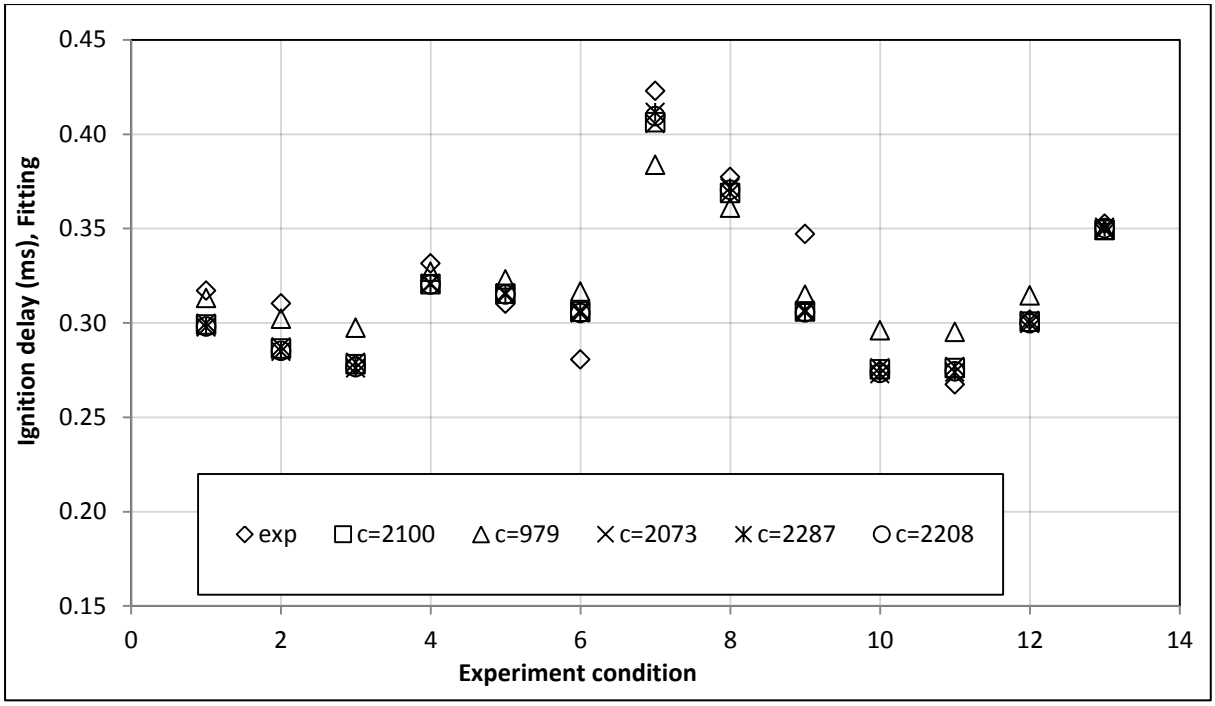

Figure (7.6): Variation of ignition delay by considering different values for constant *C* for E1-E13. *A* and *n* were calculated by fitting a non-linear least square function.

7.6.Discussion

7.6.1. Analytical, Line fitting and Fitting a least square methods

According to figures 7.4-7.6 even though the *C* values varies over a wide range from 979 to 2287, the calculated values and experimental data are relatively closer to each other. The constants *A* and *n* compensated for the effect of inaccurate value for *C*.

According to table (7.2) and comparing *n* values using three techniques as discussed in sections 7.52, 7.5.3 and 7.5.4 show that the values of *A* and *n* corresponding to *C*=979 from Hardenberg [96] is considerably different and it is attributed to the large difference between *C* value from Hardenberg (*C*=979) and other techniques which were discussed in this chapter (*C*=2073,2287 and 2208).

The benefits of using analytical techniques are more dominant when a new fuel is investigated. Due to high number of investigations performed on diesel fuel research, the range of variation for A , n and C are relatively well known in the literature but this fact does not apply on any other fuel such as bio-diesels, therefore the proposed analytical method can provide a precise value for A , n and C.

7.6.2.New correlation

Equation (7.20) in section 7.4 is providing a new correlation to calculate ignition delay. The value of C in the new correlation is dependent upon fuel properties and engine operating conditions which can be calculated by the technique discussed in section 7.3.3 equation (7.17). As discussed in this work the values of constants A and n in equation (2.44) can affect the predicted values for ignition delay, consequently the new correlation cannot be affected by values of constants A and n since the new correlation is not expressed in terms of constants.

The new correlation is taking the effect of all experimental data into account to calculate the ignition delay at a given operating condition. Also the new correlation was calculated by using the dimensionless parameters defined in this work (Δ,Π) which are relative combustion properties, consequently they can cancel out some errors in data which results in better accuracy of ignition delay prediction. Figure 7.3 presents the values of ignition delay calculated by using new correlation. In this figure three sets of ignition delay, produced by using new correlation and two calculating techniques (analytical and Line fitting approaches) were plotted along with experimental data for operating conditions E1-E13.

7.6.3.Error propagation function

Error propagation function was used to compare the calculated ignition delay values for operating conditions E1-E13. Error propagation value (ω) were calculated for each set of τ values by using equation (7.21) and using *A* ,*n* and *C* values from table (7.2).

$$\omega = \sqrt{\sum_{i=1}^{13}(\tau_i - \tau_{ex})^2} \qquad (7.21)$$

Where τ_{ex} refers to experimental data. The absolute ignition delay error propagation values calculated by new correlation along with fifteen sets of calculated ignition delay using table (7.2) were plotted in figure 7.7 .

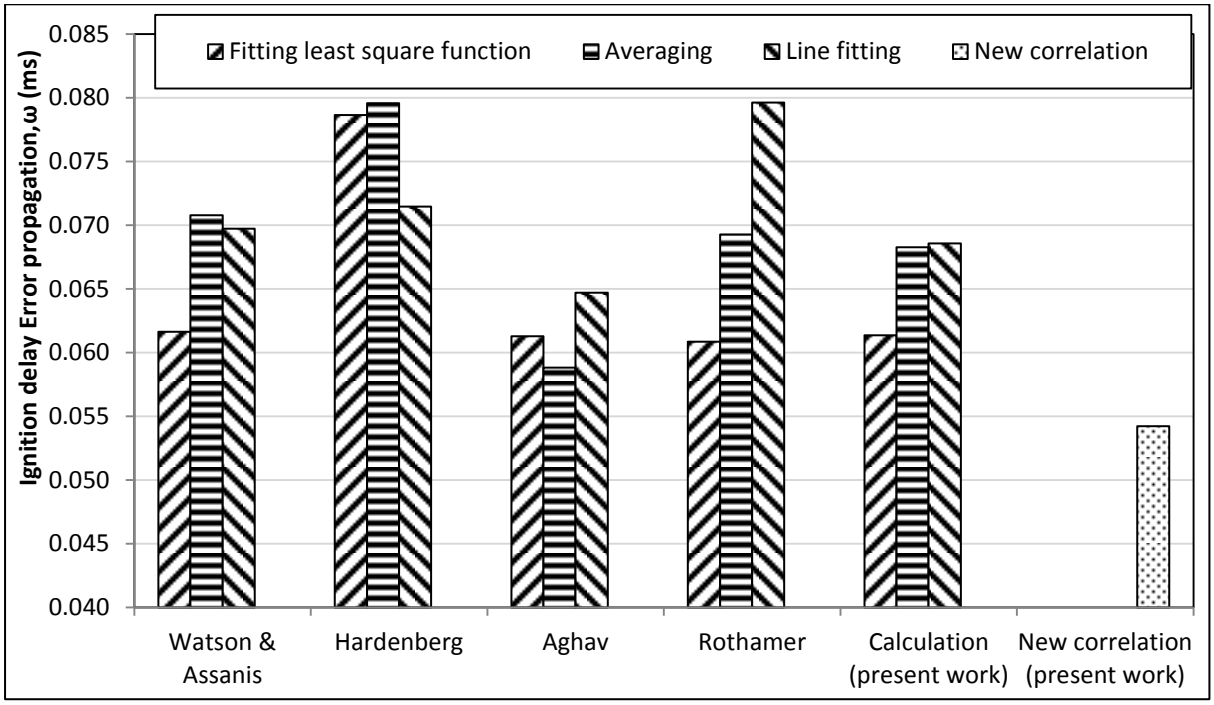

Figure (7.7): Error propagation values (ω) determined for *A* and *n* for different values of *C* obtained from [96, 100&109, 137, 139] along with analytical calculation in present work (analytical) and new correlation.

According to this figure the value of ω varies for fitting least square function, analytical and line fitting approaches due to different values of *C*. Calculated values of ω in figure 7.7

indicates that the predicted ignition delay values by using analytical , line fitting approaches and fitting least square function are relatively close to experimental data. Of Watson&Assanis, Hardenberg, Aghav, Rothamer and calculation by equation (7.17) corresponding to *C*=2100, 979, 2073, 2287 and 2208 respectively, it was found that *C* values corresponding to Aghav and calculation by equation (7.17) produce better results.

As it was stated, the new correlation can be used to calculate ignition delay directly without any of calculated *A* and *n* values. According to figure 7.7 the new correlation provides better results in terms of lower ω value.

The new correlation can be used for any fuel, provided the value of *C* for a fuel is accurately estimated. There is no need to determinate *A* and *n* as the new correlation is expressed by combustion properties.

7.7.Conclusion

The Arrhenius type expression for predicting the ignition delay (τ) which is known as a most widely used correlation was considered in this work.

$$\tau = Ap^{-n} \exp \frac{C}{T}$$

Where *p* is the in-cylinder pressure at start of combustion, *T* is in-cylinder temperature at start of combustion, *t* is the ignition delay period and *A* and *n* are constants and $C = \frac{E_A}{R}$. *R* is the universal gas constant and E_A is the apparent activation energy for the fuel auto ignition process.

1. It was found that the constant values can affect the accuracy of ignition delay correlation significantly. The induced error on τ with respect to *A, n* and *C* were calculated and compared. It was found that the value of τ is more affected by the uncertainty of *A, n* and *C* in the order to *n>A>C.*
2. Analytical techniques were introduced to calculate the value of *A, n* and *C* without using fitting least square function. The new proposed techniques for calculating *A, n* and *C* have been compared against those values which were reported in literature and concluded that the proposed techniques can improve the accuracy of the correlation. The proposed techniques could be ideal methods to study new fuels which are not fully analysed and the fuel properties are not known completely.
3. A new correlation was introduced to calculate τ in this work.

$$\tau_n = \tau_o . \exp\left[\left(\frac{\left[\sum_{i=1}^{n}(-\ln \Pi_i)\right].\left[\sum_{i=1}^{n-1}(-\ln \Pi_i).(\ln \Delta_i)\right] - \left[\sum_{i=1}^{n}(-\ln \Pi_i)^2\right].\left(\sum_{i=1}^{n-1}\ln \Delta_i\right)}{\left[\sum_{i=1}^{n}(-\ln \Pi_i)^2\right] - \left[\sum_{i=1}^{n}(-\ln \Pi_i)\right].(-\ln \Pi_n)}\right) + C\left(\frac{1}{T_n} - \frac{1}{T_o}\right)\right]$$

4. It was found that the results from the new correlation matched well with experimental data.
5. The new correlation is not expressed in terms of constants. The relative combustion properties were used to determine τ. Consequently some errors can be cancelled out as a result of using dimensionless values.
6. It was found that the calculated values for τ by the new correlation were accurate compared to those calculated by the considered Arrhenius type expression in this work.
7. There was no parameter characterized for diesel fuel specifically in the new correlation, consequently this correlation can be used to calculate τ for bio-diesels too.

Chapter 8

Conclusion and recommendation for future work

Diesel engines are in wide use in many fields of industry and commerce. The data indicates that the number of diesel engines is increasing due to their high performance as it was discussed in section 1.2. Diesel engines can power huge trucks and marines as well as little lawnmowers for gardening. Parallel to growth of number of diesel engines in human daily life a real concern grows due to harmful effect of diesel engines.

In order to reduce the harmful effect of these type of engines continues investigation is in progress since Rudolf Diesel developed diesel engine in 1892. In result of this investigation significant improvement were made on diesel engines in terms of material, design, fuel as well as engine research techniques as discussed in section 2.3.

Improving diesel engine analysis as a key factor in understanding of diesel engine combustion can result in engines with higher performances.

In order to improve diesel engine analysis several correlations which widely are in use by researchers were discussed and calculation was carried out to minimize the induced error. Also a new technique was proposed to calculate heat capacities ratio which results in more accurate heat release analysis.

Wiebe equation was studied in chapter 5 and the achievements are discussed in section 8.1. Similarly the achievement from heat release analysis which was discussed in chapter 6 are discussed in section 8.2. The achievement from chapter 7 in regard to ignition delay

calculation is discussed in section 8.3. Finally the recommendation for future work is discussed in section 8.4.

8.1. Wiebe equation

Wiebe equation (equation (5.1)) was discussed as a strong tool in heat release analysis in chapter 5. It was found that the accuracy of Wiebe equation can be affected significantly by inaccurate calculation of constants in the Wiebe equation (*A* and *n*). The error induced on combustion burn fraction (*f*) with respect to constants (*A* and *n*) were calculated and found that *f* can be affected more by *n* in compare to *A*. New techniques were proposed to calculate accurate value for *A* and *n*.

In order to improve the accuracy of Wiebe equation, a modified version of Wiebe equation was proposed. The modified Wiebe equation contains only one constant instead of two constants in Wiebe equation, in original form (equation (5.1)). It was found that using modified Wiebe equation can improve the accuracy of heat release analysis considerably.

8.2. Heat capacities ratio

Heat release calculation is used by many researchers as an important tool for analysis of diesel engine combustion (section 3.1). As a standard technique the in-cylinder pressure data along with equation (3.8) are used to calculate valuable parameters as in-cylinder temperature, apparent heat release, cumulative heat release, location of centre of combustion, combustion duration and some other parameters, dependent on the nature of study.

The error induced on apparent heat release rate (*AHRR*) with respect to in-cylinder pressure (p) and Heat capacities ratio (γ) was calculated and compared in chapter 6. It was found that the γ can affect *AHRR* significantly in comparison to p, consequently it is important to calculate the value of γ accurately.

Using p-V diagram in logarithm scale was discussed in chapter 6 and following to this discussion a new technique was proposed to calculate γ value. It was found that the newly defined technique can provide accurate values and can improve the accuracy of heat release analysis.

Using the concept of Wiebe equation a new dimensionless parameter, called Combustion Burn Factor which was denoted by C_i was introduced in this chapter. It was shown that the Wiebe equation is the function of C_i only. The benefits of using C_i was discussed extensively in this work and concluded that plotting *AHRR* against the C_i can improve the heat release analysis.

8.3. Ignition delay

Ignition delay is an important parameter which can provide valuable information about performance of the diesel engine combustion in chapter 7. Many investigations were carried out by researchers to study the relation between ignition delay and diesel engine combustion main parameters as fuel spray pattern, fuel specifications, diesel engine design and many more.

Wolfer equation (equation (2.44)) as an important tool to predict the ignition delay in diesel engine combustion was discussed in chapter 7. It was found that Wolfer equation can be affected by the constants and the error induced on ignition delay (τ) with respect to A,n and C

were calculated and compared. It was found that τ is affected significantly by n in comparison to A and C. New techniques were proposed to calculate accurate values for constants in Wolfer equation. It was found that the accuracy of Wolfer equation was improved by using the new techniques to obtain the constants.

In order to improve the accuracy of ignition delay calculation and also remove the effect of using inaccurate constants, a new correlation was proposed to calculate ignition delay. In the new correlation τ is expressed in terms of combustion parameters only, and no constant exists in the new correlation. It was found that the new correlation provides accurate values in comparison to those which were calculated by the Arrhenius type expression.

Since no parameter was characterised for diesel fuel in the new correlation, consequently the new correlation can be used to calculate ignition delay for bio-diesels too.

8.4. Recommendation for future work

Dimensionless parameters were used to improve the heat release analysis in this work. Modified Wiebe equation, a new ignition delay correlation and a new technique to calculate Heat capacities ratio were proposed in this work. A diesel engine was employed to demonstrate the results from proposed correlations as well as the calculation of Heat capacities ratio. The engine was kept at constant speed and naturally aspirated with no EGR applied to the system. It is beneficial to demonstrate the proposed correlations by applying engine operating conditions varying EGR, engine speed, load and super charge at intake manifold.

A new dimensionless parameter called Combustion Burn Factor denoted as C_i was introduced in this work and the benefits of expressing the apparent heat release in terms of C_i was

discussed. Further investigation is required to study the effect of EGR, engine load, super charged conditions and emission performance of combustion on variation of C_i.

References

1. http://epp.eurostat.ec.europa.eu/tgm/table.do?tab=table&init=1&plugin=1&language=en&pcode=tsdpc340. (15.05.2014)
2. Rajput R K. Internal Combustion Engines, Laxmi Publications, 2005.
3. Heywood J B. Internal Combustion Engine Fundamentals, 1988 (McGraw-Hill). ISBN: 0-07-100499-8.
4. Makartchouk A. Diesel Engine Engineering Thermodynamics, Dynamics, Design and Control. Marcel Dekker, Inc 2002. ISBN: 0-8247-0702-8.
5. Heisler H. Vehicle and engine technology. Edward Arnold Publication, (1999). ISBN: 03406917
6. Suzuki T. The romance of engines. Society of Automotive Engineers, (1997). ISBN: 1560919116.
7. VanWylen G J, Sonntag R E. Fundamentals of classical thermodynamics. John Wiley &Sons, Inc. ISBN 0-471-90124-5.
8. Sharp J. The public health impact of diesel particulate matter. Sierra club of Canada. May 2003.
9. Zimmerman N, Pollitt K J G, Jeong C H, Wang J M, Jung T, Cooper J M, Wallace J S, Evans G J. Comparison of three nanoparticle sizing instruments: The influence of particle morphology. Atmospheric Environment 86 (2014) 140-147.
10. Crua C. Combustion processes in a diesel engine. A PhD thesis submitted in December 2002. School of engineering Brighton University.

11. Ghojel J I. Review of the development and applications of Wiebe function: a tribute to the contribution of Ivan Wiebe to engine research. International Journal of Engine Research, Volume 11, November 4/2010.

12. Zhao H. Laser Diagnostics and Optical Measurement Techniques in Internal Combustion Engines. SAE International. ISBN 978-0-7680-5782-9.

13. Espey C, Dec J E. Diesel engine combustion studies in a newly designed optical-access engine using high-speed visualization and 2-D laser imaging. SAE paper 1993 no. 930971.

14. Hentschel W, Schindler K. Flow, spray and combustion analysis by laser techniques in the combustion chamber of a direct-injection diesel engine. Optics and Lasers in Engineering 1996, 25, 401-413.

15. Nakagawa H, Endo H, Deguchi Y. LIF imaging of diesel spray combustion. JSME Combustion and Modelling Symposium, COMODIA1998, 359-364, Kyoto.

16. Su D S, Jentoft D E, Muller J O, Jacob E, Simpson C D, Tomovic Z. Microstructure and oxidation behaviour of Euro IV diesel engine soot: a comparative study with synthetic model soot substances. Catalysis Today 2004;90:127–32.

17. Kittelson J. Engine and nanoparticles: a review. Journal of Aerosol Sience 998; 5(6):575-88.

18. Liu Y, Tao F, Foster D E, Reitz R D. Application of an improved multi-step phenomenological soot model to a HSDI diesel multiple injection modelling. SAE paper 2005-01-0924; 2005.

19. Tao F, Golovitchev V I, Chomiak J A. Phenomenological model for the prediction of soot formation in diesel spray combustion. Combustion and Flame 2004;136:270-82.

20. Tian L, Cheung C S, Huang Z. Effects of engine operating conditions on the size and nanostructure of diesel particles. Journal of Aerosol Science 47(2012) 27-38.

21. La Rocca A, Di Liberto G, Shayler P J, Fay M W. The nano-structure of soot-in-oil particles and agglomerates from an automotive diesel engine. Tribology International 61(2013) 80-87.

22. Patel M, Leonor Azanza Ricardo C, Scardi, Pranesh B. Aswath P. Morphology, structure and chemistry of extracted diesel soot-part I: Transmission electron microscopy , Raman spectroscopy, X-ray photoelectron spectroscopy and synchrotron X-ray diffraction study. Tribology International 52 (2012) 29-39.

23. Patel M, Pranesh B. Aswath P. Morphology, structure and chemistry of extracted diesel soot-part II: X-ray absorption near edge structure (XANES) spectroscopy and high resolution transmission electron microscopy. Tribology International 52 (2012) 17-28.

24. Ishiguro T, Takatori Y, Akihama K. Microstructure of diesel soot particles probed by electron microscopy : first observation of inner core and outer shell. Combustion and Flame (1997), 108, 231–234.

25. Park K, Kittelson D B, McMurry P H. Structural properties of diesel exhaust particles measured by transmission electron microscopy (TEM): relationships to particle mass and mobility. Aerosol Science and Technology (2004), 38, 881–889.

26. Vander Wal R L. Soot nanostructure: definition, quantification and implications. SAE paper 2005-01-0964,2005.

27. Neer A, Koylu U O. Effect of operating condition on the size, morphology and concentration of sub micro-meter particulates emitted from a diesel engine. Combustion and Flame (2006), 146, 142–154.

28. Lapuerta M, Martos F J, Herreros J M. Effect of engine operating conditions on the size of primary particles composing diesel soot agglomerates. Journal of Aerosol Science (2007), 38, 455–466.

29. Song J H, Lee K O. Fuel property impacts on diesel particulate morphology nano-structures ,and NOx emissions. SAE paper no 2007-01-0129 ,2007.

30. Li Z, Song C L, Song J O, Lv G, Dong S R, Zhao Z. Evolution of the nanostructure, fractal dimension and size of in-cylinder soot during diesel combustion process. Combustion and Flame (2011), 158, 1624–1630.

31. Tao F, Srinivas S, Reitz R D, Foster D E. Comparison of three soot models applied to multi-dimenssional diesel combustion simulations. JSME International Journal Series B 2005;48(4):671-8.

32. Hessel R P, Foster D E, Steeper R R, Aceves S M, Flowers D L. Pathline analysis of full cycle four stroke HCCI engine combustion using CFD and multi zone modelling. SAE paper 2008-01-0048;2008.

33. Faizal Wan Mahmood W M, La Rocca A, Shayler P J, Bonatesta F, Pegg I. Predicted paths of soot particles in the Cylinders of a DI Diesel Engine. SAE paper 2012-01-0148; 2012.

34. Samson R J, Mulholland G W, Gentry J W. Structural analysis of soot agglomerates. Langmuir 1987;3(2):272-81.

35. Bandin J S M, Prieto G, Sarmiento F. Fractal aggregates in tennis ball systems. Physics Education 2009;44:499-502.

36. Manickavasagam S, Menguc M P. Scattering matrix elements of fractal like soot agglomerates. Applied Optics 1997;36:1337-51.

37. Agar Scientific, Elektron Technology UK Ltd, Unit 7, M11 Business Link, Parsonage Lane, Stansted, Essex CM24 8GF. United Kingdom.

38. Eastwood P. Particulate Emissions from Vehicles. John Willey & Sons Ltd, Chichester, 2008, ISBN:978-0470724552.

39. Krieger R. Applications of Engine Combustion Models: An Introductory Overview. Combustion Modelling in Reciprocating Engines, 1980: p. 485–503.

40. Schröder O, Bünger J, Munack A, Knothe G, Krahl J. Exhaust emissions and mutagenic effects of diesel fuel, biodiesel and biodiesel blends. Fuel 2013; 103: 414–420.

41. Tan P Q, Zhao J Y, Hu Z Y, Lou D M , Du A M. Effects of fuel properties on exhaust emissions from diesel engines. Jornal of Fuel Chemistry and Technology 2013; 41(3): 347-355.

42. Karabektas M, Ergen G , Hosoz M. Effects of the blends containing low ratios of alternative fuels on the performance and emission characteristics of a diesel engine. Fuel 2013; 112: 537–541.

43. Squaiella L L F, Martins C A, Lacava P T. Strategies for emission control in diesel engine to meet Euro VI. Fuel 2013; 104: 183–193.

44. Yu L, Ge Y, Tan J, He C, Wang X, Liu H, Zhao W,Guo J, Fu G, Feng X, Wang X. Experimental investigation of the impact of biodiesel on the combustion and emission characteristics of a heavy duty diesel engine at various altitudes. Fuel 2013; http://dx.doi.org/10.1016/j.fuel.2013.06.056.

45. Pinzi S, Rounce P, Herreros J M, Tsolakis A, Dorado M P. The effect of biodiesel fatty acid composition on combustion and diesel engine exhaust emissions. Fuel 2013; 104: 170–182.

46. Lenin M A, Swaminathan M R, Kumaresan G. Performance and emission characteristics of a DI diesel engine with a nanofuel additive. Fuel 2013; 109: 362–365.

47. Rakopoulos C D, Antonopoulos K A, Rakopoulos D C. Experimental heat release analysis and emissions of a HSDI diesel engine fuelled with ethanol–diesel fuel blends. Energy 2007; 32: 1791–1808.

48. Theobald MA, Alkidas AC. On the heat-release analysis of diesel engines: effects of filtering of pressure data. SAE paper no. 872059; 1987.

49. Homsy SC, Atreya, A. An experimental heat release rate analysis of a diesel engine operating under steady state conditions. SAE paper no. 970889; 1997.

50. Rakopoulos C D, Antonopoulos K A, Rakopoulos D C, Giakoumis E G. Study of combustion in a divided chamber turbocharged diesel engine by experimental heat release analysis in its chambers. Applied Thermal Engineering 2006; 26: 1611–20.

51. Gupta M, Bell SR, Tillman ST. An investigation of lean combustion in a natural gas-fueled spark-ignition engine. J.Energy Resour. Technol. 1996; 118: 145-151.

52. Rousseau S, Lemoult B, Tazerout M. Proceeding of the Instituation of Mechanical Engineers, Part D: Journal of Automobile Engineering 1999: 213- 481.

53. Watts P A, Heywood J B. Simulation studies of the effects of turbo charging and reduced heat transfer on spark ignition engine operation. SAE paper no. 800289; 1980.

54. Johansson T, Borgqvist P, Johansson B, Tunestal P. HCCI Heat Release Data for Combustion Simulation, Based on Results from a Turbocharged Multi Cylinder Engine. SAE paper no. 2010-01-1490; 2010.

55. Ravaglioli V, Moro D, Serra G, Marelli M, Ponti F. MFB50 On-Board Evalution Based on a Zero-Dimensional Rate Of Heat Release Model, SAE paper no. 2011-01-1420; 2011.

56. Kumar R, Reader G T, Zheng M. A Preliminary Study of Ignition Consistency and Heat Release Analysis for a Common-Rail Diesel Engine. SAE paper no. 2004-01-0932; 2004.

57. Miyamoto N, Chikahisa T, Murayama T, Sawyer R. Description and analysis of diesel engine rate of combustion and performance using Wiebe's functions. SAE paper no. 850107; 1985.

58. Liu Z, Karim G A. Simulation of combustion process in gas-fuelled diesel engines. Part A, Journal of Power and Energy 1997; 211(A2): 159-169.

59. Cesario N, Muscio C, Farina M, Amato P, Lavorgna M. Modelling the Rate of Heat Release in Common Rail Deisel Engines: a Soft Computing Approach, SAE paper no. 2004-01-2967; 2004.

60. Galindo J, Climent H, Plá B, JiménezV.D. Correlations for Wiebe function parameters for combustion simulation in two-stroke small engines. Applied Thermal Engineering 2011; 31: 1190-1199.

61. Kim J, Bae C, Kim G. Simulation on the effect of the combustion parameters on the piston dynamics and engine performance using the Wiebe function in a free piston engine. Applied Energy 2013; 107: 446–455.

62. Yeliana Y, Cooney C, Worm J, Michalek D.J, Naber J.D. Estimation of double-Wiebe function parameters using least square method for burn durations of ethanol-gasoline blends in spark ignition engine over variable compression ratios and EGR levels. Applied Thermal Engineering 2011; 31: 2213-2220.

63. Yasar H, Soyhan H S, Walmsley H, Head B, Sorusbay C. Double-Wiebe function: An approach for single-zone HCCI engine modelling. Applied Thermal Engineering 2008; 28: 1284–1290.

64. Shipinski J, Uyehara O A, Myers P S. Experimental correlation between rate of injection and rate of heat release is a diesel engine. ASME paper 68-DGP-11, 1968.

65. Johnson T. Vehicular Emissions in Review. SAE paper 2012 No: 2012-01-0368.

66. Johnson T. Diesel Engine Emissions and Their Control. Corning Environmental Technologies, Corning Incorporated, HP-CB-2-4, Corning, NY 14831, U.S.A. DOI: 10.1595/147106708X248750. Platinum Metals Rev., 2008, 52, (1), 23–37.

67. Tan P Q, Zhao J Y, Hu Z Y, Lou D M , Du A M. Effects of fuel properties on exhaust emissions from diesel engines. Jornal of Fuel Chemistry and Technology 2013,41(3), 347-355.

68. Karabektas M , Ergen G , Hosoz M. Effects of the blends containing low ratios of alternative fuels on the performance and emission characteristics of a diesel engine. Fuel 112 (2013) 537–541.

69. Zhang J. Particle matter emission control and related issues for diesel engines. A thesis submitted to The University of Birmingham for the degree of DOCTOR OF PHILOSOPHY, 2010.

70. Catania A E, Ferrari A. Development and performance assessment of the new-generation CF fuel injection system for diesel passenger cars. Applied Energy 91 (2012) 483–495.

71. HK S. Investigations of multiple injection strategies for the improvement of combustion and exhaust emissions characteristics in a low compression ratio (CR) engine. Applied Energy 88(2011):5013–9.

72. Chiodi M,Mack O,Bargende M,Paule K,Brandt J,Fackh V,Wichelhaus D. Improvement of a high-performance diesel-engine by means of investigation on different injection strategies. SAE paper 2009 No: 2009-24-0008.

73. Catania A E, Ferrari A,Spessa E. Numerical–experimental study and solutions to reduce the dwell time threshold for fusion-free consecutive injections in a multijet solenoid-type C.R. system, ICE best paper award. J Eng Gas Turb Power 2009;131(1). 022804-1–022804-14.

74. Ghaffarpour M,Noorpoor A R. NOx reduction in diesel engines using rate shaping and pilot injection. Int J Automotive Technol Manage 2007;7(1):15.

75. Yri R,Salvador F J,Gimeno J,Morena J D. Influence of injector technology on injection and combustion development – Part 1: Hydraulic characterization. Applied Energy 88(2011):1068–74.

76. Zamboni G,Capobianco M. Experimental study on the effects of HP and LP EGR in an automotive turbocharged diesel engine. Applied Energy 94 (2012) 117–128.

77. I. Al-Hinti I,Samhouri M,Al-Ghandoor A,Sakhrieh A. The effect of boost pressure on the performance characteristics of a diesel engine: A neuro-fuzzy approach. Applied Energy 86 (2009) 113–121.

78. Agarwal D,Kumar Singh S,Agarwal A. Effect of Exhaust Gas Recirculation (EGR) on performance, emissions, deposits and durability of a constant speed compression ignition engine. Applied Energy 88 (2011) 2900–2907.

79. Wei H, Zhu T, Shu G ,Tan L,Wang Y. Gasoline engine exhaust gas recirculation – A review. Applied Energy 99 (2012) 534–544.

80. Aithal S M. Impact of EGR fraction on diesel engine performance considering heat loss and temperature-dependent properties of the working fluid. Int J Energy Res 2008;33:415–30.

81. Breda K. Influence of biodiesel on engine combustion and emission characteristics. Applied Energy 88(2011) 1803–12.

82. Varuvel E G,Mrad N,Tazerout M,Aloui F. Experimental analysis of biofuel as an alternative fuel for diesel engine.Applied Energy 94(2012) 224-231.

83. Muralidharan K,Vasudevan D. Performance, emission and combustion characteristics of a variable compression ratio engine using methyl esters of waste cooking oil and diesel blends. Applied Energy 88 (2011) 3959–3968.

84. Labecki L,Cairns A,Xia J,Megaritis A,Zhao H,Ganippa L C. Combustion and emission of rapeseed oil blends in diesel engine. Applied Energy 95 (2012) 139–146.

85. Labecki L,Ganippa L C. Effects of injection parameters and EGR on combustion and emission characteristics of rapeseed oil and its blends in diesel engines. Fuel 98 (2012) 15–28.

86. Abbaszadehmosayebi G,Ganippa L C. Characterising Wiebe Equation for Heat Release Analysis based on Combustion Burn Factor (Ci). Fuel 119(2014) 301-307.

87. Brunt M F J,Rai H. The Calculation of Heat Release Energy from Engine Cylinder Pressure Data.SAE paper No: 981052,1998.

88. Brunt M F J,Platts K C. Calculation of Heat Release in Direct Injection Diesel Engines. SAE paper No: 1999-01-0187, 1999.

89. Baratta M, Misul D. Development and assessment of a new methodology for end of combustion detection and its application to cycle resolved heat release analysis in IC engines. Applied Energy 98(2012) 174-189.

90. Ceviz M A,Kaymaz I. Temperature and air-fuel ratio dependent specific heat ratio functions for lean burned and unburned mixture. Energy Conversion and Management 46 (2005) 2387-2404.

91. Horn U, Egnell R, Johansson B, Andersson Ö. Detailed Heat Release Analyses with Regard to Combustion of RME and Oxygenated Fuels in an HSDI Diesel Engine. SAE paper 2007,No:2007-01-0627.

92. Klein M,Eriksson L. A Specific Heat Ratio Model for Single-Zone Heat Release Models. SAE paper 2004,No:2004-01-1464.

93. Klein M,Eriksson L. A comparison of specific heat ratio models for cylinder pressure modeling, Vehicular systems, Dept of EE Linköpings Universitet,SWEDEN.

94. Ebrahimi R. Effect of specific heat ratio on heat release analysis in a spark ignition. Scientia Iranica B(2011) 18(6), 1231-1236.

95. Asad U, Zheng M. Fast heat release characterization of a diesel engine. International Journal of Thermal Sciences 47 (2008) 1688-1700.

96. Hardenberg H O, Hase F W. An Empirical Formula for Computing the Pressure Rise Delay of a Fuel From Its Cetane Number and From the Relevant Parameters of Direct-Injection Diesel Engines. SAE paper No. 790493, 1979.

97. Wolfer H H. Der Zundverzug im Dieselmotor. VDI.Foresh-ht,1938, 392,15.

98. Aradi A, Ryan T III. Cetane effect on diesel ignition delay times measured in a constant volume combustion apparatus. SAE Technical Paper 952352, 1995.

99. Davidson D F, Gauthier B M, Hanson R K. Shock tube ignition measurements of iso-octane/air and toluene/air at high pressures. Proceedings of the Combustion Institue 30(2005) 1175-1182.

100. Assanis D N, Filipi Z S, Fiveland S B, Syrimis M. A Predictive Ignition Delay Correlation Under Steady-State and Transient Operation of a Direct Injection Diesel Engine. Journal of Engineering for Gas Turbines and Power 125(2003) 450-458.

101. Alkhulaifi K, Hamdalla M. Ignition delay correlation for a direct injection diesel engine fuelled with automotive diesel and water diesel emulsion. World Academy of science, Engineering and Technology 58(2011) 905-917.

102. Kwon S, Arai M, Hiroyasu H. Effects of cylinder temperature and pressure on ignition delay in direct injection diesel engine. Journal of MESJ 1988, Vol. 24, No.1. Department of Mechanical Engineering, University of Hiroshima, Japan.

103. Kobori S, Kamimoto T, Aradi A A. A study of ignition delay of diesel fuel sprays.International Journal of Engine Research 2000 ,1:29 DOI: 10.1243/1468087001545245.

104. Kalghatgi G T, Hildingsson L, Harrison A J, Johansson B. Auto ignition quality of gasoline fuels in partially premixed combustion in diesel engines. Proceedings of the Combustion Institute 33(2011) 3015-3021.

105. Andrae J C G, BjÖrnbom P, Cracknell R F, Kalghatgi G T. Auto ignition of toluene reference fuels at high pressures modelled with detailed chemical kinetics. Combustion and Flame 149 (2007) 2-24.

106. Hernandez J J, Sanz-Argent J, Carot J M, Jabaloyes J M. Ignition delay time correlations for a diesel fuel with application to engine combustion modelling. International Journal of Engine research 11(2010) 199-206.

107. Reyes M, Tinaut F V, Andrés C, Pérez A. A method to determine ignition delay times for Diesel surrogate fuels from combustion in a constant volume bomb: Inverse Livengood–Wu method. Fuel 102 (2012) 289–298.

108. Rosseel E, Sierens R. The physical and the chemical part of the ignition delay in diesel engines, SAE paper No:961123, 1996.

109. Watson N, Pilley A D, Marzouk M. A combustion correlation for diesel engine simulation, SAE paper No:800029, 1980.

110. Knothe G. Dependence of biodiesel fuel properties on the structure of fatty acid alkylesters. Fuel Processing Technology 2005;86: 1059-70.

111. Demirbas A. Biodiesel, A realistic fuel alternative for diesel engines. London: Springer-Verlag;2008.

112. Sugano H, Nemoto K, Kuwayama S, Mitsui Y, Kusaka J, Daisho Y. An Experimental Study on the Effects of Combustion and Fuel Factors on DI Diesel Engine Performance (Second Report): Effects of fuel properties on premixed charge compression ignition combustion and the conventional diesel combustion. Society of Automotive Engineers of Japan Paper 20045786. 2004.

113. Risberg P, Kalghatgi G, Ångstrom H, Wåhlin F. Auto-ignition quality of Diesel-like fuels in HCCI engines. Society of Automotive Engineers Paper 2005-01-2127. 2005.

114. Li T, Okabe Y, Izumi H, Shudo T, Ogawa H. Dependence of Ultra-High EGR Low Temperature Diesel Combustion on Fuel Properties. Society of Automotive Engineers Paper 2006-01-3387. 2006.

115. Kitano K, Nishiumi R, Tsukasaki T, Tanaka T, Morinaga M. Effects of Fuel Properties on Premixed Charge Compression Ignition Combustion in a Direct Injection Diesel Engine. Society of Automotive Engineers Paper 2003-01-1815. 2003.

116. Bunting B, Crawford R, Wolf L, Xu Y. The Relationships of Diesel Fuel Properties, Chemistry, and HCCI Engine Performance as Determined by Principal Components Analysis. Society of Automotive Paper 2007-01-4059. 2007.

117. Bunting B, Wildman C, Szybist J, Lewis S, Storey J. Fuel chemistry and cetane effects on diesel homogeneous charge compression ignition performance, combustion, and emissions. International Journal of Engine Research. 8(1). 2007. pp. 15-27.

118. Rodríguez R P, Sierens R, Verhelst S. Ignition delay in a palm oil and rapeseed oil biodiesel fuelled engine and predictive correlations for the ignition delay period. Fuel 90(2011) 766-772.

119. Crua C, Kennaird D A, Sazhin S S, Heikal M R, Gold M R. International journal of Engine Research 2004,5:365. DOI:10.1243/146808704323224259.

120. Lyn W T. Study of burning rate and nature of combustion in diesel engines. In Ninth international symposium on combustion. 1963: The combustion institute.

121. Aligrot C, Champoussin J C, Guerrassi N. A correlative model to predict auto ignition delay of diesel fuels. SAE paper 970638,1997.

122. Yamada Y, Emi M, Ishii H, Suzuki Y, Kimura S, Enomoto Y. Heat loss to the combustion chamber wall with deposit in D.I. diesel engine: variation of instantaneous heat flux on piston surface with deposit. JSAE Review 23(2002) 415-421.

123. Sigurdsson E, Ingvorsen K M, Jensen M V, Mayer S, Matlok S, Walther J H. Numerical analysis of the scavenge flow and convective heat transfer in large two-stroke marine diesel engines. Applied Energy 123(2014) 37-46.

124. Xin Q. Diesel engine heat rejection and cooling. Diesel Engine System Design, 2013, Pages 825-859.

125. Taymaz I, Cakir K, Gur M, Mimaroglu A. Experimental investigation of heat losses in a ceramic coated diesel engine. Surface and Coatings Technology, 169–170(2003) 168-170.

126. Durgun O, Şahin Z. Theoretical investigation of heat balance in direct injection (DI) diesel engines for neat diesel fuel and gasoline fumigation. Energy Conversion and Management 50(2009) 43-51.

127. Awad S, Geo Varuvel E, Loubar K, Tazerout M. Single zone combustion modeling of biodiesel from wastes in diesel engine. Fuel 2013; 106: 558-568.

128. Desbazeille M, Randall R B, Guillet F, ElBadaoui M, Hoisnard C. Model-based diagnosis of large diesel engines based on angular speed variations of the crankshaft. Mechanical Systems and Signal Processing 2010; 24: 1529-1541.

129. Kawano D. Optimization of Engine System for Application of Bio-diesel Fuel, SAE paper no. 2007-01-2028; 2007.

130. Malhotra R K, Raje N R. Bio Fuels as Blending Components for Gasoline and Diesel Fuels, SAE paper no. 2003-26-0011; 2003.

131. Rakopoulos C D, Rakopoulos D C, Giakoumis E G, Dimaratos A M. Investigation of the combustion of neat cottonseed oil or its neat bio-diesel in a HSDI diesel engine by experimental heat release and statistical analyses . Fuel 89(2010) 3814-3826.

132. Rakopoulos D C. Heat release analysis of combustion in heavy-duty turbocharged diesel engine operating on blends of diesel fuel with cottonseed or sunflower oils and their bio-diesel. Fuel 96(2012) 524-534.

133. Ghojel J, Honnery D. Heat release model for the combustion of diesel oil emulsions in DI diesel engines. Applied Thermal Engineering 25(2005) 2072-2085.

134. Bueno A V, Velásquez J A, Milanez L F. Heat release and engine performance effects of soybean oil ethyl ester blending into diesel fuel. Energy 36(2011) 3907-3916.

135. Rakopoulos D C, Rakopoulos C D, Papagiannakis R G, Kyritsis D C. Combustion heat release analysis of ethanol or n-butanol diesel fuel blends in heavy-duty DI diesel engine. Fuel 90(2011) 1855-1867.

136. Lakshminarayanan P A, Aghav Y V. Modelling Diesel Combustion. Springer Netherlands publications. 2010 ISBN: 978-90-481-38845. Pages 59-78.

137. Aghav Y V, Thatte V M, Kumar M N, Lakshminarayanan P A, Babu M K G. Predicting Ignition delay and HC emission for DI diesel engine encompassing EGR and Oxygenated fuels. SAE paper 2008, No: 2008-28-0050.

138. Abbaszadehmosayebi G, Ganippa L. Determination of specific heat ratio and error analysis for engine heat release calculations. Applied Energy 122(2014) 143-150.

139. Rothamer D A, Murphy L. Systematic study of ignition delay for jet fuels and diesel fuel in a heavy-duty diesel engine. Proceedings of the Combustion Institute 34 (2013) 3021–3029.

Appendix 1

Fuel technical specifications

Property	Diesel	RME	JME	Unit
Ash content	<0.005	-	0.02	%
Calorific value	44800	45959.1	39340	kJ/kg
Carbon residue	0.2	-	-	%
Cetane Number	52.1	49.8	51	-
Cloud point	-10	-17	-	^{o}C
Density@15 ^{o}C	853.8	837.4	860-900	kg/m^{3}
Flash point	68	-	101	^{o}C
Hydrogen	13.4	13.5	-	%
Oxygen	0	<0.04	-	%
Sulphur content	10	7.5	10	mg/kg
Total aromatics	10.5	24	-	%
Carbon	86.2	86.5	-	%
Viscosity@40 ^{o}C	2.5	2.891	3.5-5	cSt
Water content	61	-	500	mg/kg

Appendix 2

By definition *Cum.Hrr* is the integration of *AHRR* function during combustion period:

$$Cum.Hrr = \int_a^b Ahrr.d\theta$$

Differentiating the definition of *Cum.Hrr* with respect to γ :

$$\frac{d}{d\gamma}Cum.Hrr = \frac{d}{d\gamma}\int_a^b Ahrr.d\theta \tag{2.1}$$

$$\frac{d}{d\gamma}Cum.Hrr = \int\left(\frac{-1}{(\gamma-1)^2}\times p\times\frac{dV}{d\theta} - \frac{1}{(\gamma-1)^2}\times V\times\frac{dp}{d\theta}\right)d\theta \tag{2.2}$$

$$\frac{d}{d\gamma}Cum.Hrr = \frac{-1}{(\gamma-1)^2}.pV \tag{2.3}$$

Appendix 3

Equation (7.19) in the text has been re-written to express the Δ term in the n^{th} form as equation (3.1).

$$\sum_{i=1}^{n}(-\ln\Pi_i)^2.[(\sum_{i=1}^{n-1}\ln\Delta_i)+(\ln\Delta_n)]-[\sum_{i=1}^{n}(-\ln\Pi_i)].\{[\sum_{i=1}^{n-1}(-\ln\Pi_i.\ln\Delta_i)]+[(-\ln\Pi_n).(\ln\Delta_n)]\}=0$$

(3.1)

Equation (3.2) has been restructured to determine the n^{th} term of Δ by using equation (3.1) which is expressed as:

$$\Delta_n = \exp\left(\frac{[\sum_{i=1}^{n}(-\ln\Pi_i)].[\sum_{i=1}^{n-1}(-\ln\Pi_i).(\ln\Delta_i)]-[\sum_{i=1}^{n}(-\ln\Pi_i)^2].(\sum_{i=1}^{n-1}\ln\Delta_i)}{[\sum_{i=1}^{n}(-\ln\Pi_i)^2]-[\sum_{i=1}^{n}(-\ln\Pi_i)].(-\ln\Pi_n)}\right) \tag{3.2}$$

In equation (3.2) the right hand side parameters are all known in terms of the engine parameters (Π_i to Π_n) and (Δ_i to Δ_{n-1}) consequently the value of Δ_n can be calculated.

Equation (3.3) has been determined from the main definition of Δ.

$$\tau_n = \tau_o.\Delta_n.\exp\left(\frac{C}{T}-\frac{C}{T_o}\right) \tag{3.3}$$

Replacing Δ_n from equation (3.2) in equation (3.3) results in the determination of the new correlation for ignition delay as:

$$\tau_n = \tau_o.\exp[(\frac{[\sum_{i=1}^{n}(-\ln \Pi_i)].[\sum_{i=1}^{n-1}(-\ln \Pi_i).(\ln \Delta_i)] - [\sum_{i=1}^{n}(-\ln \Pi_i)^2].(\sum_{i=1}^{n-1}\ln \Delta_i)}{[\sum_{i=1}^{n}(-\ln \Pi_i)^2] - [\sum_{i=1}^{n}(-\ln \Pi_i)].(-\ln \Pi_n)}) + C(\frac{1}{T_n} - \frac{1}{T_o})] \quad (3.4)$$

The equation (3.4) is a new correlation to calculate ignition delay directly by using combustion parameters (*p*,*T* and *C*).

Publications of this work

1. Abbaszadehmosayebi G,Ganippa L C. Characterising Wiebe Equation for Heat Release Analysis based on Combustion Burn Factor (Ci). Fuel 119(2014) 301-307.
2. Abbaszadehmosayebi G, Ganippa L. Determination of specific heat ratio and error analysis for engine heat release calculations. Applied Energy 122(2014) 143-150.
3. Abbaszadehmosayebi G, Ganippa L. Characterising ignition delay correlation for diesel engine by using newly proposed analytical methods. To be submitted to Applied Energy Journal.
4. Abbaszadehmosayebi G, Ganippa L. Analysis of combustion heat release and engine performance by using newly defined dimensionless parameters (C_θ, C_H). Ander preparation.